AD-A119 800 MASSACHUSETTS INST OF TECH CAMBRIDGE DEPT OF OCEAN E--ETC F/G 13/10
EXPERIMENTAL AND THEORETICAL STUDIES OF THE EFFECT OF GAS CONTE--ETC(U)
JAN 82 R J VAN HOUTEN, H C SAYRE N00014-80-C-0224

UNCLASSIFIED 82-1 NL

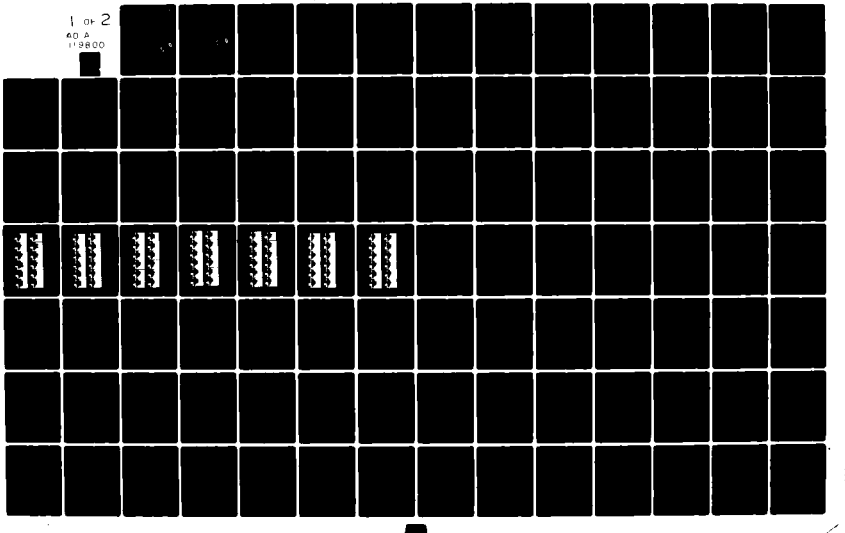

EXPERIMENTAL AND THEORETICAL STUDIES OF THE EFFECT OF GAS CONTENT ON UNSTEADY CAVITY FLOWS

by

Robert J. Van Houten
and
H. Clayton Sayre

January 1982
Report No. 82-1

This research was carried out under the Naval Ship Systems Command General Hydromechanics Research Program Subproject SR 009 01 01 administered by the David W. Taylor Naval Ship Research and Development Center Contract N00014-80-C-0224

Department of Ocean Engineering

EXPERIMENTAL AND THEORETICAL STUDIES OF THE EFFECT OF GAS CONTENT ON UNSTEADY CAVITY FLOWS

by

ROBERT J. VAN HOUTEN
and
H. CLAYTON SAYRE

January 1982

Report No. 82-1

This research was carried out under the
Naval Ship Systems Command General Hydromechanics
Research Program Subproject SR 009 01 01
administered by the David W. Taylor Naval Ship Research
and Development Center Contract N00014-80-C-0224

Department of Ocean Engineering
Massachusetts Institute of Technology
Cambridge, Massachusetts 02139

Unclassified

SECURITY CLASSIFICATION OF THIS PAGE (When Data Entered)

REPORT DOCUMENTATION PAGE	READ INSTRUCTIONS BEFORE COMPLETING FORM
1. REPORT NUMBER: 82-1	2. GOVT ACCESSION NO.: A119802
	3. RECIPIENT'S CATALOG NUMBER:
4. TITLE (and Subtitle): Experimental and Theoretical Studies of the Effect of Gas Content on Unsteady Cavity Flows	5. TYPE OF REPORT & PERIOD COVERED: Final 10-1-79 to 1-31-81
	6. PERFORMING ORG. REPORT NUMBER:
7. AUTHOR(s): Robert J. Van Houten H. Clayton Sayre	8. CONTRACT OR GRANT NUMBER(s): N00014-80-C-0224
9. PERFORMING ORGANIZATION NAME AND ADDRESS: Department of Ocean Engineering Massachusetts Institute of Technology Cambridge, Mass. 02139	10. PROGRAM ELEMENT, PROJECT, TASK AREA & WORK UNIT NUMBERS: SR 009 01 01
11. CONTROLLING OFFICE NAME AND ADDRESS: David W. Taylor Naval Ship Research and Development Center Bethesda, Maryland 20084	12. REPORT DATE: January, 1982 13. NUMBER OF PAGES: 110
14. MONITORING AGENCY NAME & ADDRESS (if different from Controlling Office)	15. SECURITY CLASS. (of this report): Unclassified 15a. DECLASSIFICATION/DOWNGRADING SCHEDULE

16. DISTRIBUTION STATEMENT (of this Report)

Approved for Public Release: Distribution Unlimited

17. DISTRIBUTION STATEMENT (of the abstract entered in Block 20, if different from Report)

18. SUPPLEMENTARY NOTES

Prepared under Naval Sea Systems Command General Hydromechanics Research Program

19. KEY WORDS (Continue on reverse side if necessary and identify by block number)

Cavity Flow
Ventilation
Hydrofoils

20. ABSTRACT (Continue on reverse side if necessary and identify by block number)

A partially cavitating two-dimensional hydrofoil was oscillated in pitch while air was bled into the cavity at a controlled rate. By varying the ambient pressure and air flow rate simultaneously, a constant ventilation number was maintained for a series of cavity air partial pressures. Unsteady forces and cavity pressures were measured, and photographs taken. It was found that cavity air caused fluctuating cavity pressures, and (cont)

DD FORM 1 JAN 73 1473 EDITION OF 1 NOV 65 IS OBSOLETE
S/N 0102-014-6601

SECURITY CLASSIFICATION OF THIS PAGE (When Data Entered)

tended to stabilize cavity length. Its effect on force coefficients was relatively modest. These trends were also found from a parallel theoretical investigation in which a computer program which predicts unsteady cavitation of 2-D foils was modified to allow for cavity gas.

THEORETICAL AND EXPERIMENTAL STUDIES OF THE EFFECT OF GAS CONTENT ON UNSTEADY CAVITY FLOWS

by

R. J. Van Houten
and
H. C. Sayre

ABSTRACT

A partially cavitating two-dimensional hydrofoil was oscillated in pitch while air was bled into the cavity at a controlled rate. By varying the ambient pressure and air flow rate simultaneously, a constant ventilation number was maintained for a series of cavity air partial pressures. Unsteady forces and cavity pressures were measured, and photographs taken. It was found that cavity air caused fluctuating cavity pressures, and tended to stabilize cavity length. Its effect on force coefficients was relatively modest. These trends were also found from a parallel theoretical investigation in which a computer program which predicts unsteady cavitation of 2-D foils was modified to allow for cavity gas.

TABLE OF CONTENTS

LIST OF FIGURES

NOMENCLATURE

A	sectional area of cavity
$AR = s/c$	aspect ratio
c	chord
$C_D = \frac{D}{\frac{1}{2}\rho U^2 S}$	drag coefficient
$C_L = \frac{L}{\frac{1}{2}\rho U^2 S}$	lift coefficient
$C_M = \frac{M}{\frac{1}{2}\rho U^2 Sc}$	moment coefficient
$C_{pa} = \frac{P_a}{\frac{1}{2}\rho U^2}$	air partial pressure coefficient
$C_{pc} = \frac{P_c}{\frac{1}{2}\rho U^2}$	cavity pressure coefficient
fm , Fm	measured force vector and matrix
fa , Fa	applied force vector and matrix
$\underline{H}$	transfer function
k	wave number of gust
$k_R = \frac{kc}{2}$	reduced wave number

ℓ	cavity length
L	lift force
$\dot{M}_a$	air mass flux
M	moment about 1/4 chord, positive when nose down
P_a	air partial pressure
P_{atm}	atmospheric pressure
P_c	cavity pressure
P_o	ambient tunnel pressure
P_v	vapor pressure
$Re = \frac{Uc}{\nu}$	Reynold's number
R_o	radius of spherical cavity
s	span
S	planform area
U	free stream velocity
V	cavity volume
$\dot{V}_a$	air volume flux

$\dot{V}_c$	cavity volume flux
$(\bar{})$, $(\ )_o$	time average
$(\ )_n$	amplitude of n^{th} harmonic
α	angle of attack
γ	polytropic exponent
ν	kinematic viscosity of water
ρ	density of water
$\sigma_c = \frac{P_o - \bar{P_c}}{\frac{1}{2}\rho U^2}$	ventilation number
$\sigma_v = \frac{P_o - P_v}{\frac{1}{2}\rho U^2}$	cavitation number
ω	frequency of oscillation
$\omega_R = \frac{\omega c}{2U}$	reduced frequency

INTRODUCTION

Hydrofoils operating in a marine environment generally cavitate when the combined effects of high speed and low ambient pressures cause the pressure at the surface of the foil to become sufficiently low. When the presssure minimum is located near the leading edge of the foil, the cavitation generally takes the form of a sheet-like cavity which extends from the leading edge of the foil to some other point on the foil (partial cavitation) or to some point behind the trailing edge of the foil (super cavitation). The cavity is filled with water vapor and the pressure within the cavity is the vapor pressure the fluid.

Once a cavity forms, however, its nature can change to the presence in sea water of free and dissolved air. This air can enter the cavity in two ways - through the cavity surface and by way of the re-entrant jet which typically forms at the trailing edge of the cavity. This re-entrant jet is a turbulent jet which forces fluid forward into the cavity. The jet breaks down into droplets of fluid, from which air can be expected to escape fairly readily.

Other means by which air can enter a cavity is by natural ventilation from the atmosphere, or by injection. Possible reasons for injecting air into a cavity include noise and erosion control on propeller blades and enhanced control of hydrofoil craft. In the case of natural ventilation and

injection, the foil need not first develop a vapor cavity.

Although there are several means by which air can enter a cavity, the results are the same, namely the existence of a two-phase cavity, part gas and part vapor. Since air (and vapor) are entrained by the turbulent wake behind the cavity, an equilibrium condition is reached where the proportions of air and vapor do not vary with time. In steady flow, the existence of the gaseous phase changes the basic flow only insofar as it changes the cavity pressure. In unsteady flow, however, the gaseous phase behaves quite differently than does the vapor phase. Because the kinematics of evaporation are quite rapid, as is the heat transfer from the cavity surface [Brennan, 1969], the vapor phase remains at a constant pressure when the cavity volume changes. This was shown experimentally by Shen and Petersen (1978). However, diffusion of air into the cavity and the loss of air through the wake of the cavity are relatively slow processes, so the gaseous phase compresses when the volume decreases and expands when the volume increases. The cavity pressure therefore changes with time, and this affects the cavity dynamics.

Klose and Acosta (1969) reported experiments on ventilated unsteady super cavitation, in which they found large variations in the lift coefficient with air injection rate. These variations were of the same order of magnitude as the variations in

the cavity pressure, although complete correspondence between lift and pressure fluctuation did not exist.

Jiang and Leehey (1977) investigated the unsteady performance of unventilated supercaviting 3-D hydrofoils, and reported that short supercavities, under their experimental conditions, contained significant amounts of air. At certain reduced frequencies, the measured pressure in these cavities showed large fluctuations, and the foil experienced correspondingly large oscillatory lift coefficients. It was postualted that these large lift coefficients were due to resonance of the air-filled cavity. The experimentally obtained resonant frequency was compared with that calculated for a spherical air-vapor bubble of the same volume in a fluid at rest, and fairly good agreement was found. In addition, the damping ratios calculated for such a bubble agreed in a qualitative sense with the experimental observations.

The work reported here consisted of both an experimental and a theoretical investigation. The experimental phase investigated the effect of cavity air on a partially cavitating hydrofoil. A 2-D hydrofoil was oscillated in pitch about its quarter-chord point. Air was bled through a tap in the foil surface, to give air partial pressures of from 0 to 80 percent of the total cavity pressure. As the bleed rate was varied the ventilation number (cavitation number based on measured cavity pressure)

was kept constant, so that the effect of air on mean cavity characteristics was minimized. Unsteady forces and cavity pressures were measured, and photographs were taken at a series of times during the oscillation cycle. In addition to the above experiment, an investigation was made into the natural entrainment of air into a cavity on the above-mentioned hydrofoil.

The theoretical work consisted of extending the capabilities of an existing numerical method for the calculation of unsteady 2-dimensional cavity flows in order to be able to predict the effect of cavity gas. A direct comparison between theory and experiment was not possible, but certain trends can be compared.

EXPERIMENTS

Experimental Facility

All experiments discussed in this report were performed in the Marine Hydrodynamics Laboratory at the Massachusetts Institue of Technology, Cambridge, Massachusetts. The laboratory contains a variable pressure water tunnel of a recirculating design with a water capacity of 23 cubic meters. At its maximum test section velocity of 10 meters per second (mps), it has a cycle time of 10 seconds. The test section is 51 centimeters (cm) square and 140 cm long, surrounded on all four sides by 112 cm by 42 cm by 5 cm thick clear plexiglass windows. A vacuum apparatus provides test section static pressures as low as 80 millimeters (mm) mercury above absolute; these pressures are measured as the average of the static pressures immediately ahead of and behind the model in the test section. Velocities are measured by manometers sensing static pressure differences across a contraction ahead of the test section. The area ratio of this contraction is 4.9.

The laboratory is equipped with a Digital Equipment Corporation MINC-11 mini-computer and analog-to-digital (A/D) converter, which permits high frequency data acquisition and storage as well as convenient data reduction. The A/D converter is capable of dividing its 16 kilohertz maximum sampling rate among up to sixteen analog inputs. A Tektronix 4662 plotter is part of the system to provide graphical presentation of reduced data.

Hydrofoil and Oscillator Drive

The hydrofoil tested was supported in the water tunnel by two shafts bolted to the foil at its quarter chord point. These shafts were fixed in bearing cases mounted in dynamometers on both sides of the tunnel. Figure 1 shows the foil and dynamometer; Appendix A describes the two dynamometers in detail.

One of the shafts supporting the foil passed through seals outside the tunnel and was used to oscillate the foil. A 23 cm arm was clamped to the shaft. This arm was connected to a pushrod which was driven by an eccentric and variable speed electric motor. The configuration described produced adequately sinusoidal pitch motion, variable from 1 to 13 hertz and from .5 to 10 degrees double amplitude in angle of attack. The pushrod has turnbuckle threads for continuous adjustment of mean angle of attack.

A steel nipple on the driving eccentric created a pulse each time it passed a magnetic pickup. This signal was recorded with the other data and was used to determine instantaneous angle of attack. The point of asymmetry in the pulse was considered to be the point at which the nipple passed directly over the pick-up; a strobe and time delay fired by the positive going pulse was used to exactly determine minimum angle of attack in the time record.

Mean angle of attack was measured with respect to the angle of zero lift for the foil. With the eccentric at a known extreme

position (e.g. minimum angle of attack in the pitch cycle) the turnbuckle pushrod backed the foil down until negative flat plate loading exactly cancelled camber loading and zero lift was measured. The zero lift angle is defined by the design lift coefficient of the foil and lift curve slope, and so can be used as a reference to position the foil. This technique is extremely precise, and it is adequately accurate provided that flat plate and camber loading are affected equally by three-dimensional effects and fluid viscosity. These were considered to be reasonable assumptions.

The hydrofoil model was a 66-309 section with its thickness distribution modified as discussed by Brockett (1966). The leading edge radius was .83 mm, the chord was 23 cm; the material was anodized aluminum. The 66-309 section was selected as a likely choice for prototype design. It is characterized by good boundary layer characteristics resulting in low drag.

Leakage between the tunnel walls and the foil was inevitable inasmuch as end clearance between the foil and walls was necessary to permit free motion of the foil. It is, however, difficult to estimate this end clearance inasmuch as the tunnel windows draw in as the tunnel is depressurized for cavitation studies. Minimum clearance is that for which the foil does not interfere with the windows under maximum vacuum.

Despite the foil's relatively sharp leading edge, a .5 mm trip wire was glued to the foil 3 mm downstream of the leading edge to insure sheet cavitation beginning uniformly near the leading dege. The details of boundary layer transition, separ-

ation, and cavitation inception are poorly understood for the unsteady problem. Whereas early transition and leading edge sheet cavities are likely at prototype Reynold's numbers of 100 million they are uncertain at model test Reynold's numbers of 3 million. The addition of a trip wire to the model caused sheet cavitation at every point in the pitching cycle, and this was felt to most correctly duplicate prototype conditions

Pressure Measurement

A 6 mm air passageway from a point one quarter chord from the leading edge and at mid-span on the suction side of the foil led outside the tunnel through the driving shaft. After an operating condition was achieved where cavities never smaller than a quarter chord were formed, air could be bled through this line into the cavity. A Fisher Scientific Mark III flowmeter measured average air flow.

Separate devices were used to measure average and unsteady cavity pressures. A Bruel and Kjaer type 8103 hydrophone was placed in the air line to the cavity in order to measure unsteady pressures. The accuracy of remote reading of unsteady pressures was initially a concern. This configuration was calibrated by connecting the hydrophone, enclosing chamber and 70 cm length of 6 mm diameter air line to a fluctuating pressure, and then comparing the resulting response to the response of the hydrophone when directly connected to the same fluctuating pressure. This test demonstrated that no adjustment need be made to the harmonics of measured cavity pressure up to 35 hertz.

Mean pressures were measured by the manometer device shown in figure 2. This manometer has two interfaces: vapor to liquid water and liquid water to mercury. The vertical location of each of the interfaces must be known in order to sum the hydrostatic pressures created by the water and mercury phases. The motivation behind the conglomeration of glassware and tubing of figure 2 was to insure the known location of a stable vapor-liquid interface. With reference to figure 2, the vapor region "A" in the glass bottle communicates through the hole in the drive shaft and foil to the cavity. Since there is a single negligible density vapor phase in all this tubing, the pressure in the vapor region "A" is the cavity pressure. The fluid in the bottle is connected through a single phase fluid line to the mercury manometer. This manometer (corrected for the hydrostatic water head from the vapor-fluid interface to the fluid-mercury interface) measures the pressure in the vapor region of the bottle and so the mean cavity pressure. Note that if pressures as low as vapor pressure of water at room temperatures are to be measured, it is necessary that all tubing containing liquid be lower than the vapor-liquid interface.

Air is bled directly into the glass bottle and then flows into the cavity. The frictional pressure drop due to this air flow was estimated and was found to be negligible.

Experimental Procedure

The nature of the experiment and the equipment available presented certain restrictions upon the cavitation conditions. In order to be able to bleed air continuously into the cavity, the minumum length of the oscillating cavity could be no less than one quarter of the foil chord. Also, the oscillating angle of attack was set so that the maximum unventilated cavity length would be about a full chord. In order to minimize the risk of fatique failure of the shaft welds, unsteady lift loading was to be less than 2500 Newtons. Pressures below 100 mm mercury absolute provided low cavitation numbers without high fluid velocities and loading, but these pressures cause evolving free tunnel air to make photographs impossible to interpret. The other consideration guiding the choice of experimental conditions was the thought that variations in angle of attack near ideal angle of attack would represent the most realistic prototype conditions. Within these five limitations operating conditions for the experiment were selected.

Unsteady data was taken for one unventilated case and six ventilated cases. The ventilation number (cavitation number based on measured cavity pressure rather than vapor pressure) was constant to within 3% for all seven cases.

Test conditions were as follows:

Frequency, ω	8.5 Hz
Reduced frequency, ω_R	1.00
Velocity, U	6.1 mps
Reynold's number, Re	1.5 million
Mean angle of attack, α_o	2.25 degrees
Amplitude of angle of attack, α_1	1.25 degrees
Nominal ventilation number, σ_c	.58
Tunnel temperature	26.0 degrees Centigrade
Vapor pressure, P_v	25.7 mm hg
Cavity pressures, P_c	26.7 30.5 44.2 61.5 81.7 100. 127. mm hg
Air bleed rates, $\dot{V}_a$	0.00 1.67 10.8 24.2 31.7 40.0 55.8 cc/sec
Cavitation numbers, σ_v	0.59 0.62 0.71 0.83 0.98 1.11 1.30
$\bar{C}_{pa} = \sigma_v - \sigma_c$	0.00 0.03 0.14 0.25 0.40 0.53 0.72

When unsteady cavities of the desired character were established, air was continuously introduced into the cavity. The mean cavity pressure was measured and the water tunnel pressure was adjusted so as to maintain constant ventilation number between tests. The system and measurement electronics were given 30 seconds to come to equilibrium and then the computer started recording data. The magnetic pulse from the pickup on the drive eccentric, firing just before minimum angle of attack, was used to initialize the Schmidt trigger on the A/D converter. The length of the sampling record was adjusted such that 1.2 oscillation cycles of data were recorded. Three hundred data points were taken from each of the five load cells, the pressure transducer and the eccentric pickup.

As soon as the computer finished storing this acquired data, it waited for another pulse from the eccentric; this was repeated

until 45 cycles had been read and averaged. Integer arithmetic was used to the extent possible to speed the averaging of data, and the time required for the 45 cycles of data acquisition at a cycle frequency of 8.5 hertz was 50 seconds. Stationarity of the process did not appear to be a problem. Tunnel velocity, tunnel pressure, cavity pressure and air bleed rate were recorded by the two technicians during the 50 seconds of data storage and then given to the computer, which stored them along with the unsteady force and pressure data on a floppy disk. A series of these experiments were performed at air bleed rates giving a range of cavity pressures from vapor pressure to 130 mm mercury absolute.

After the data had been collected and stored, preparations were made for photographing the cavities. The tunnel was deaerated to improve visibility in the photos and the camera, tripod, strobe and time delay were readied. It was felt that the ease and reproducibility of recreating a given cavitation state (as determined by cavitation and ventilation numbers) justified taking the photos after the data acquisition was completed. Variations in tunnel air content were not considered of importance inasmuch as the continuous air bleed dominated the postulated natural entrainment of air by the cavity.

Photographic illumination was provided by a General Radio model 1540 strobe which was triggered by a variable time delay.

This time delay started counting on an impulse generated by the magnetic pickup on the drive eccentric. Twelve photos of the cavity were taken during each oscillation period. It is to be noted that a set of photos does not represent the growth and collapse of a single cavity, but rather of randomly selected cavities present at a given time in the oscillation cycle. It may allay the fears of skeptics, however, to comment that when the apparent frequency of oscillation was reduced using non-synchronous strobe illumination, cavitation appeared smooth and continuous. This suggests that the characteristics of a cavity at any given point in the pitch cycle are extremely repeatable.

Both the acquisition and analysis of the experimental data were performed on the MINC-11. The points corresponding to the beginning and end of the oscillation cycle were found from analysis of the time record of the magnetic pickup on the drive eccentric. Traces from the five load cells were combined to give measured lift, moment and drag; the static coupling between moment and drag was removed by subtracting the force read by the moment cell from the forces read by the drag cells.

The digitized time records of lift, moment, drag and pressure, and the oscillation period as determined from the record of the eccentric pickup were fed to a numerical Fourier series routine. Amplitude and phase of harmonics to 70 hertz were calculated. Next, the transfer function of the coupled measurement system,

consisting of the foil and two dynamomenters, was used to correct the strength of the measured forces in frequency space to give the actual forces. The inertial "tare" loading was subtracted from the actual forces to give the applied hydrodynamic forces. There was no adjustment to the pressure data. Appendix A describes corrections to the force data in detail.

A summary of the experimental conditions and the analysis of the data was printed out with the corrected harmonics for lift, moment, drag and pressure. A time trace was then reassembled from the corrected harmonics of hydrodynamics forces. This time trace was plotted on the Tetronix plotter.

Cavity length was estimated by eye from the 12 photographs taken throughout the oscillation cycle at each cavitation condition. This information was plotted in the same format as the force and pressure data for ready comparison.

Experimental Accuracy

It has already been mentioned that in order to allow the foil to oscillate, it was necessary to leave a gap between the foil ends and the tunnel walls. This caused the "two dimensional" foil to have a finite apparent aspect ratio and reduced the lift curve slope from the ideal two dimensional value of 6.28. The lift curve slope for the experimental foil was measured and found to be 5.2, corresponding to an apparent aspect ratio of 11.5.

This aspect ratio was considered to be sufficiently high so as to make the data useful in interpreting two dimensional numerical results.

Brockett (1966) reported that in steady flow a 7% viscous reduction in lift occurs for the modified 66 series at Reynold's numbers characteristic of model tests. For a foil with a 23 cm chord, the presence of the water tunnel walls 25 cm above and below the foil cause a 7% increase in steady lift (Sayre, 1980), coincidently cancelling the viscous attenuation. The estimation of these two effects in the unsteady case is a challenging task; it was felt they would be of lesser magnitude and would tend to cancel one another as happened in the steady case. They were ignored in the following presentation of data.

In order to demonstrate the validity of the design of the experiment and the accuracy of the data reduction programs, measurements were made for an unsteady condition which was tractible analytically. The fully wetted foil was oscillated in a fluid stream between ideal and ideal plus 2.5 degrees angle of attack at the same velocity as cavitating test conditions, and lift and moment coefficients were measured as described above. Three reduced frequencies were investigated: .5, 1.0, and 1.5. The results are shown in the table below. Lift and moment are expressed as non-dimensional coefficients; moment is about the quarter chord, positive nose down. Phase is in degrees.

		ANALYTIC			EXPERIMENTAL		
FORCE	(FRQ)	MEAN	AMP	PHASE	MEAN	AMP	PHASE
LIFT	(.5)	.337	.100	33	.324	.099	21
MOMENT	(.5)	.053	.021	127	.054	.015	99
LIFT	(1.0)	.337	.139	67	.323	.120	48
MOMENT	(1.0)	.053	.037	111	.054	.028	103
LIFT	(1.5)	.337	.200	87	.326	.174	68
MOMENT	(1.5)	.053	.051	104	.055	.045	110

The closeness of the experimental values to the computed ones indicates the correctness of the measurement and data reduction techniques.

Fully wetted unsteady sinusoidal oscillation for small angles of attack is expected to be fully linear, which is to say the strength in overtones of the fundamental oscillation frequency should be zero. The data shows reduction by a factor greater than 100 for frequencies above the fundamental in lift and moment, which confirms the linearity of the drive system.

Results

Twelve photographs of cavity growth and collapse were taken at each of the seven cavity mean pressures and are shown in figures 3 to 9. The first photo of each set was taken 7 msec after minimum angle of attack, the next 10 every 10 msec, and the last at 114 msec. The oscillation period was 117 msec.

Cavity length data has been read from the photographs and is plotted in figures 10 to 16 as length in percent of chord. Zero

time corresponds to minimum angle of attack.

Time histories of lift, moment, drag, and pressure coefficients are shown in figures 17 to 49. The mean value has been removed from the pressure plots, which are plotted as the negative of pressure, to aid comparison with lift.

The mean value and amplitudes and phases of harmonics of lift, moment, drag, and pressure are printed on the time record plots of the data. The phase angle is reported such that the following equation is satisfied:

$$f(t) = A \cos (\omega t - \phi)$$

Where $f(t)$ is the function tracing the time history of the data, A is the amplitude and ϕ is the phase angle. Inasmuch as zero time is defined by the rotating eccentric and so is the time at which the foil passes through minimum angle of attack, the quasi-steady first harmonic of lift would have a phase angle of 180 degrees , not zero. A reported phase angle ϕ less than 180 degrees indicates that the data leads the oscillation cycle by $180 - \phi$ degrees.

Figures 45 to 48 show the mean and first harmonic amplitude of lift, moment, and drag coefficients, and the first harmonic amplitude of cavity pressure coefficient (C_{pa}), plotted against the non-dimensional mean air pressure in the cavity, $\bar{C}_{pa}$, which can be obtained by subtracting the ventilation number from the cavitation number.

The most striking feature of the expermental results is the effect of air partial pressure on the unsteady cavity length. The unventilated cavity varies in length from .25 to 1.05 chord length. At a mean cavity pressure of 61.5 mm hg, or a mean air partial pressure of 36 mm hg, the range in cavity length was reduced to .60 to .95. At the maximum air partial pressure measured of 101 mm hg, the cavity length was essentiallly unchanging at .35 chord lengths.

A subjective observation made during these experiments was that the violence of cavity collapse was greatly reduced by air content. The unventilated cavity was observed in the experiment to lose about 80% of its volume in violent cloud collapse during a single 10 msec time step. At an air partial pressure of 36 mm hg, the cloud collapse was delayed about 20 msec and greatly reduced in severity. This condition was far quieter to observers outside the water tunnel. At air partial pressures of near 50 mm hg, the cavity shed air steadily with no sudden loss of cavity volume.

Although the observed volume fluctuations decreased with increased air partial pressure, the first harmonic of cavity pressure coefficient varied almost linearly with mean air pressure. This probably reflects the lessened severity of the cavity collapse at high air partial pressures, which causes the mass of cavity gas to vary less over an oscillation cycle.

The first harmonics of the lift, moment, and drag coefficients change rapidly with air partial pressure over the first three air partial pressures tested, but are relatively constant at higher air partial pressures. The low partial pressures are those pressures where the cavity length varied approximately between .3 chord and 1.0 chord. A small change in the maximum extent could have a strong effect on the force coefficients, since they will depend on the extent to which the Kutta condition is satisfied. The larger air partial pressures yielded cavities which were always smaller than one chord in length.

The increased amplitude of the unsteady cavity pressure with air content does not appear to be reflected in the lift coefficient. The negative of the cavity pressure lags the lift by 60-90 degrees.

Mean values of the force coefficients varied much more smoothly than did the first harmonics over the range of air partial pressures investigated.

THEORY

Background

During the past several years, there has been developed at MIT a lifting surface method for the prediction of unsteady cavitation of hydrofoils and propellers. This work was first reported by Jiang and Leehey (1977) for the case of 2-D and 3-D super cavitating hydrofoils. Van Houten (1979) extended the method to the case of partially cavitating high-aspect-ratio foils, and Lee (1979) applied the method to marine propellers operating in a non-uniform wake.

The foil is represented by a distribution of vorticity over the chord and in the wake, and source strength over the cavitated region. The singularity strengths are obtained from the solution of coupled integral equations which enforce, in a linearized sense, flow tangency on the wetted portions of the foil and pressure constancy over the cavitated region. A closure condition is also applied. In order to solve these equations numerically, the singularity distributions are discretized and the integral equations are satisfied at discrete collocation points. Since the set of equations to be solved depends on the cavity length, this length is assumed to be known, and the cavitation number is allowed to be an unknown. The cavitation number which is found from the solution is compared with the acutal cavitation number, and a new guess for cavity

length is made. After sufficient iteration, the correct cavity length is found.

Since the cavity length is allowed to vary, the unsteady problem is non-linear, and the solution must be obtained in the time domain. The solution to a periodic input is obtained by starting with a steady flow and time-stepping the solution through several oscillations until the response becomes periodic.

Modeling of Ventilated Cavities

In the present work, the above method was modified to allow for air partial pressure in the cavity. It was assumed that a constant mass of air existed in the cavity at all times, and that it behaved according to the polytropic gas law:

$$P_a V^{\gamma} = C$$

Since the pressure within the cavity and the volume of the cavity are both part of the solution to the boundary value problem at any time step, cavity length can be iterated until this equation is satisfied. In this way the model can account for compression and expansion of the air in the cavity, and its effect on foil performance.

This method has the capability of predicting bubble resonance effects; both the frequency at which they occur, and the degree of damping present. It was previously mentioned that Jiang and Leehey modeled the air-vapor cavity as a spherical bubble, and

obtained reasonably good agreement with their experimentally determined natural frequencies. In addition, they found qualitative agreement between the apparent damping determined experimentally and the thermodynamic damping calculated for the spherical bubble. This calculation did not include hydrodynamic damping, which is likely to dominate other damping effects. Since the cavity cannot expand or contract without changing the lift on the foil, energy will be shed into the wake as the cavity oscillates. The lifting surface model incorporates this effect, and should provide better estimates of cavity resonance effects. Thermodynamic damping is not included in this model, since it is believed to be small.

The numerical model was developed for the case of a 2-D hydrofoil, which in reality is the inner solution of a high aspect ratio foil. The 3-D corrections developed by Van Houten are not affected by the presence of cavity air except insofar as it changes the 2-D solution.

Numerical Procedure

The numerical model was run for two series of conditions. In each series a solution was found first for the case of a purely vaporous caivty, and the mean cavity volume was found. Next, a certain amount of air was assumed to be contained in the cavity, corresponding to a value for the constant C in the polytropic gas law. The pressure of that air was estimated by

assuming that the mean cavity volume was the same as in the case of the unventilated cavity. The cavitation number was then modified so that if this mean air pressure were obtained, the ventilation number would be the same as the cavitation number in the case of the unventilated foil. In fact, the mean volume would differ somewhat from that calculated for the vaporous cavity, but not by a great deal. By following this procedure for a number of air contents, the effect of percentage air content could be investigated independently of any large-scale changes in ventilation number.

The two cases run were both for a flat plate foil at a mean angle of attack of .05, in a gust whose amplitude was also .05. The reduced frequency of the oscillation was 1.0. The two cases investigated were at nominal ventilation numbers of .7 and .5, respectively. The first of these represents a case where the cavity is always smaller than one chord in length. The second is similar to the experimental one, where the cavity length exceeds one chord length over part of the oscillation cycle when the air partial pressure is low.

The proper exponent for the ideal gas law depends on the rate at which the heat of compression is transferred to the walls of the cavity. The numerical model was run for the limiting cases of isothermal and adiabatic compression and the same trends found in each case. The results presented here are all for the isothermal situation.

Calculations were made for an aspect ratio of 100. The 3-D corrections developed by Van Houten were not applied to the results. These corrections are expected to be small, and are not expected to alter the trends with air partial pressure.

Results

Figures 49 and 50 show for a ventilation number of .7, the variation in the first harmonics of cavity pressure, lift, cavity length, and cavity volume with respect to the difference between cavitation number and ventilation number. These results extend to much larger air partial pressures than did the experiments, which were limited by the amount of air which could be bled into the cavity from a source at atmospheric pressure. However, the trends over the lower air partial pressures are similar to those observed experimentally. Lift is relatively unaffected by the air content, despite a sharp rise in the oscillatory cavity pressure. The oscillatory cavity length and volume both decrease significantly. At higher air contents, the first harmonic of cavity pressure levels off. Surprisingly, the oscillations in cavity length increase over the high air partial pressure region.

Figures 51 and 52 show similar results for a ventilation number of .5. This is a case similar to the experimental situation, where the cavity oscillates beyond the trailing edge of the foil when the air partial pressure is low, but not at higher

air contents. As in the experimental results, sudden changes in the lift coefficient accompany the transition between these regimes.

Also indicated in figures 49 and 51, is the air partial pressure of a spherical bubble with a volume equal to that of the cavity and a resonant frequency equal to the frequency of the gust. This is calculated from the simple relationship:

$$P_a = \frac{\omega^2 \rho R_o^2}{3\gamma}$$

where ω is the gust frequency, ρ the water density, and R_o the radius of the spherical bubble. This can be written:

$$\sigma_v - \sigma_c = 1.03 \frac{\omega_R^2}{\gamma} \left[\frac{A}{c^2} AR \right]^{2/3}$$

where ω_R is the reduced frequency, A is the cross sectional area of the cavity, c is the chord, and AR is the aspect ratio. It appears that this equation predicts the order of magnitude of the air partial pressure at which the cavity pressure oscillations predicted by the numerical model reach their peak value.

CONCLUSIONS

1) In the course of these experiments it becamse clear that in those cases where the cavity volume variations are large (i.e., at the lower air contents) much cavity gas is lost during the collapse phase. Since the air bleed rate is practically constant during the oscillation cycle (being proportional to the pressure difference between the atmosphere and the cavity), it can be inferred that the mass of cavity gas varies with time. Since the gas mass is probably a minimum at the time when the pressure is a maximum, it can be expected that the theoretical model, which assumes constant cavity gas, will over-predict pressure oscillations. To account for this discrepancy, a more complex model would have to be used. This model would have to incorporate experimental data on the severity of cloud collapse under various conditions.

2) Before the theoretical model is used for design applications, a direct experimental confirmation of its predictions must be made. This was not done in the present work due to uncertainties in two areas. One is the effect of a non-zero leading edge radius on the extent of cavitation. The present theory is linear and does not accurately predict pressures in the leading edge region. The second uncertainty concerns the resistance of the propeller tunnel to oscillating cavities. This effect may be important when the cavities are as large as those considered in this work.

3) A general conclusion as a result of this work is that gas content is an important variable in determining the size and variability of cavities. Its effect on the force coefficients is quite large when the cavities are in the transitional range between partial and super cavitation. Due to the complexity of the hydrodynamics in this range, a lifting surface model such as that used here is probably necessary for the prediction of prototype behavior.

REFERENCES

Brennan, C. 1969, The Dynamic Balances of Dissolved Air and Heat in Natural Cavity Flows, J. Fluid Mechanics, 37, 115-127.

Brockett, T. 1966, Minimum Pressure Envelopes for Modified NACA-66 Sections with NACA a=.8 Camber, DWTNSRDC Report 1780.

Jiang, C.-W. and Leehey, P.,1977, Experimental and Theoretical Investigation of Unsteady Supercavitating Hydrofoils of Finite Span, M.I.T., Dept. of Ocean Engineering, Report 83481-4.

Klose, G. J. and Acosta, A. J.,1969, Unsteady Forces Measurements on Superventialted Hydrofoils in Heaving Motion, J. Ship Research, 13, no. 2, 92-102.

Lee, C.-S. 1979, Prediction of Steady and Unsteady Performance of Marine Propellers with or without Cavitation by Numerical Lifting Surface Theory, M.I.T., Dept. of Ocean Engineering, Phd. Thesis.

Sayre, H. C. 1980, Laser Doppler Anemometry and the Measurement of Loading Characteristics of Lifting Sections, SNAME Student Paper.

Shen, Y. T., and Peterson, F. B. 1978, Unsteady Cavitation on an Oscillating Hydrofoil, 12th Symposium on Naval Hydrodynamics, Washington, D.C.

Van Houten, R. J. 1979, The Numerical Prediction of Unsteady Cavitation of High Aspect Ratio Hydrofoils, M.I.T. Dept. of Ocean Engineering.

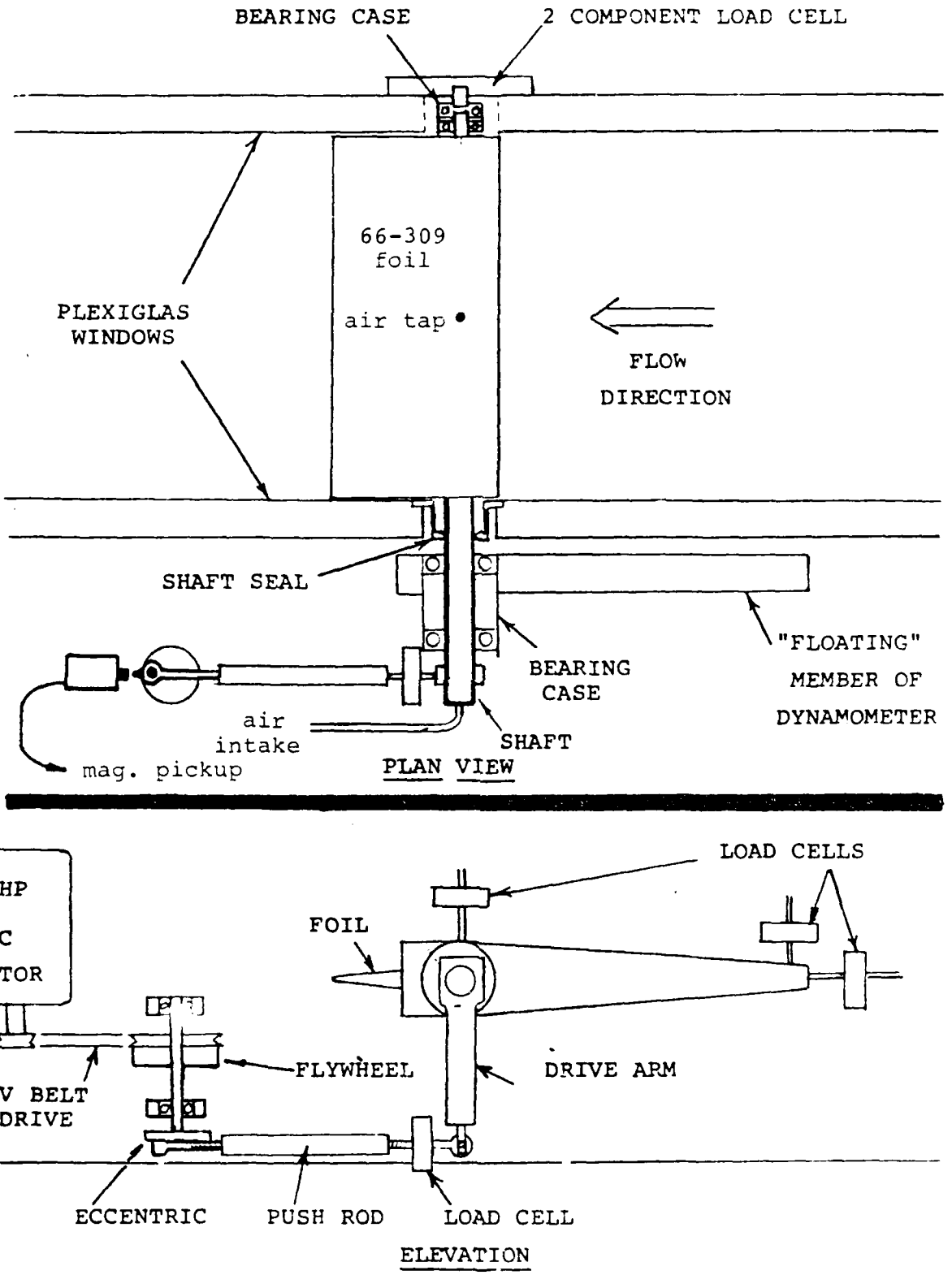

Figure 1. FOIL AND DYNAMOMETERS

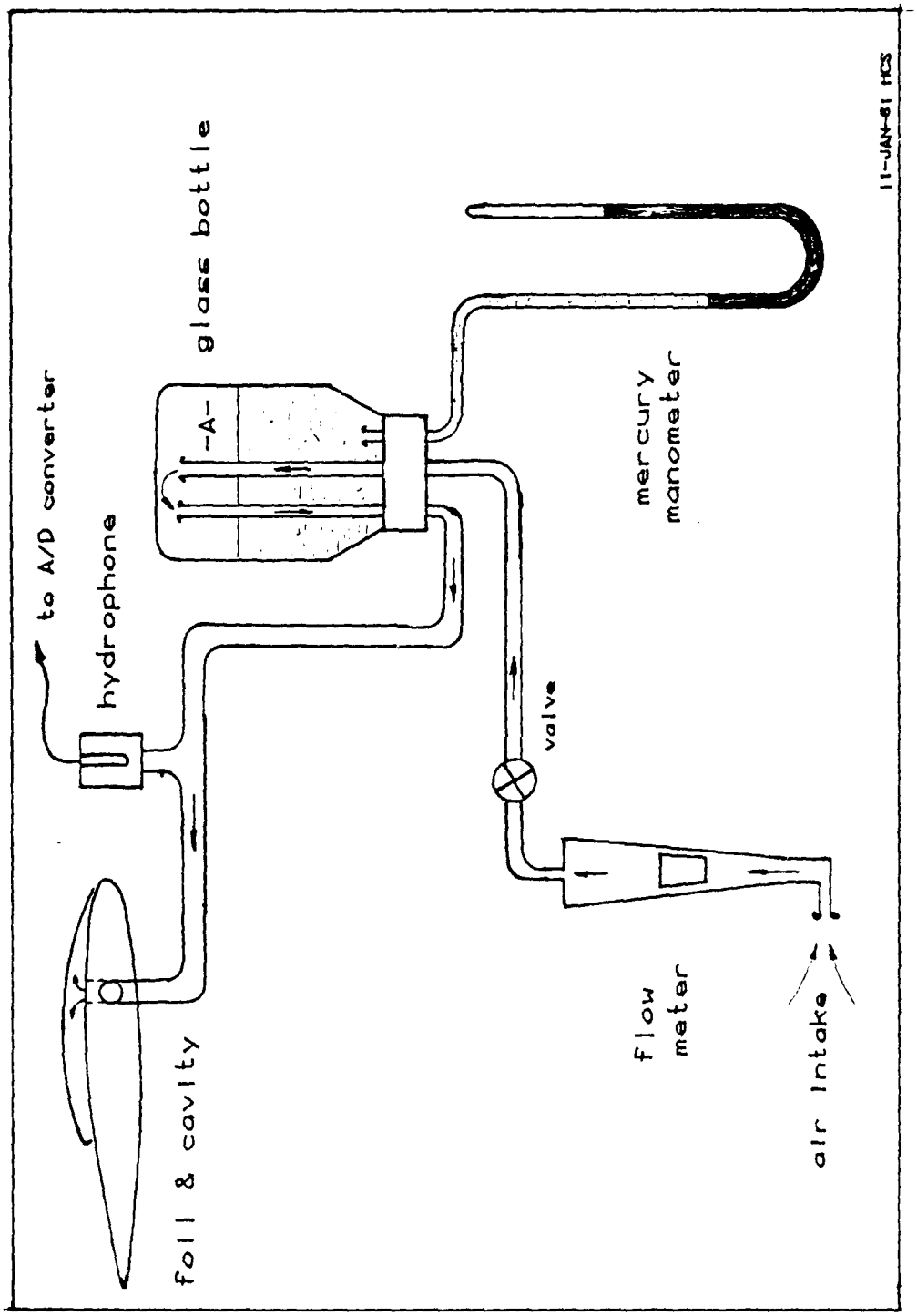

Figure 2. Pressure measurement and air bleeding

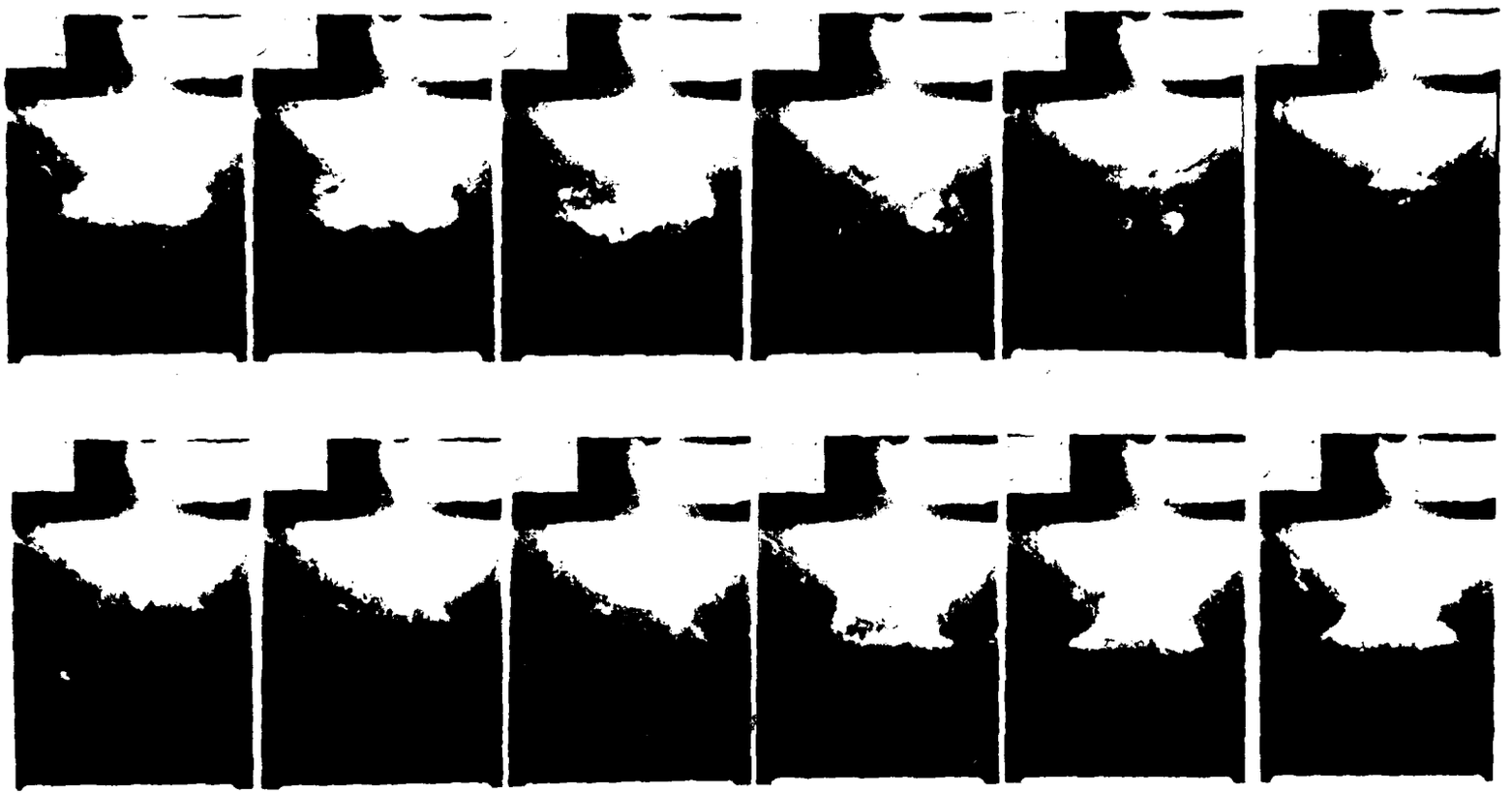

Figure 3: Cavity Photographs, $\overline{C_{pa}} = 0$

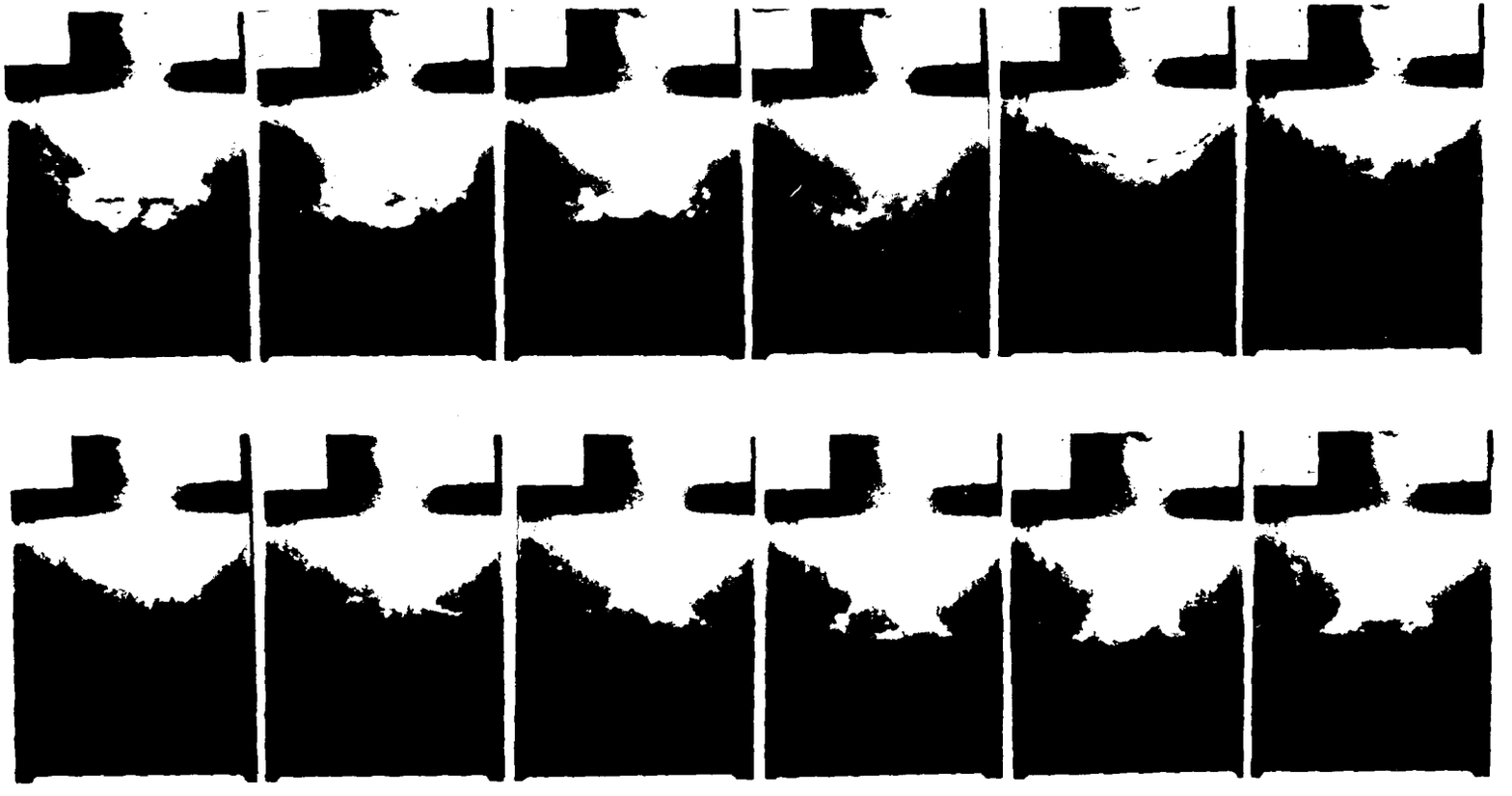

Figure 4: Cavity Photographs, $\overline{C_{pa}} = .03$

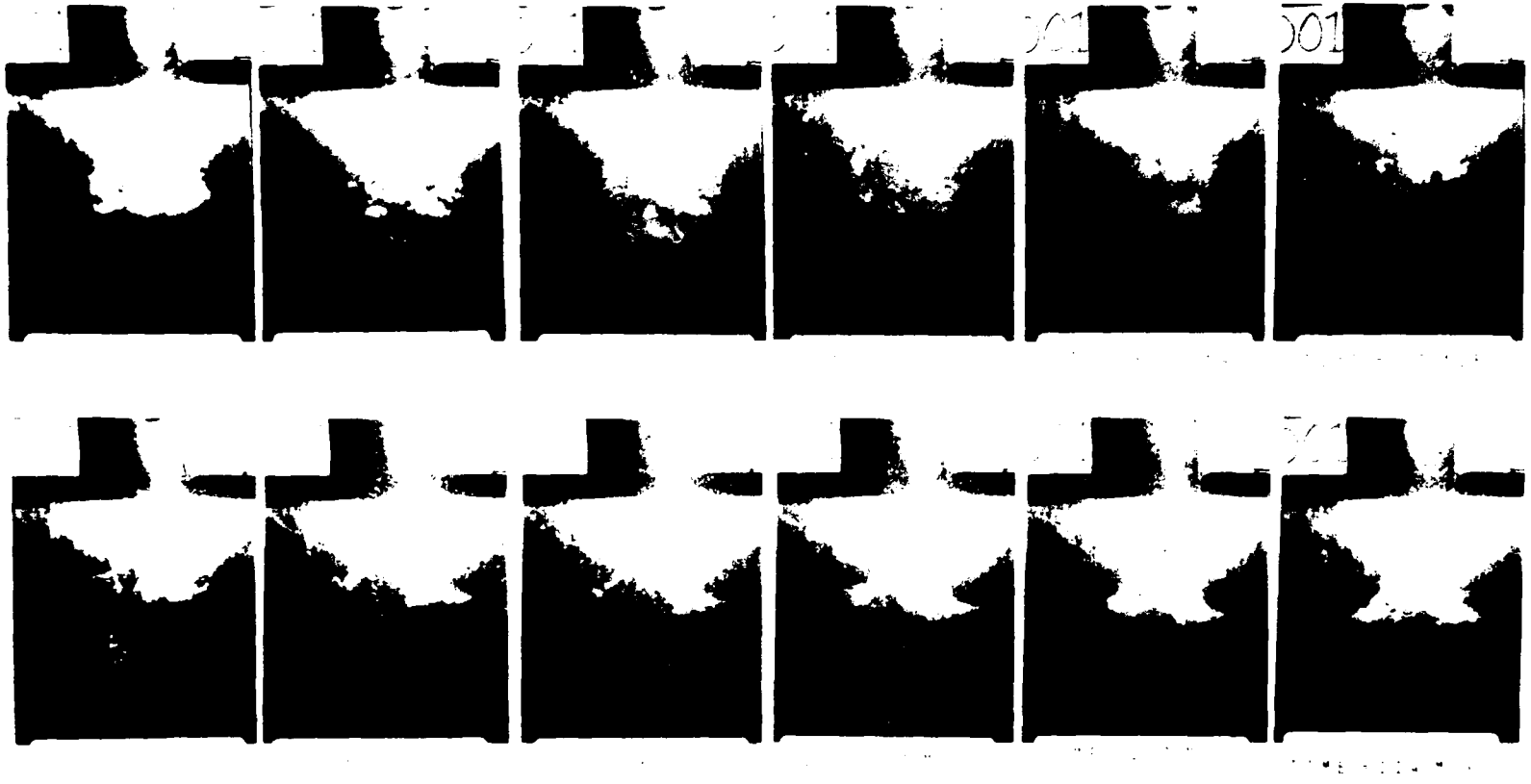

Figure 5: Cavity Photographs, $\overline{C_{pa}} = .14$

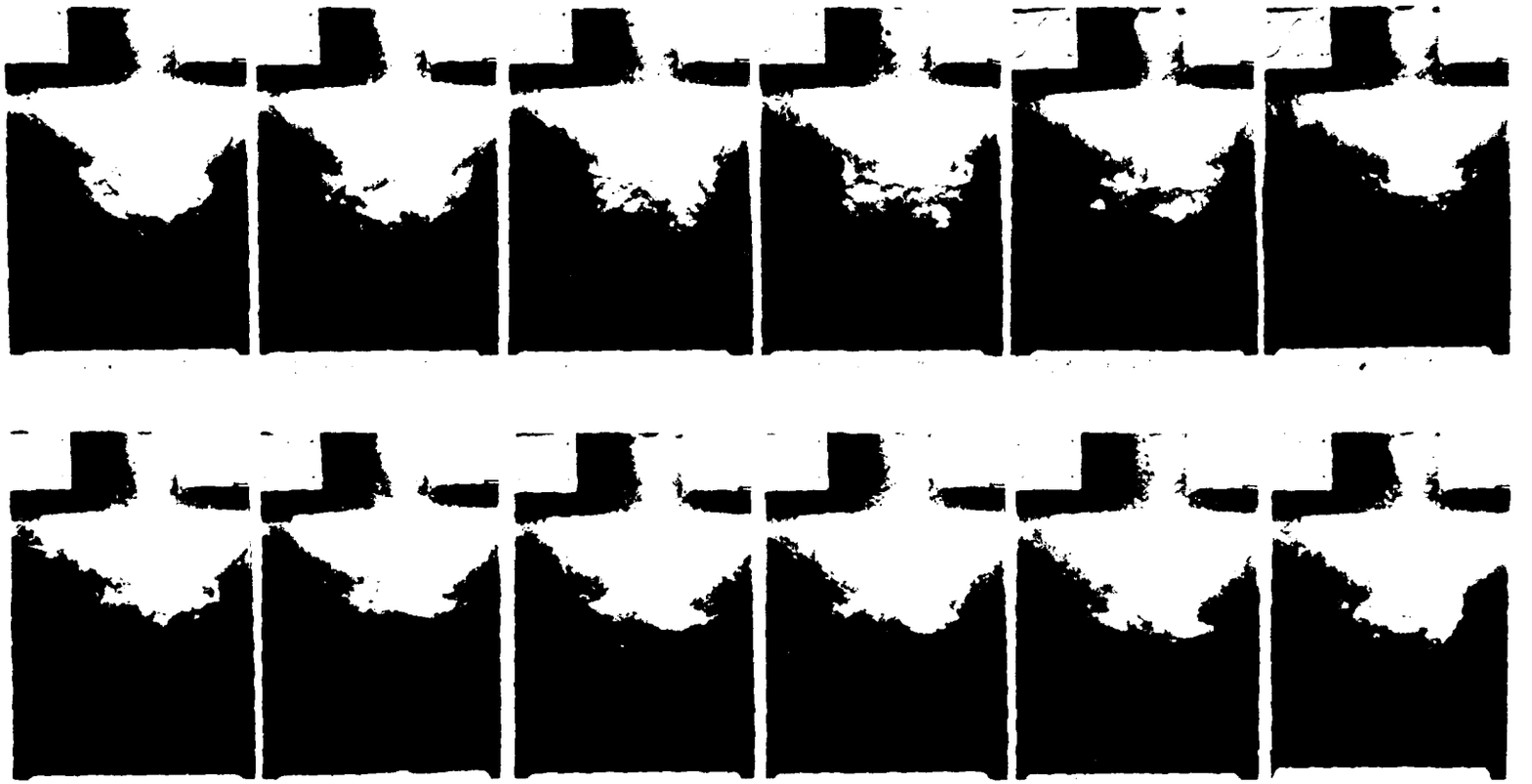

Figure 6: Cavity Photographs, $\overline{C_{pa}} = .25$

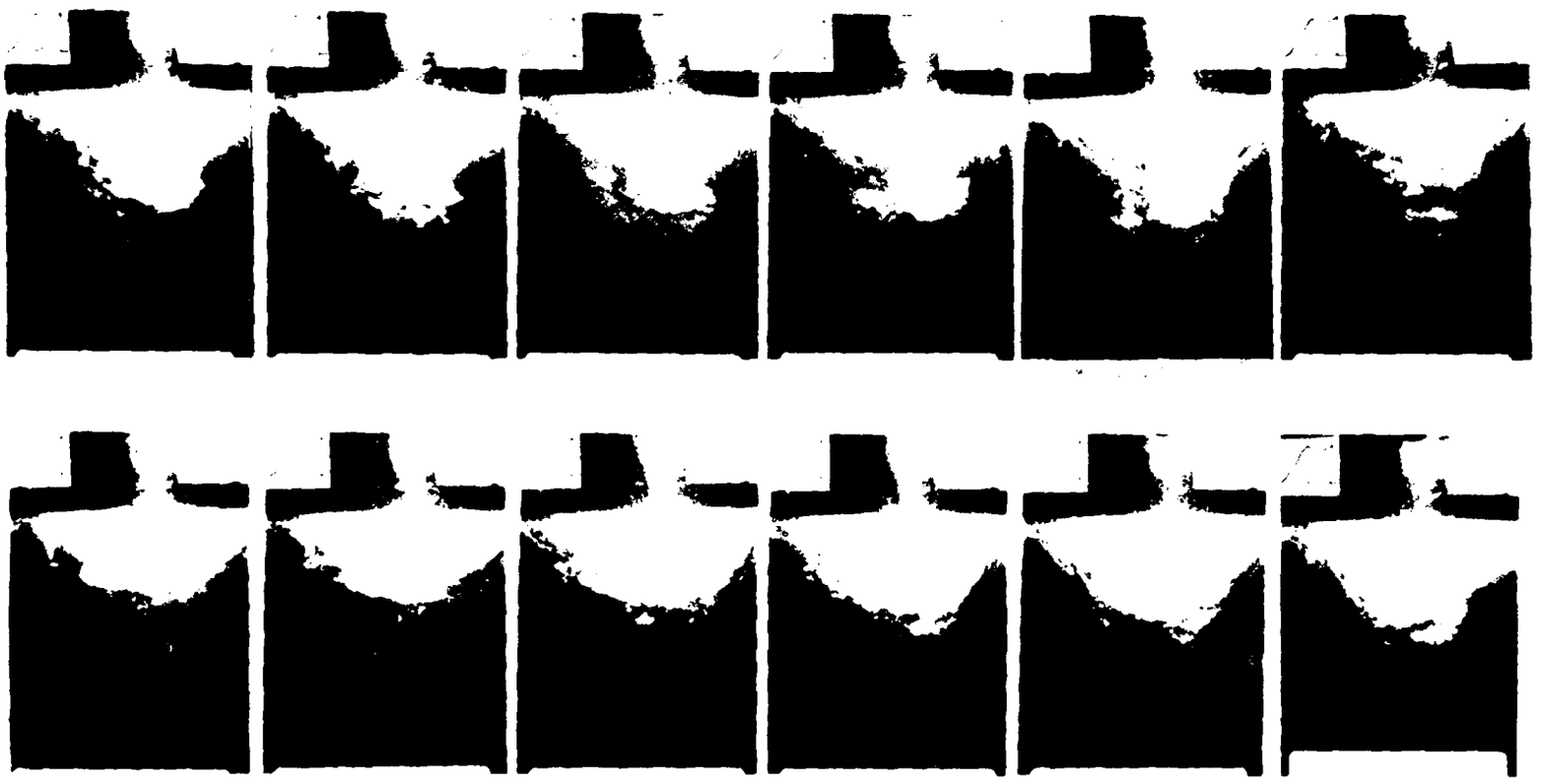

Figure 7: Cavity Photographs, $\overline{C_{pa}} = .40$

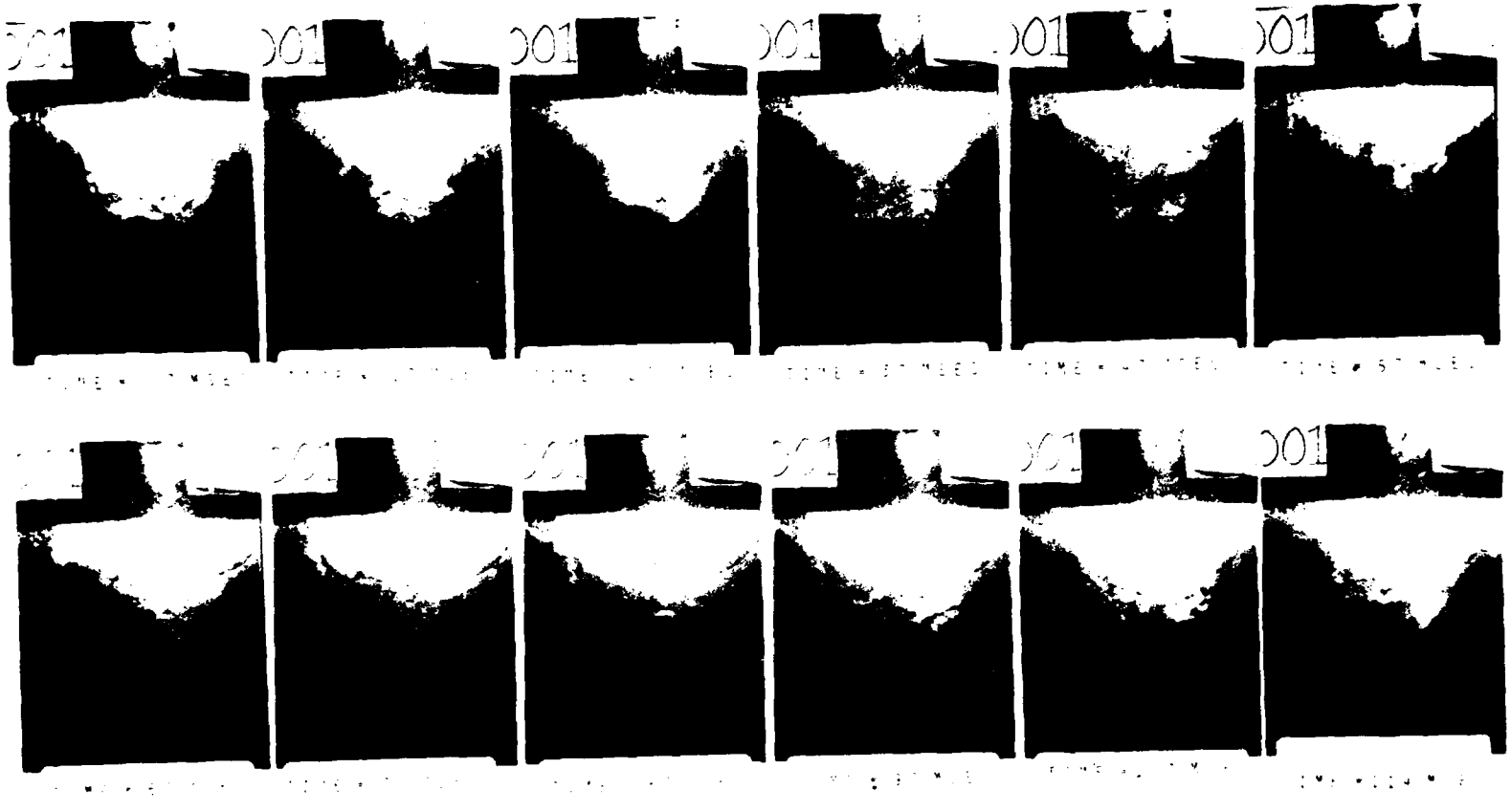

Figure 8: Cavity Photographs, $\overline{C_{pa}} = .53$

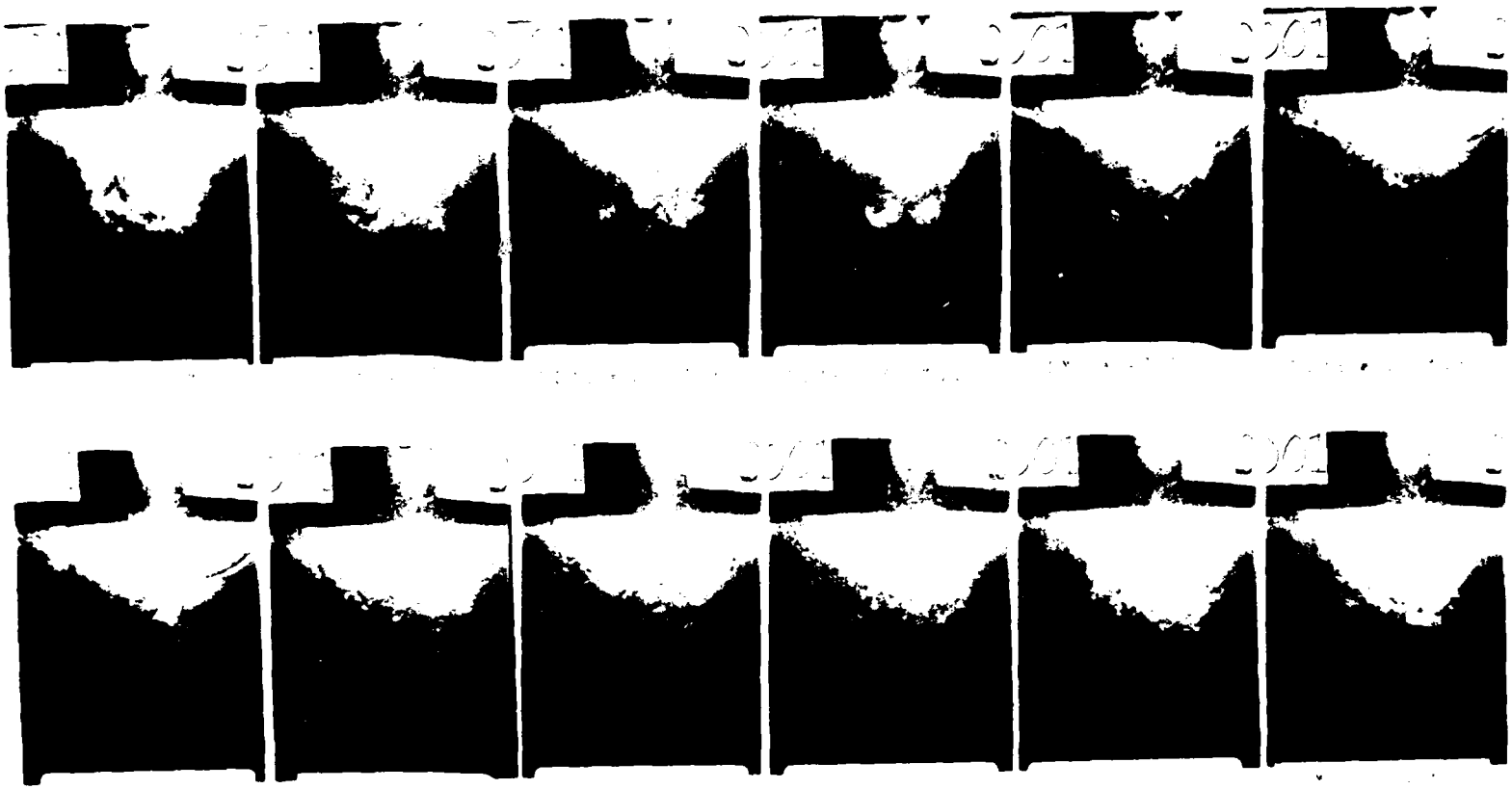

Figure 9: Cavity Photographs, $\overline{C_{pa}} = .72$

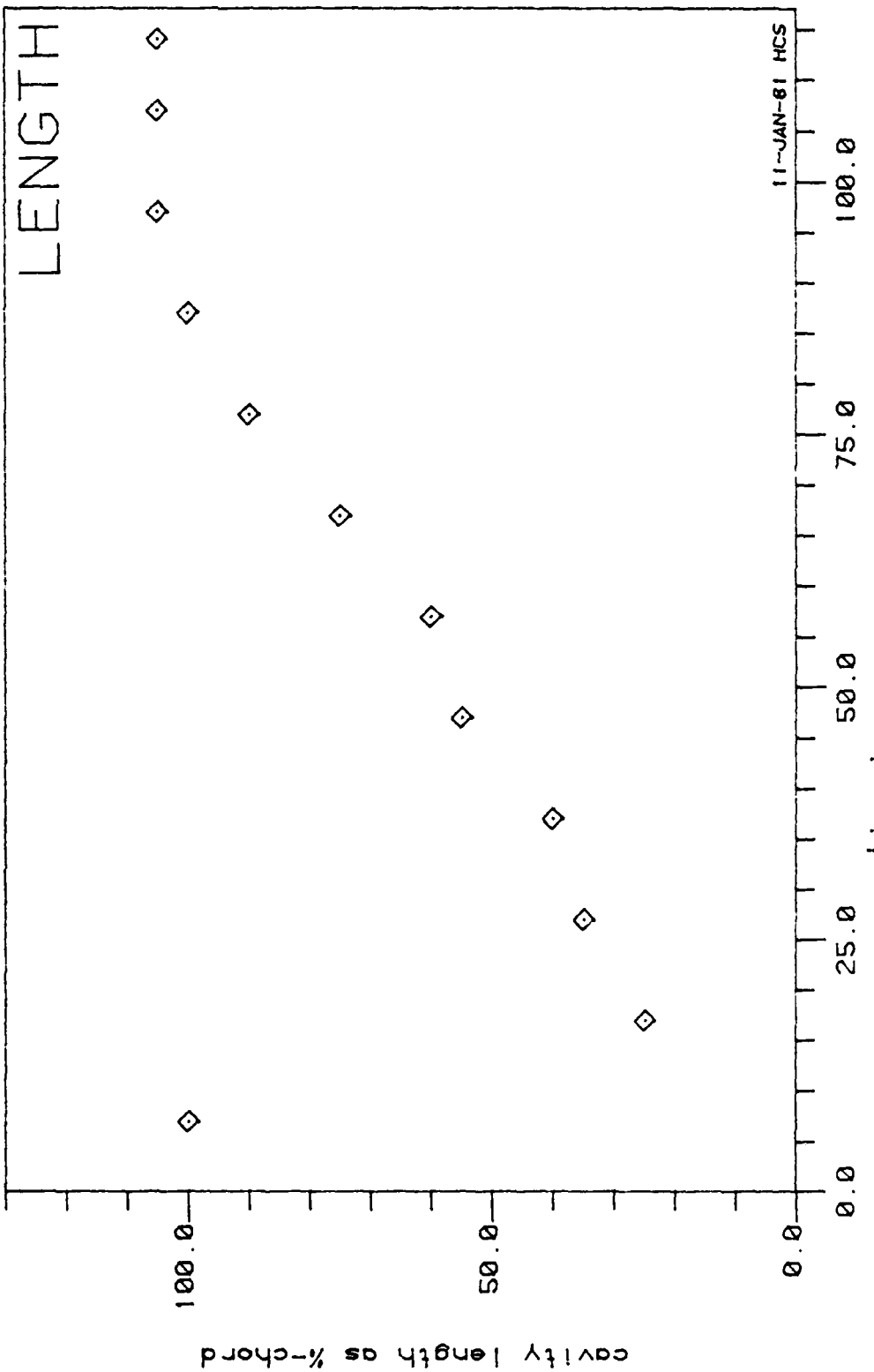

Figure 10: Cavity Length vs. Time, $\overline{C_{pa}} = 0$

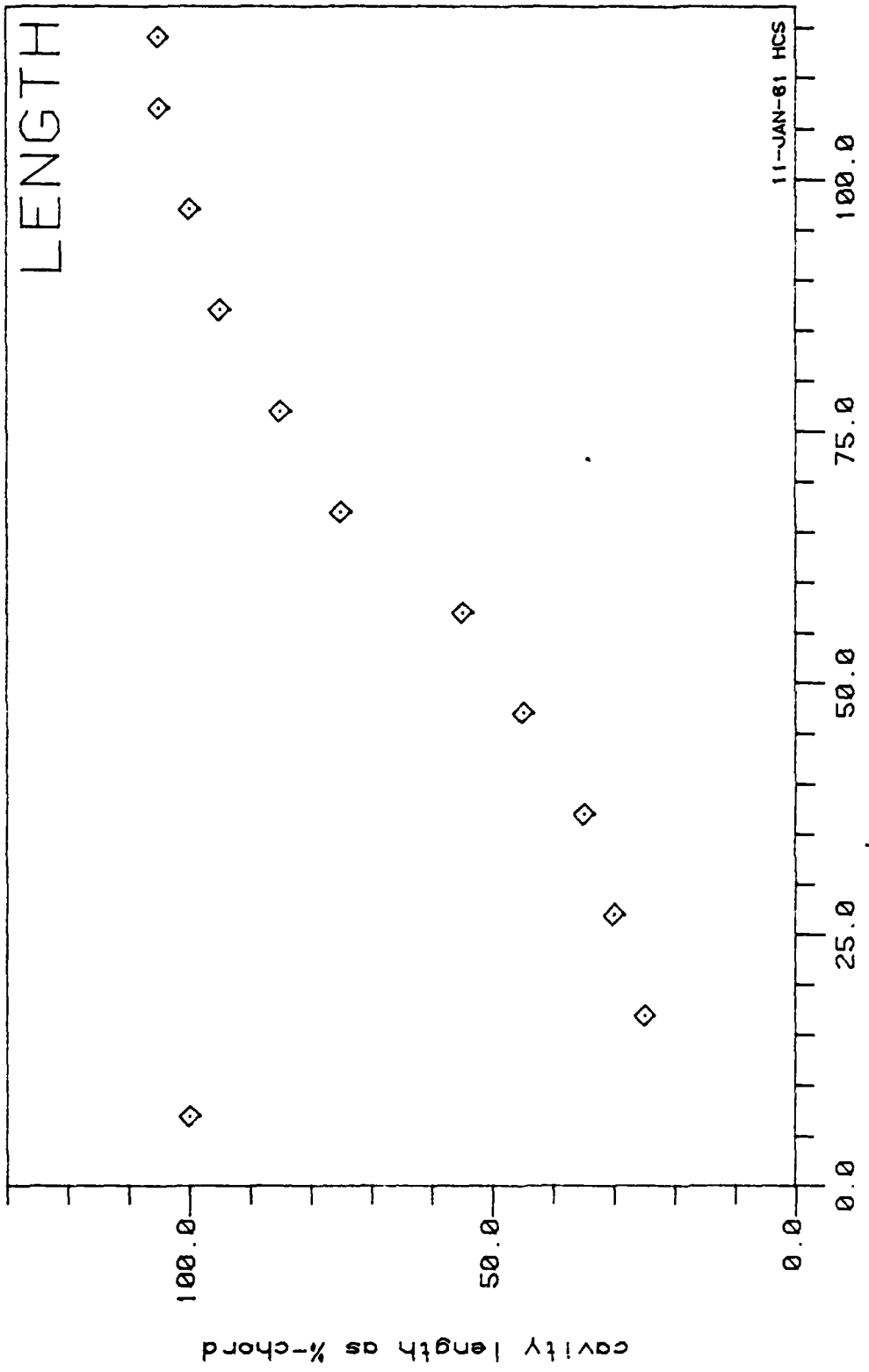

Figure 11: Cavity Length vs. Time, $\overline{C_{na}} = .03$

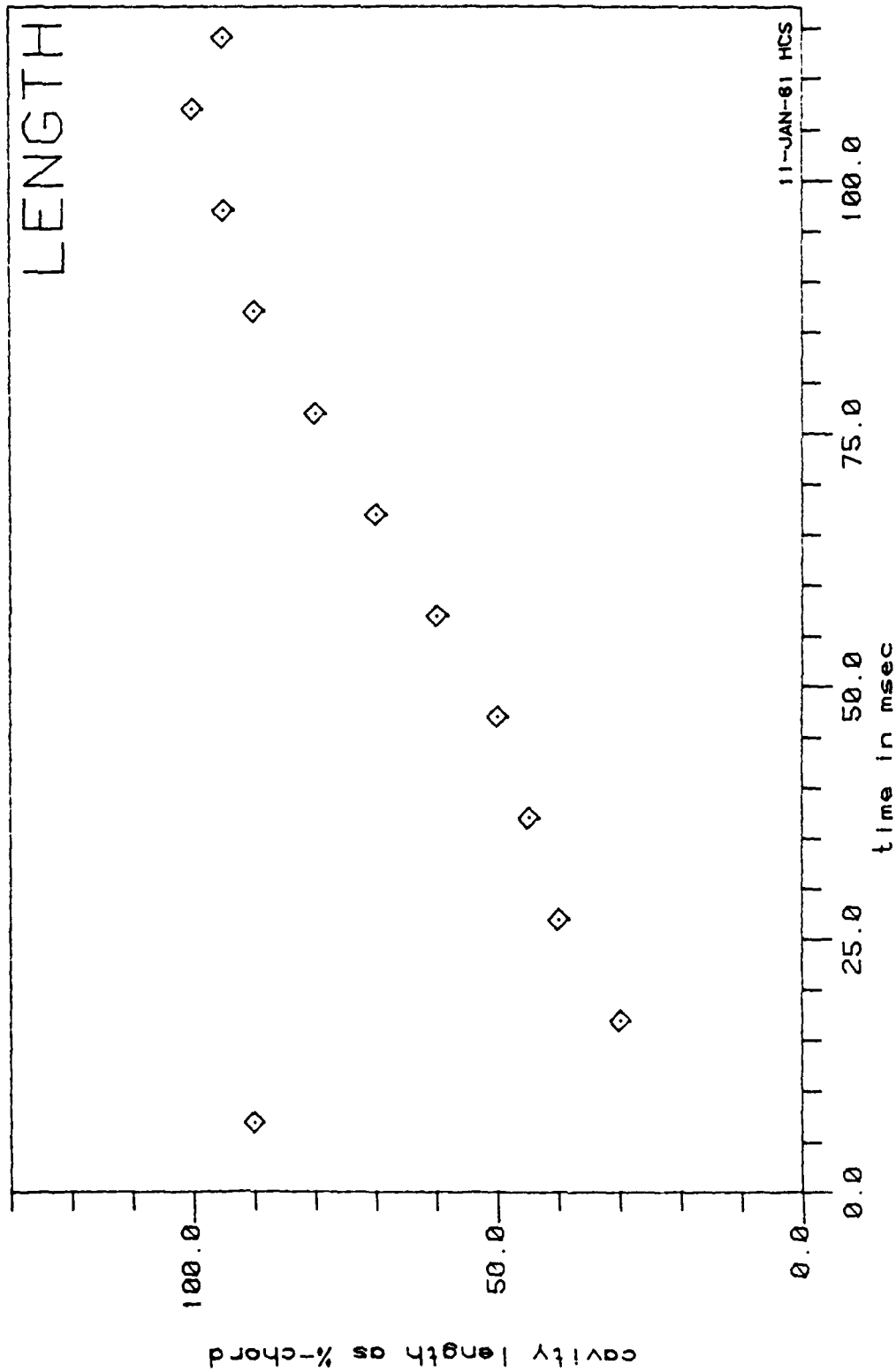

Figure 12: Cavity Length vs. Time, $\overline{C_{na}} = .14$

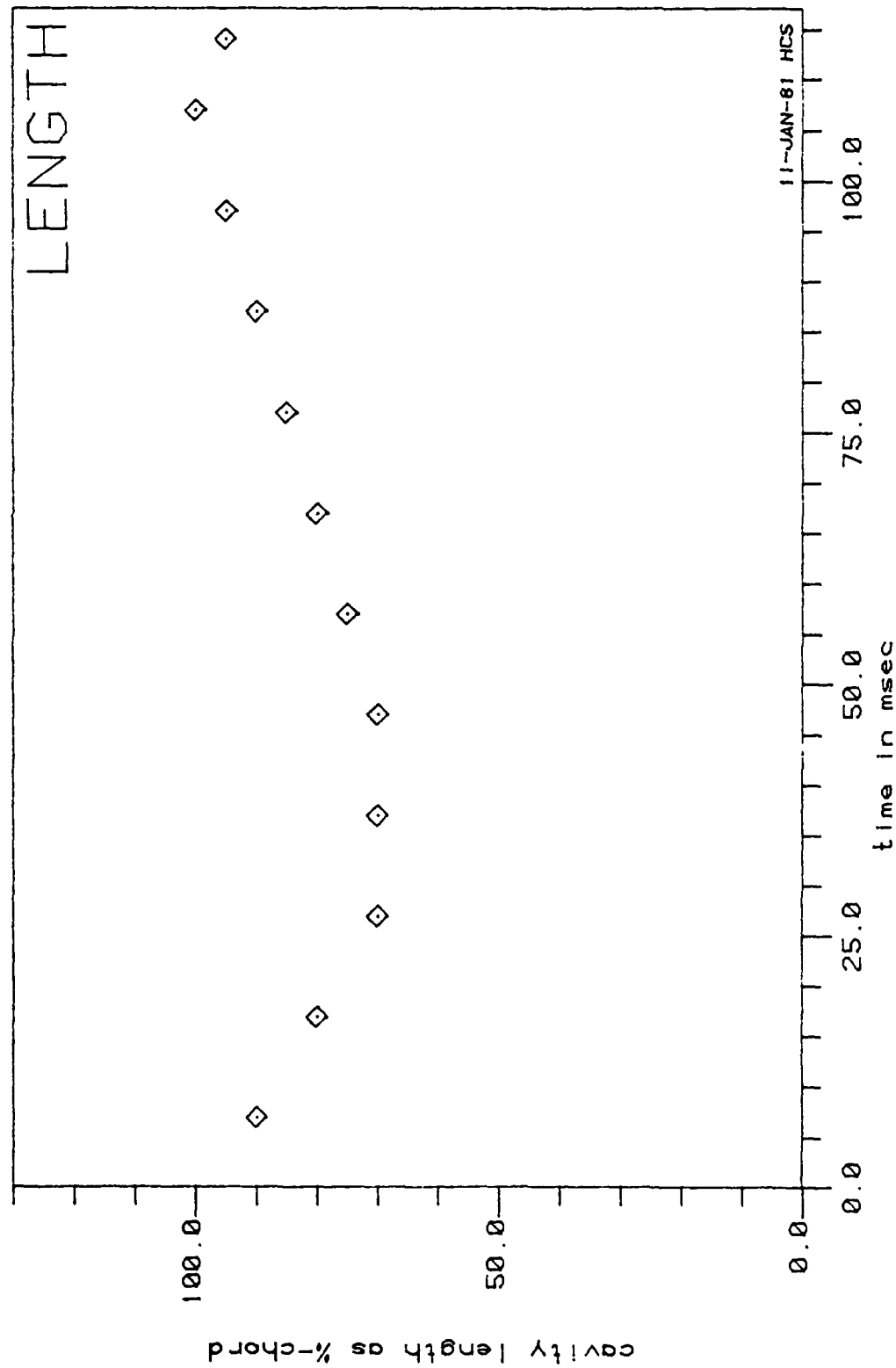

Figure 13: Cavity Length vs. Time, $\overline{C_{oa}} = .25$

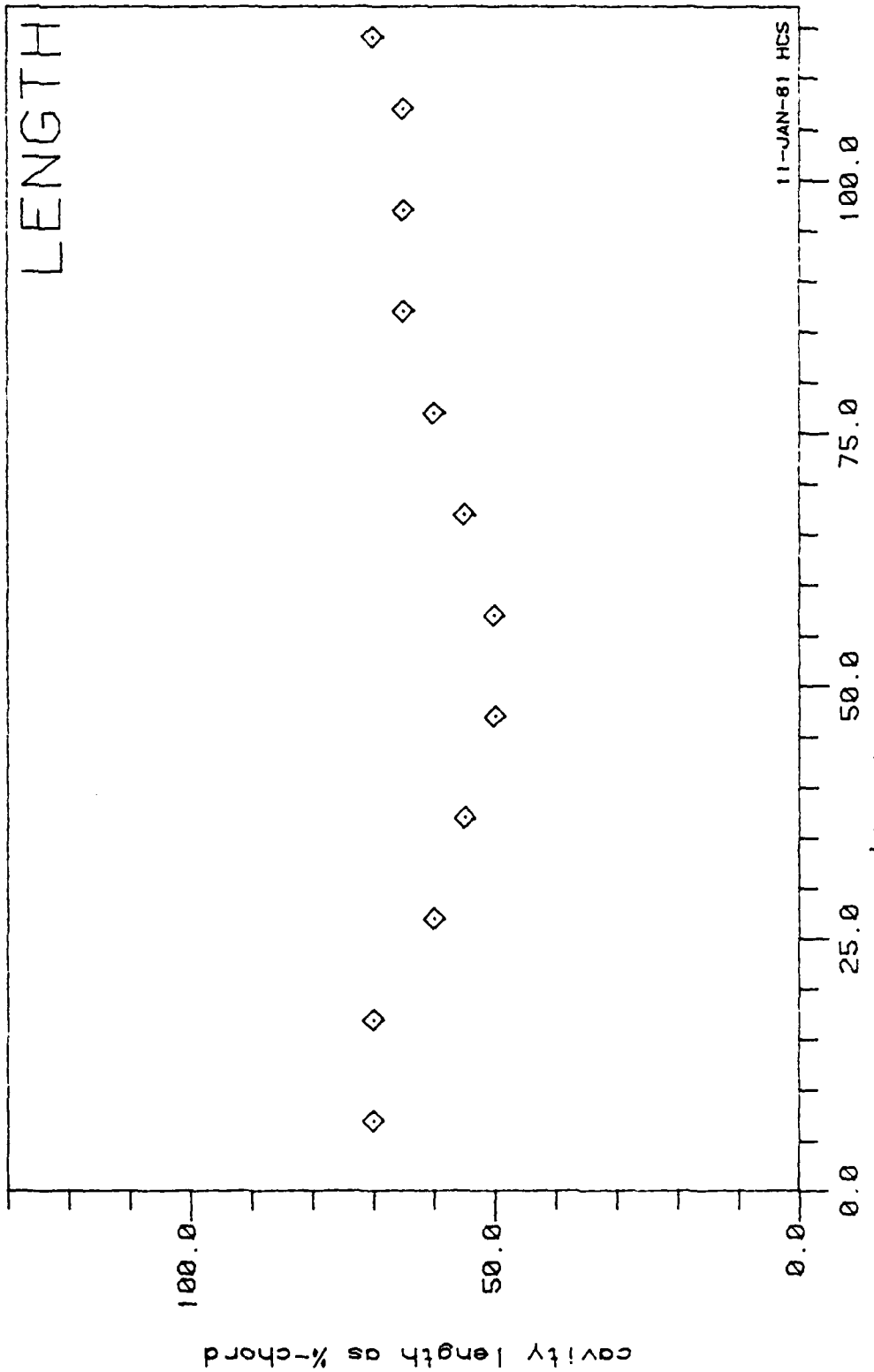

Figure 14: Cavity Length vs. Time, $\overline{C_{na}}$ = .40

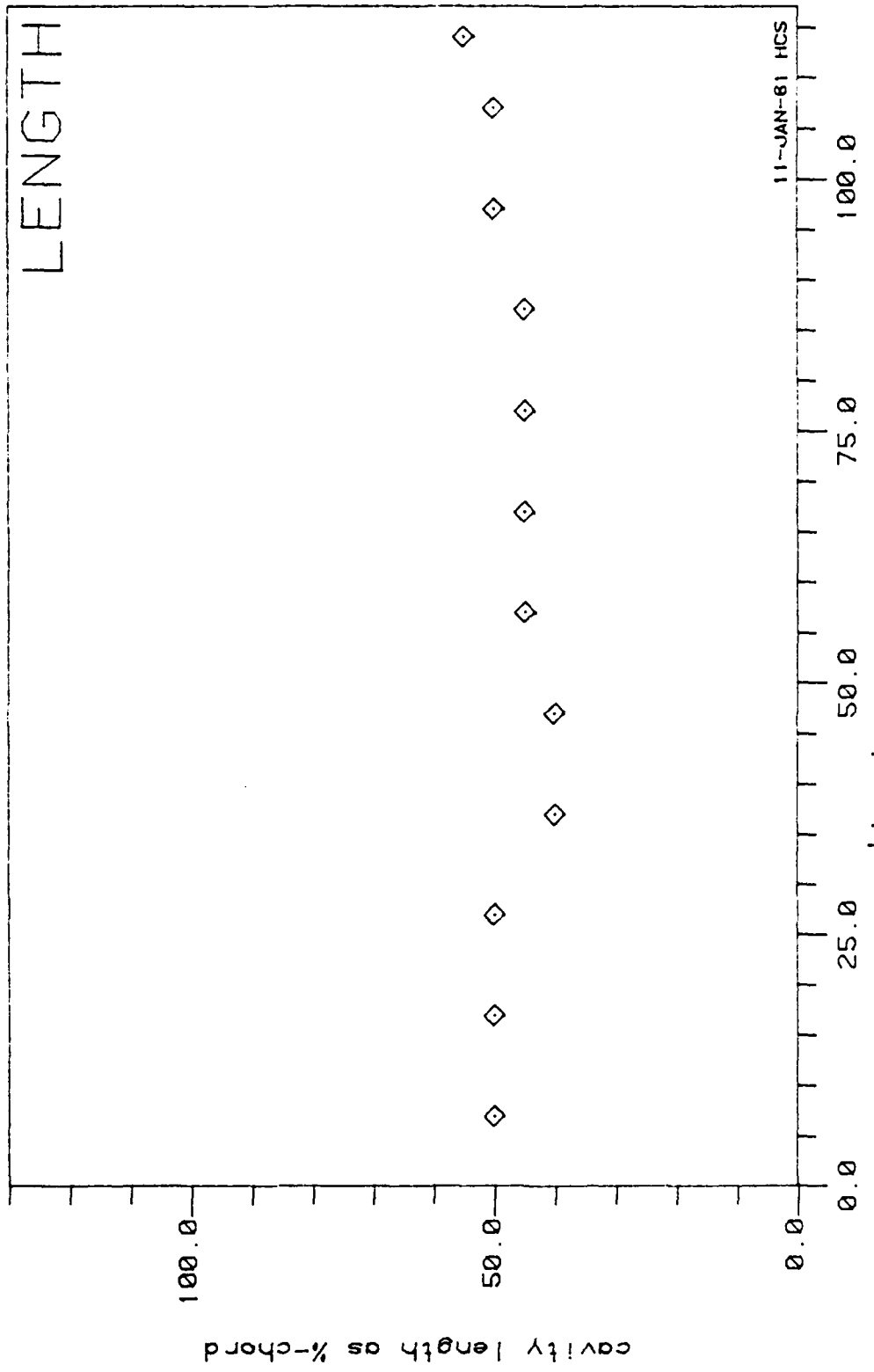

Figure 15: Cavity Length vs. Time, $\overline{C_{la}}$ = .53

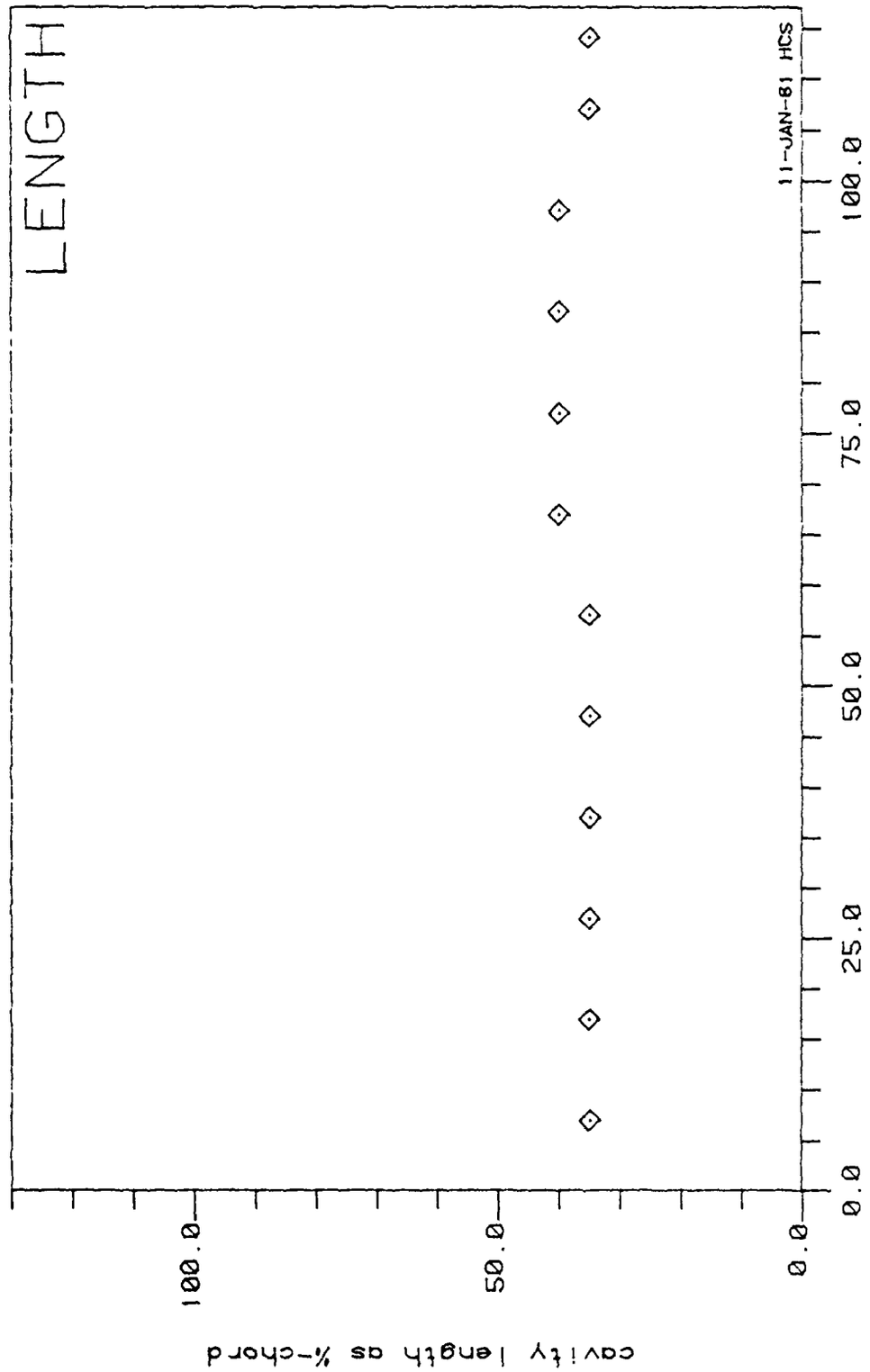

Figure 16: Cavity Length vs. Time, $\overline{C_{na}} = .72$

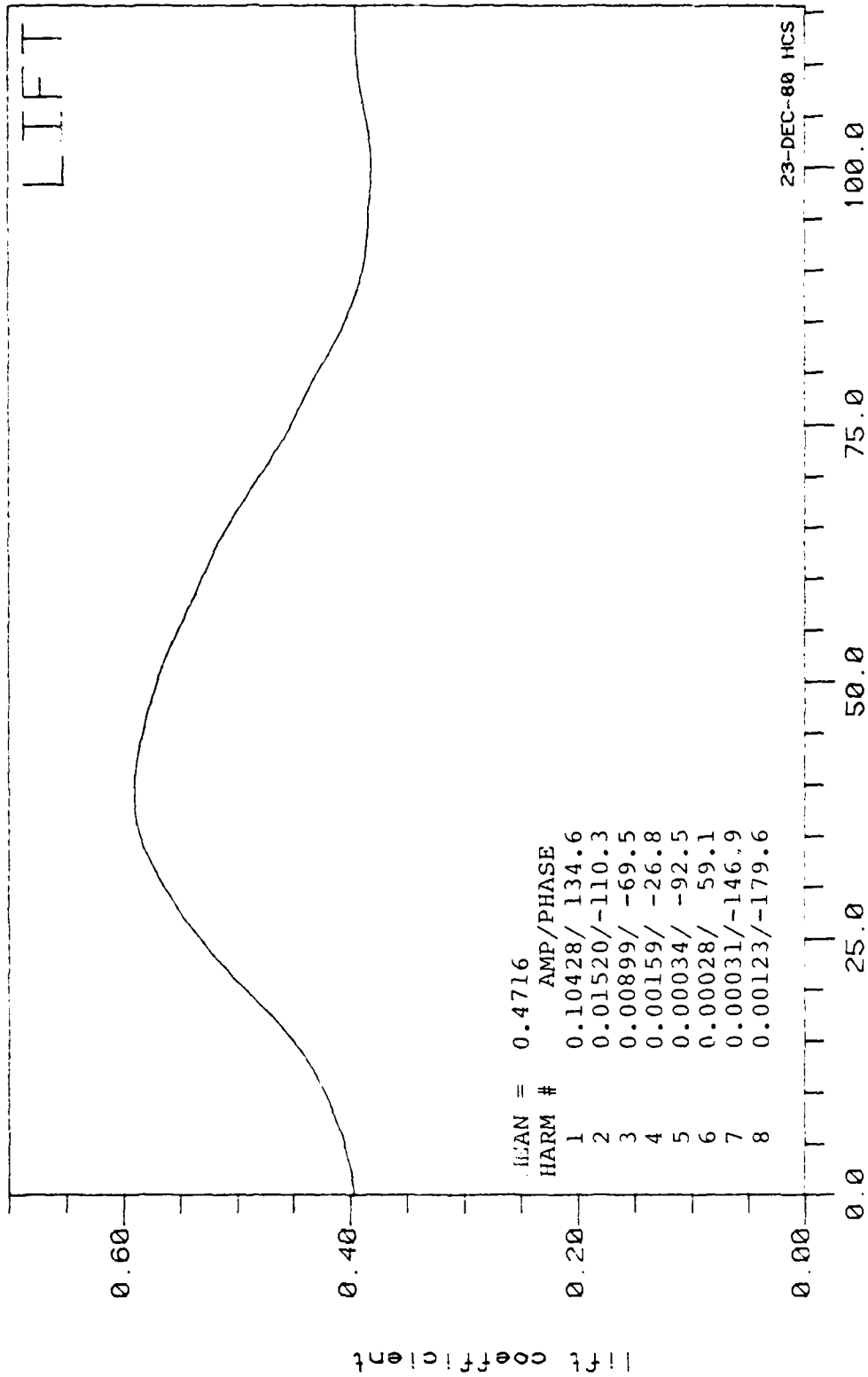

Figure 17: Lift Coefficient vs. Time, $\overline{C_{na}} = 0$

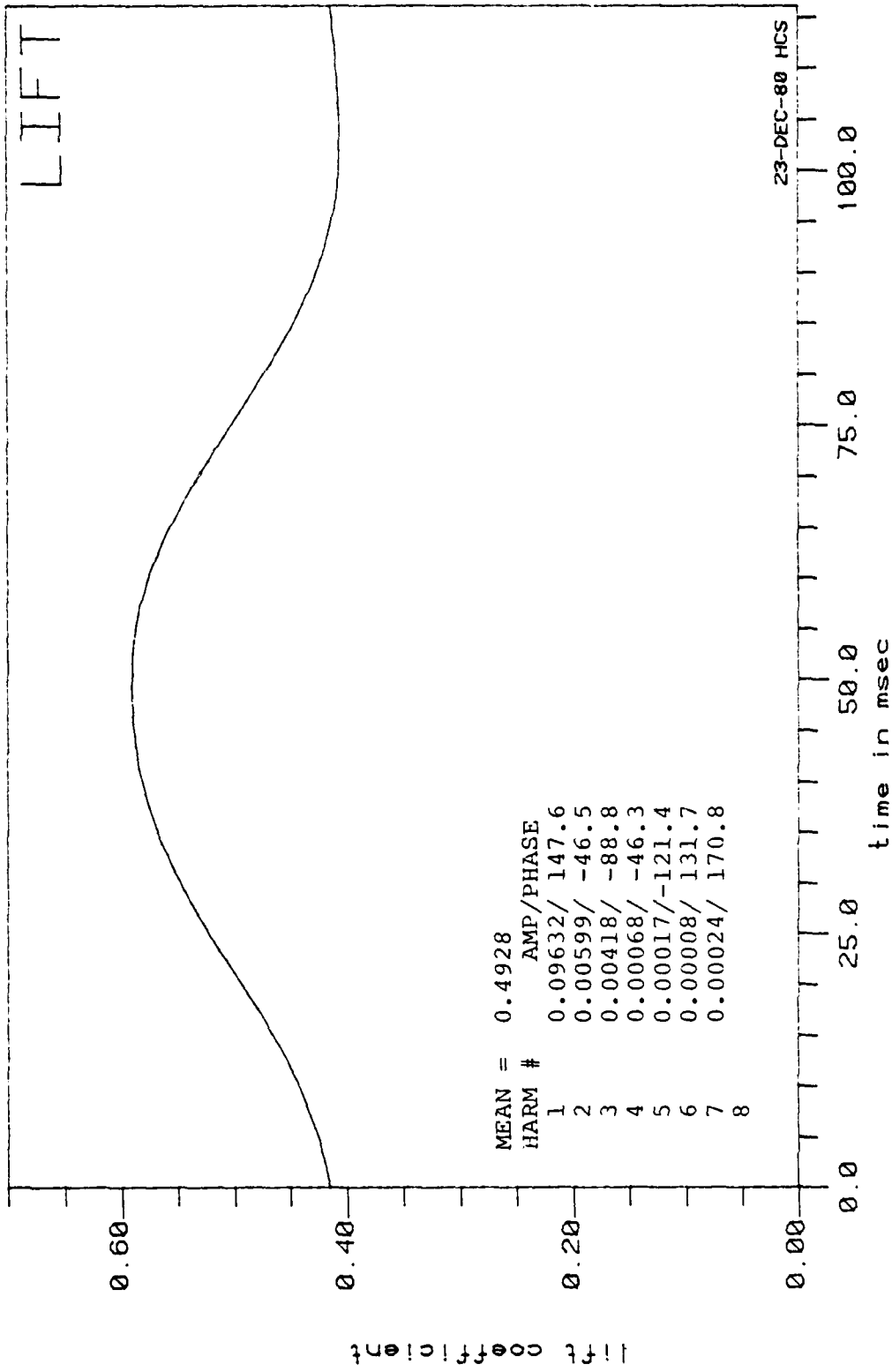

Figure 18: Lift Coefficient vs. Time, $\overline{C_{pa}}$ = .03

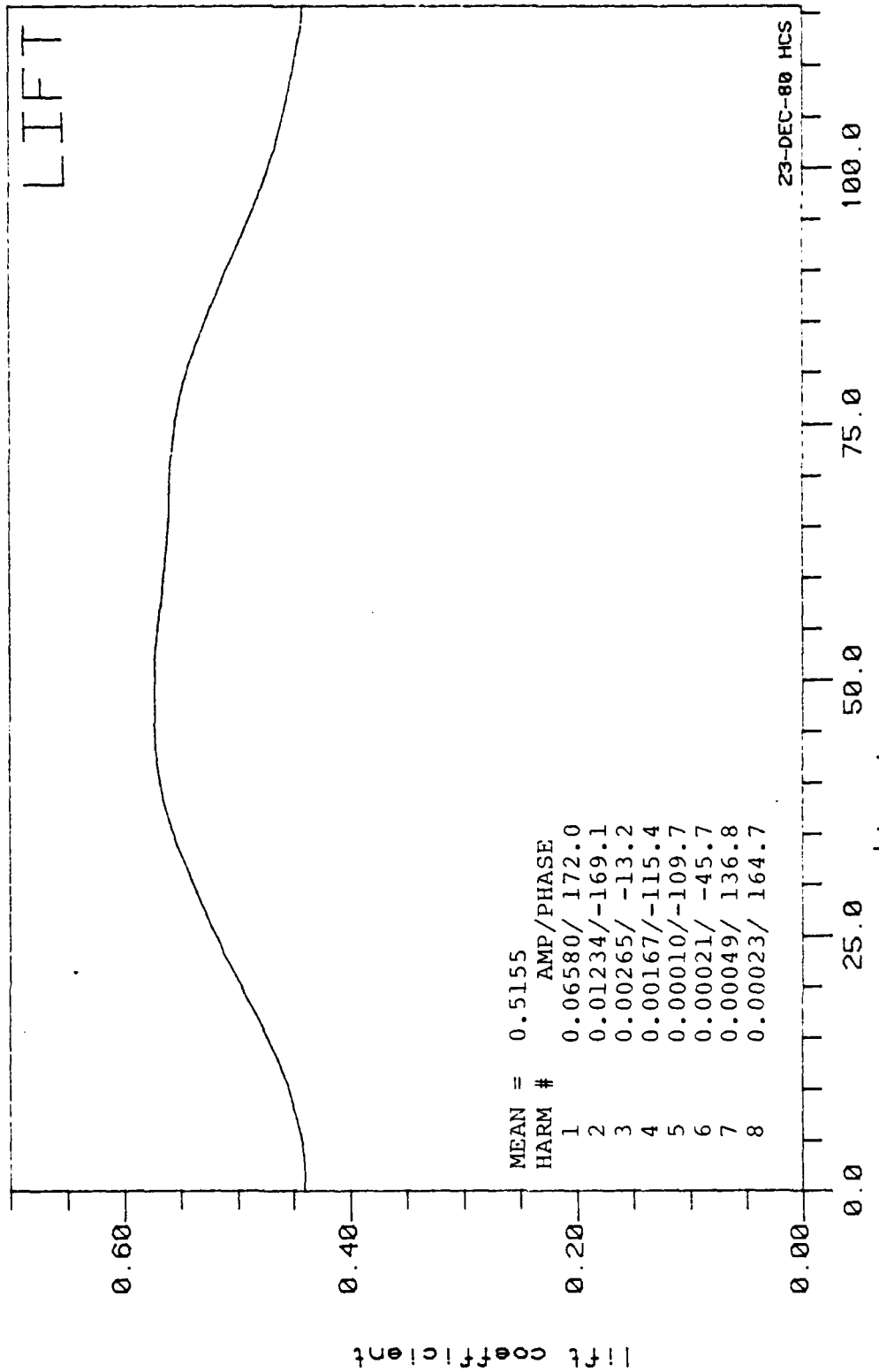

Figure 19: Lift Coefficient vs. Time, $\overline{C_{Da}} = .14$

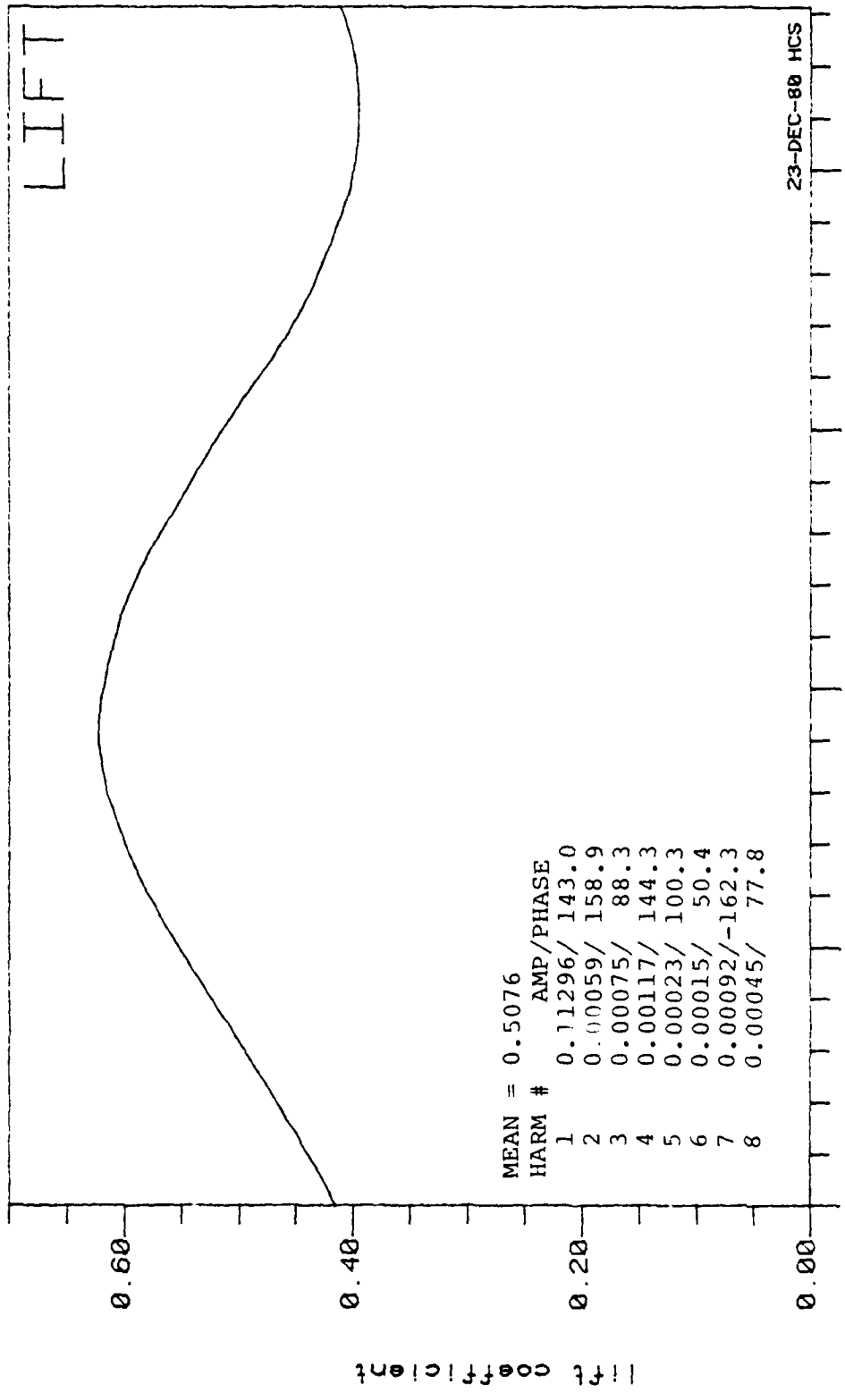

Figure 20: Lift Coefficient vs. Time, $\overline{C_{Da}}$ = .25

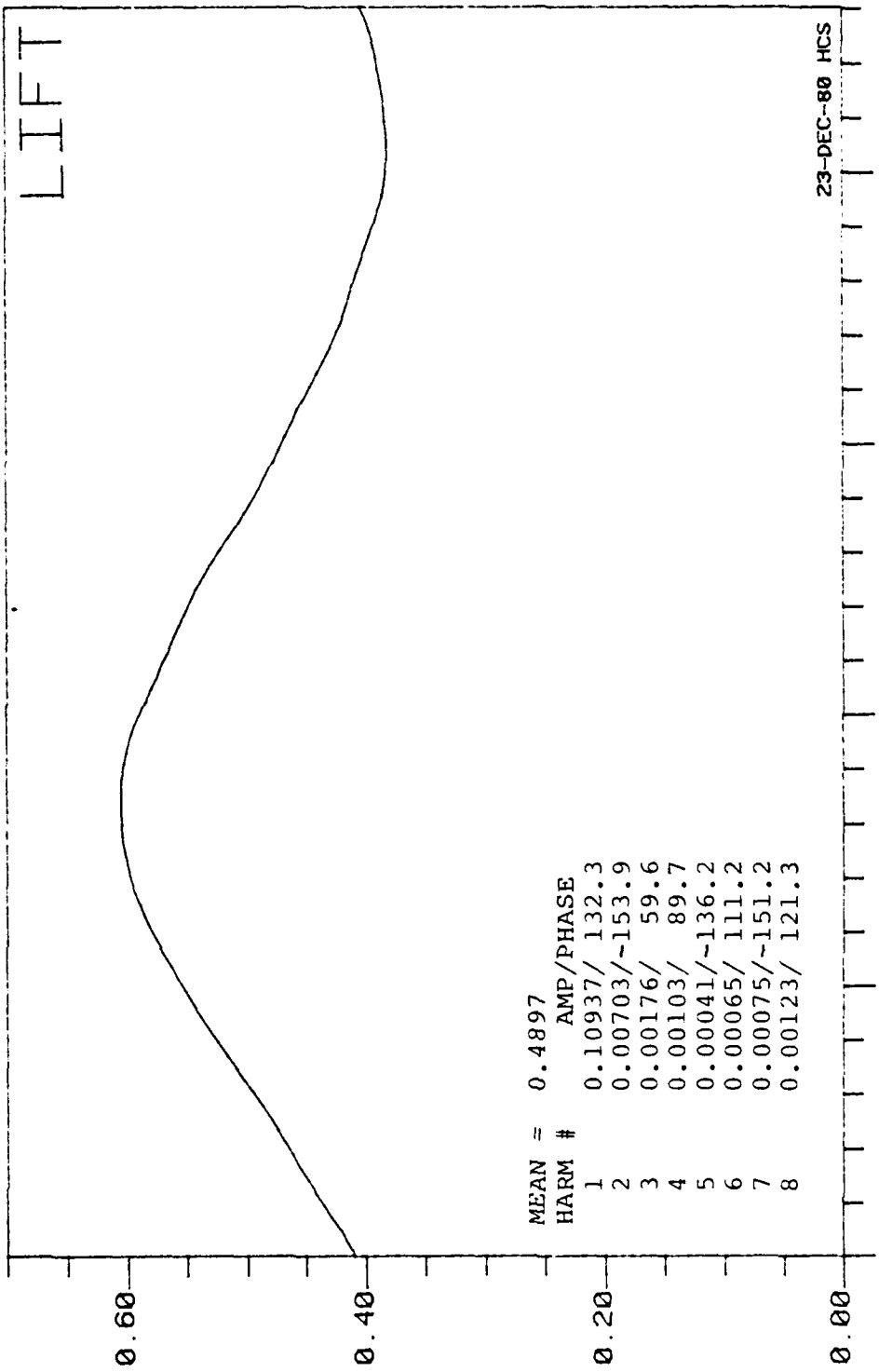

Figure 21: Lift Coefficient vs. Time, $\overline{C_{\eta a}} = .40$

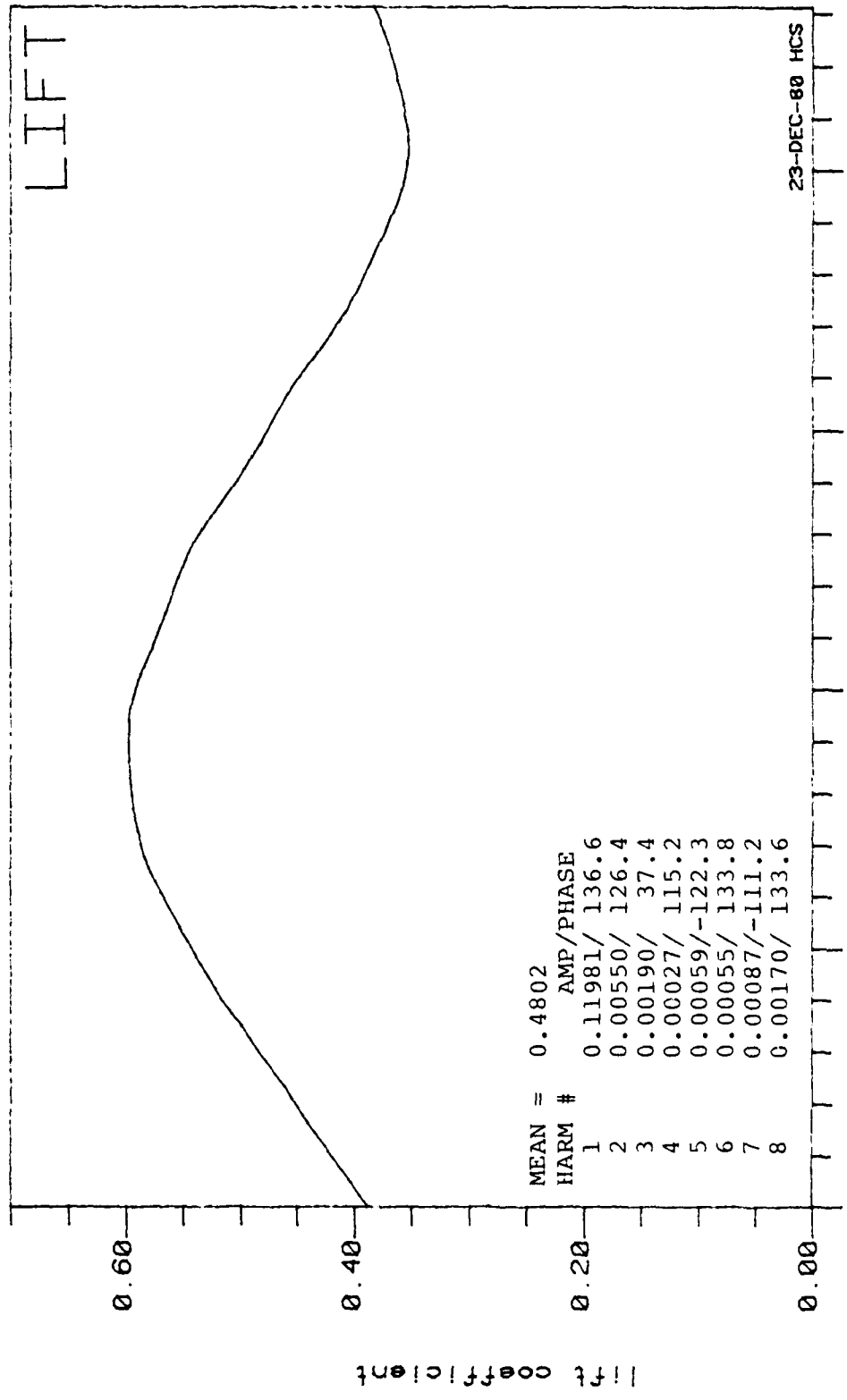

Figure 22: Lift Coefficient vs. Time, $\overline{C_{pa}} = .53$

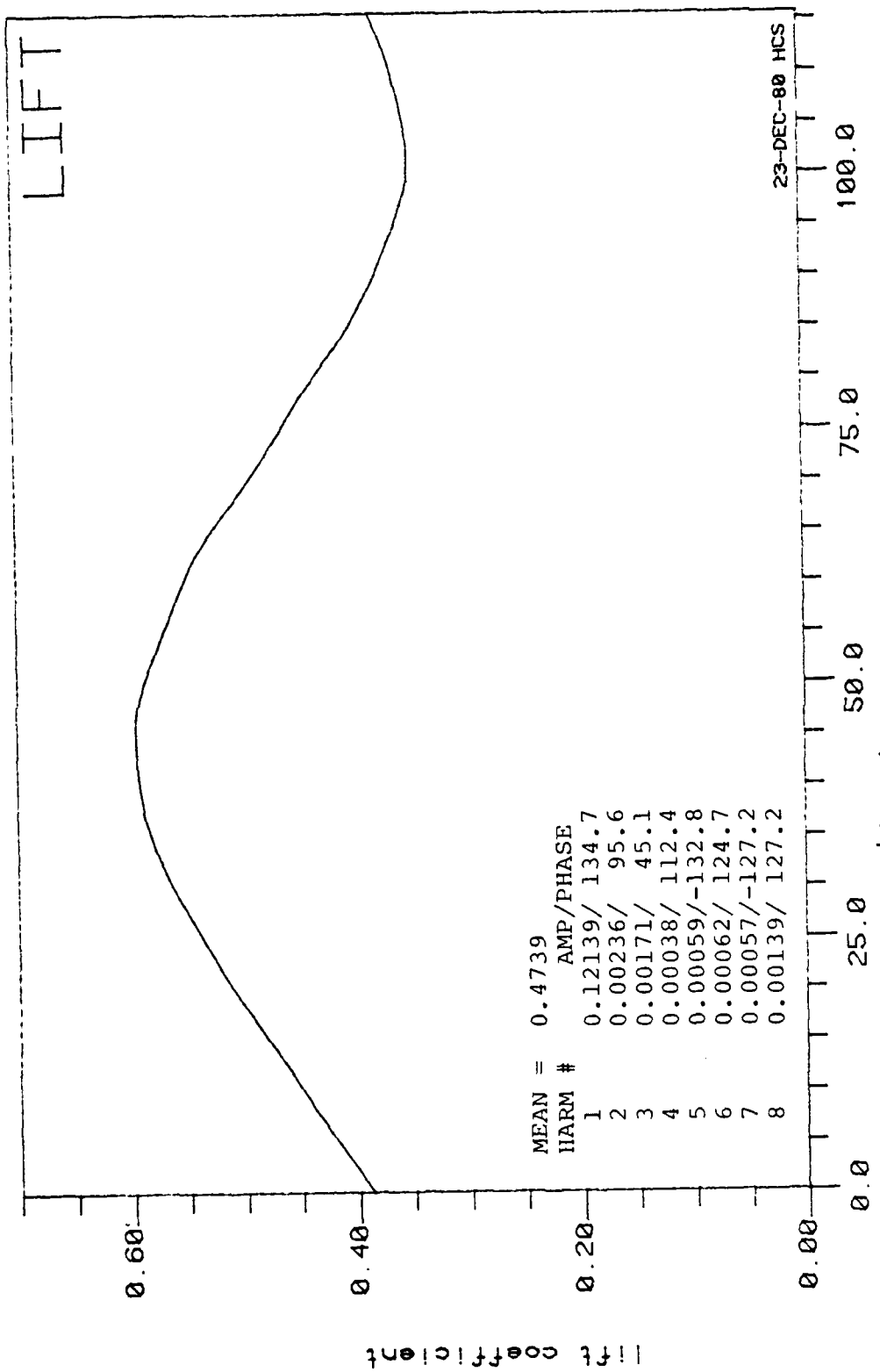

Figure 23: Lift Coefficient vs. Time, $\overline{C_{na}}$ = .72

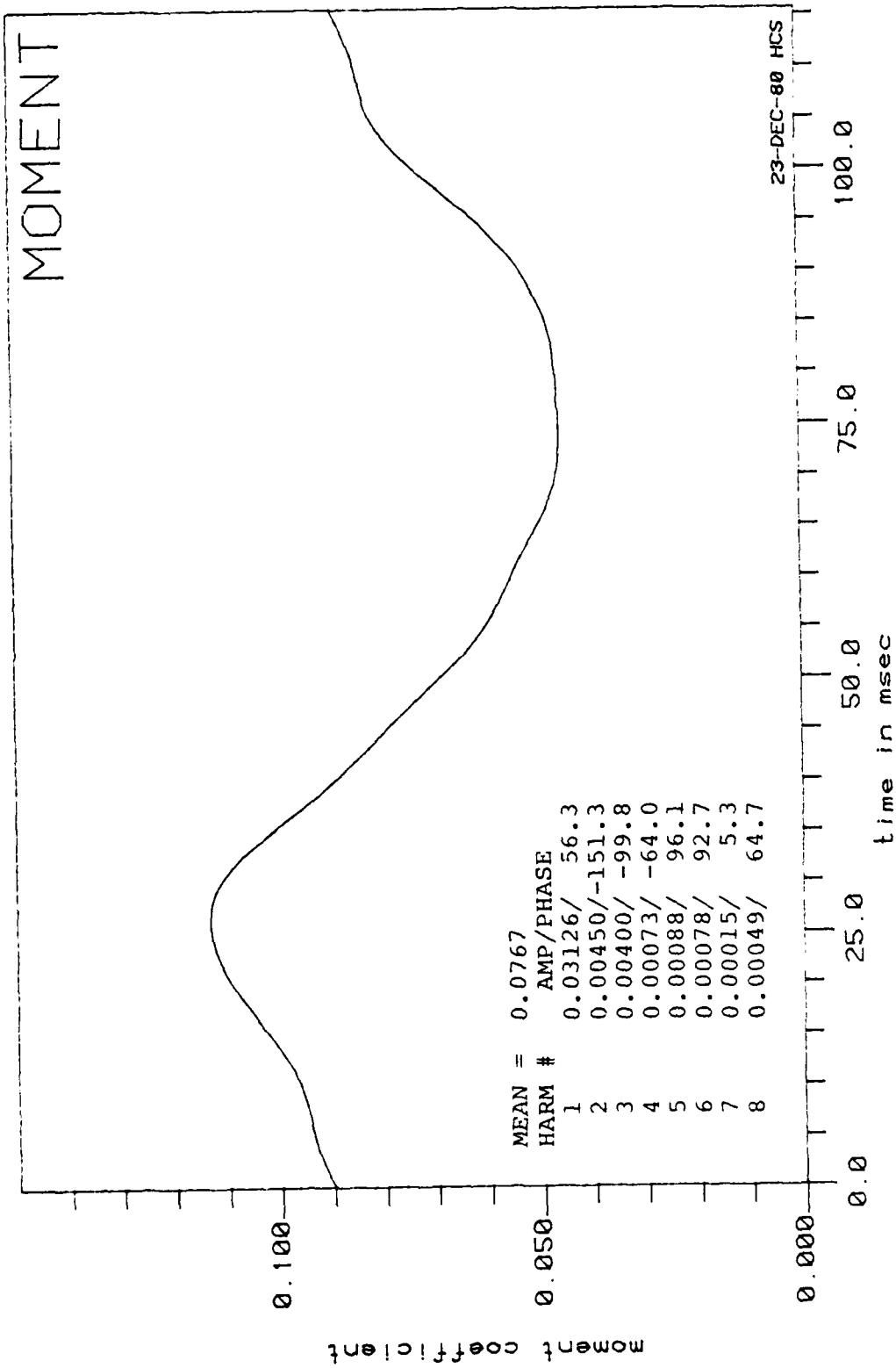

Figure 24: Moment Coefficient vs. Time, $\overline{C_{pa}} = 0$

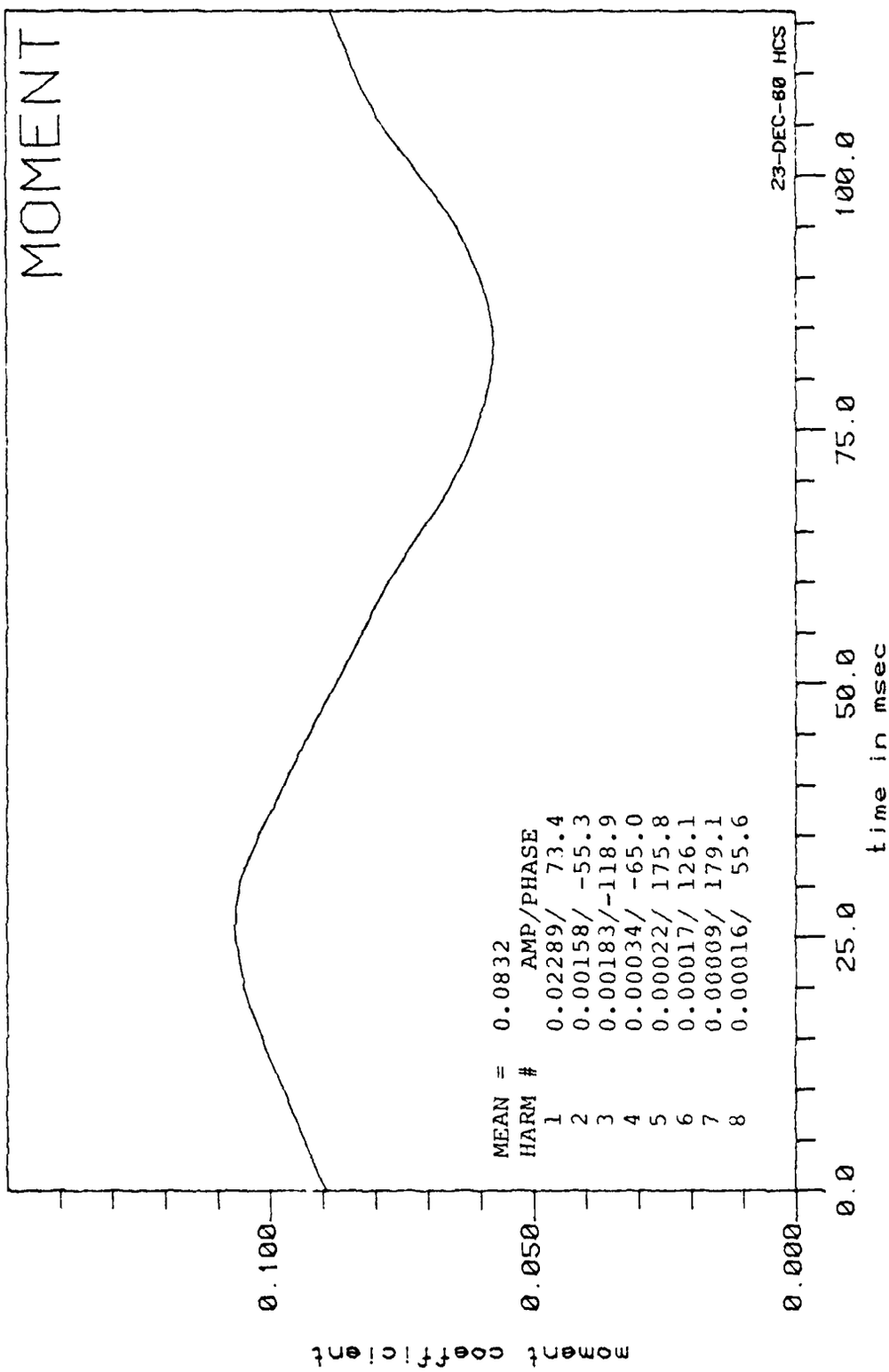

Figure 25: Moment Coefficient vs. Time, $\overline{C_{Da}}$ = .03

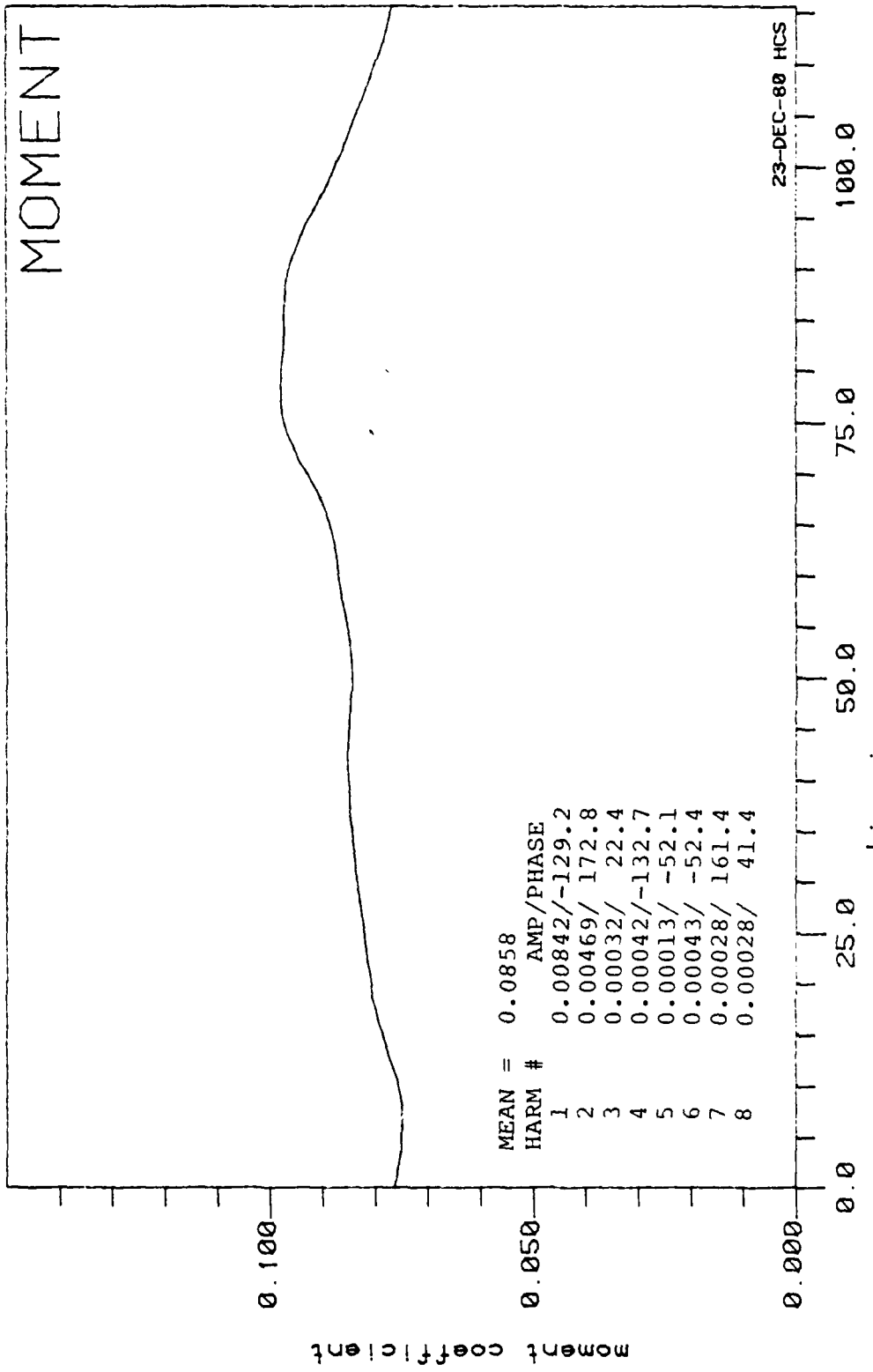

Figure 26: Moment Coefficient vs. Time, $\overline{C_{Da}} = .14$

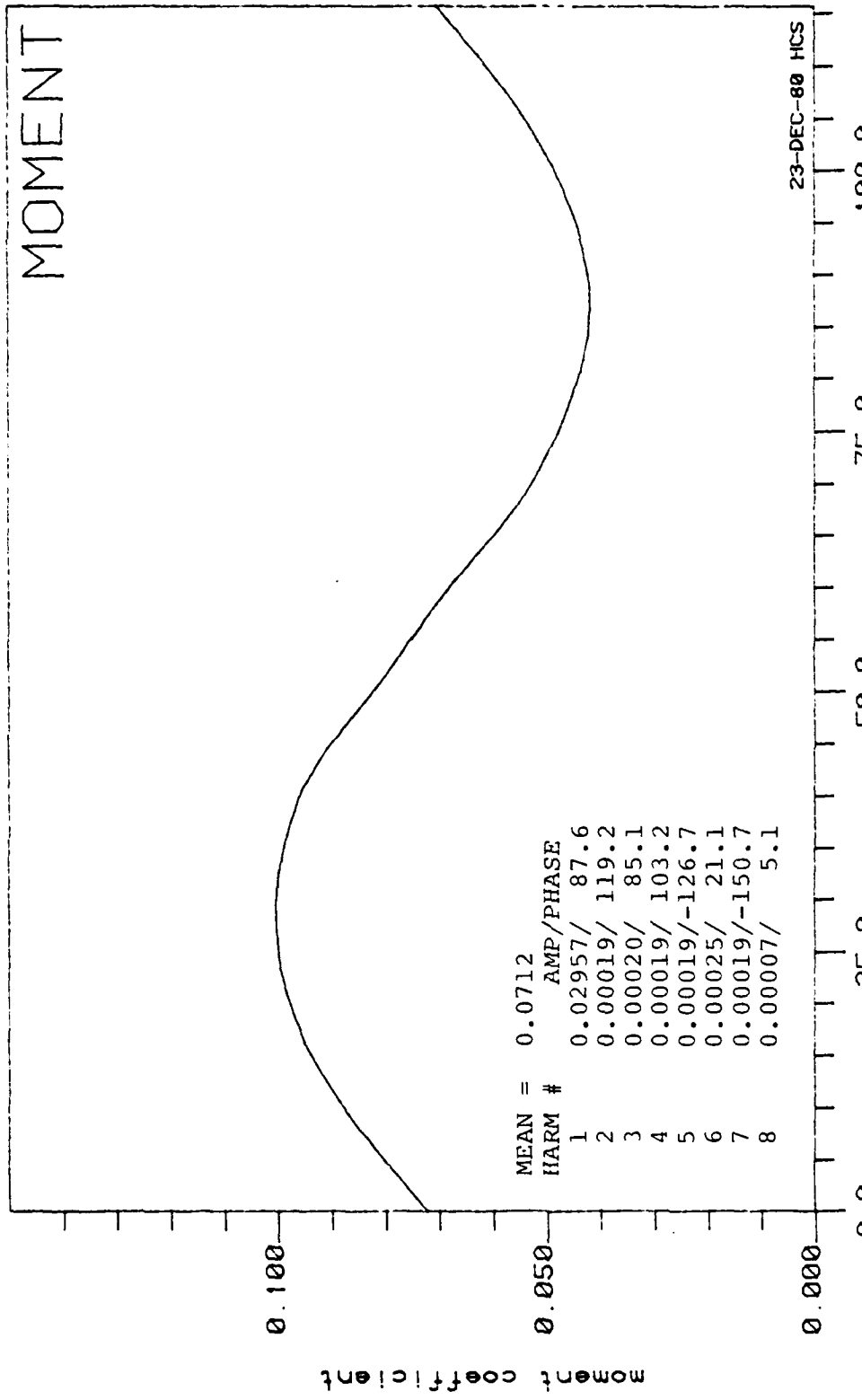

Figure 27: Moment Coefficient vs. Time, $\overline{C_{pa}} = .25$

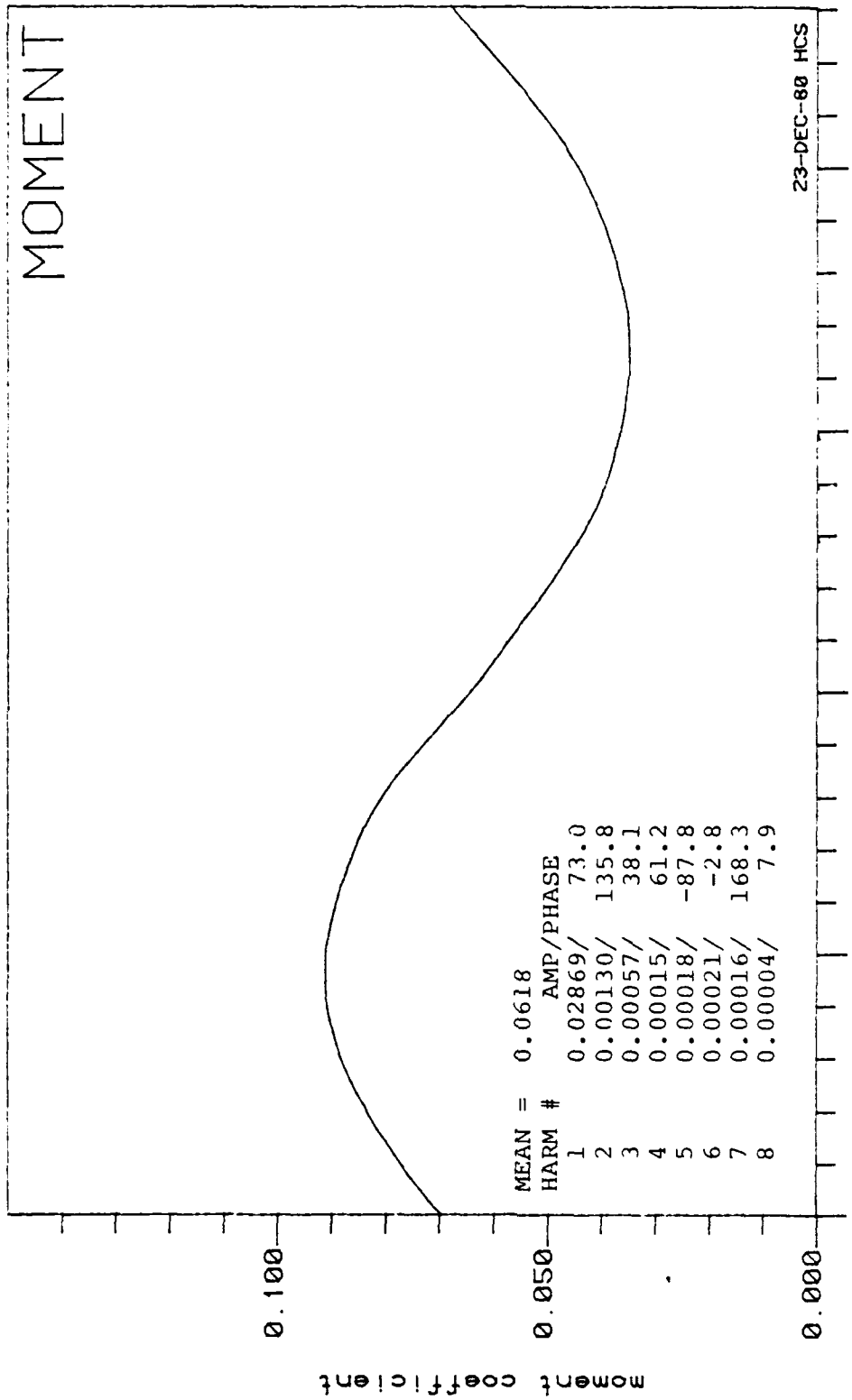

Figure 28: Moment Coefficient vs. Time, $\overline{C_{na}} = .40$

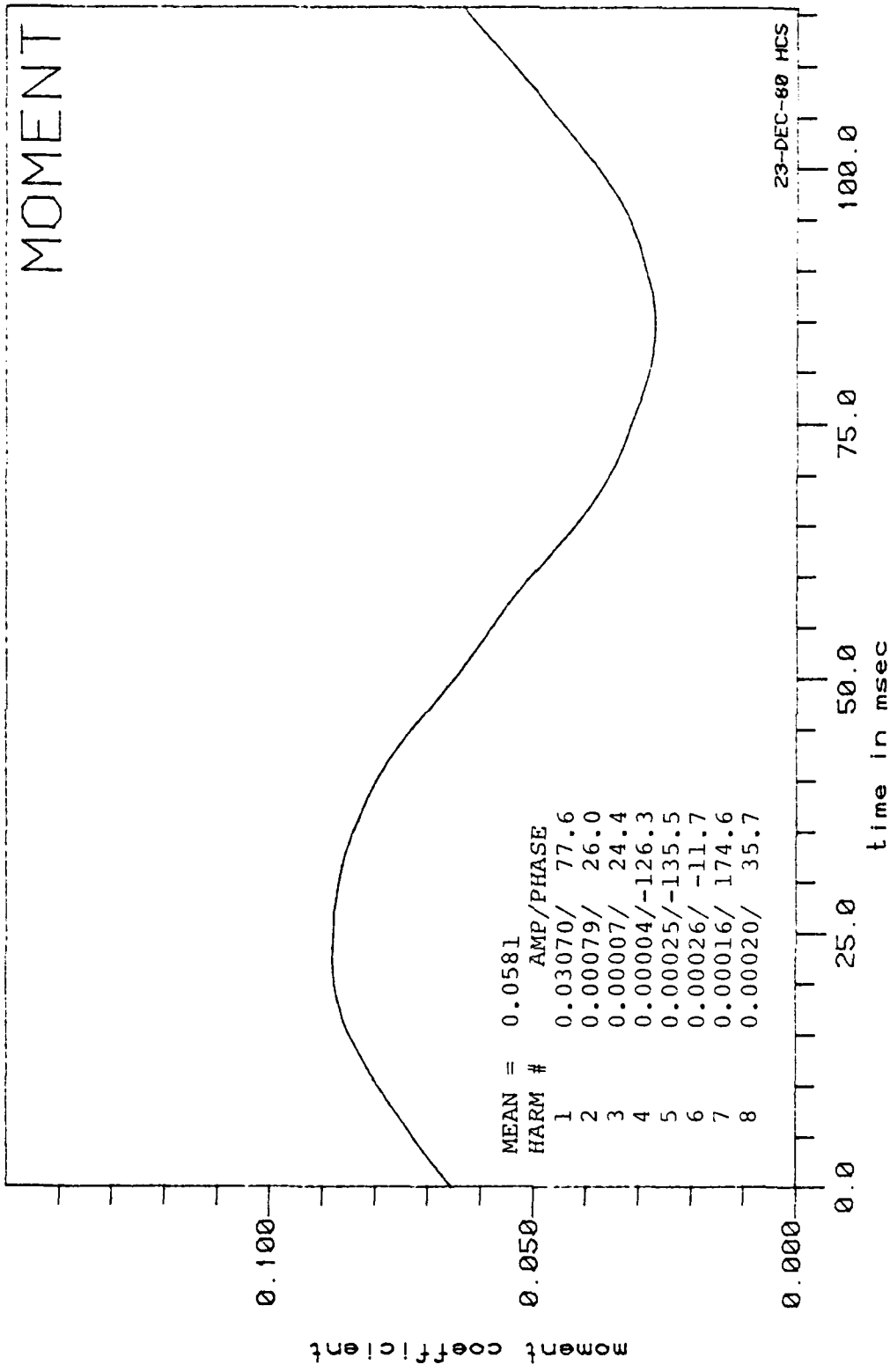

Figure 29: Moment Coefficient vs. Time, $\overline{C_{na}}$ = .53

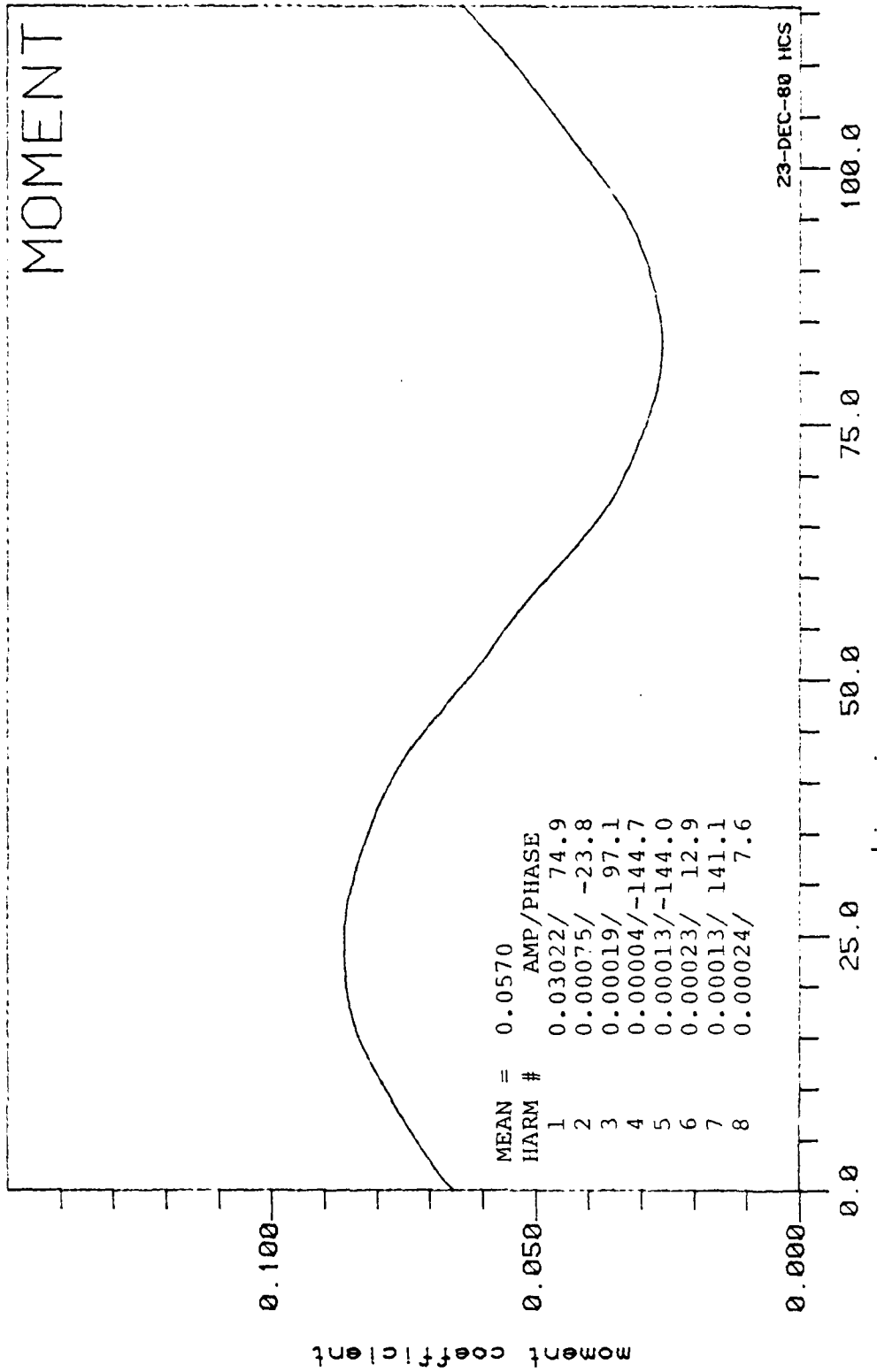

Figure 30: Moment Coefficient vs. Time, $\overline{C_{na}} = .72$

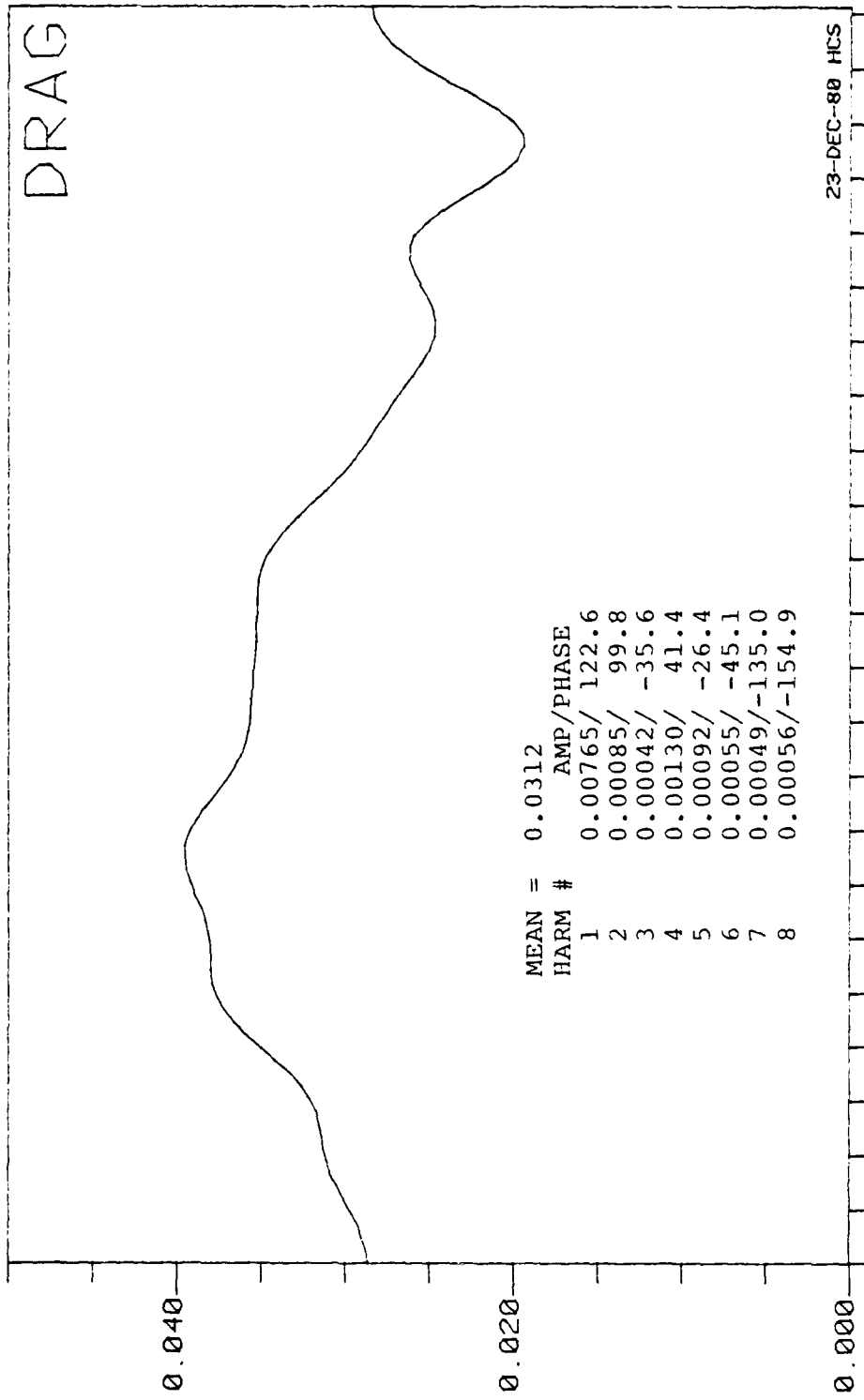

Figure 31: Drag Coefficient vs. Time, $\overline{C_{na}} = 0$

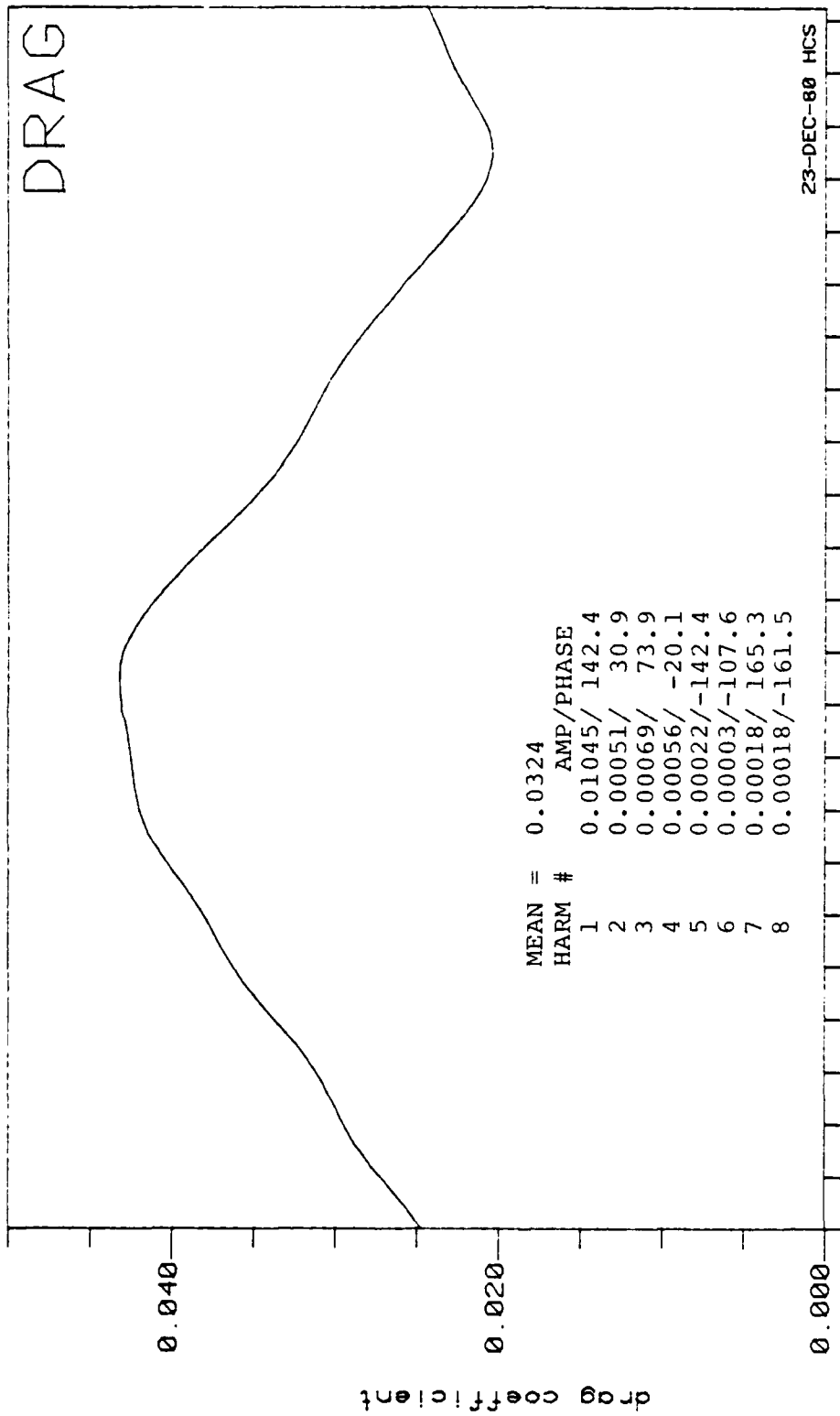

Figure 32: Drag Coefficient vs. Time, $\overline{C_{pa}} = .03$

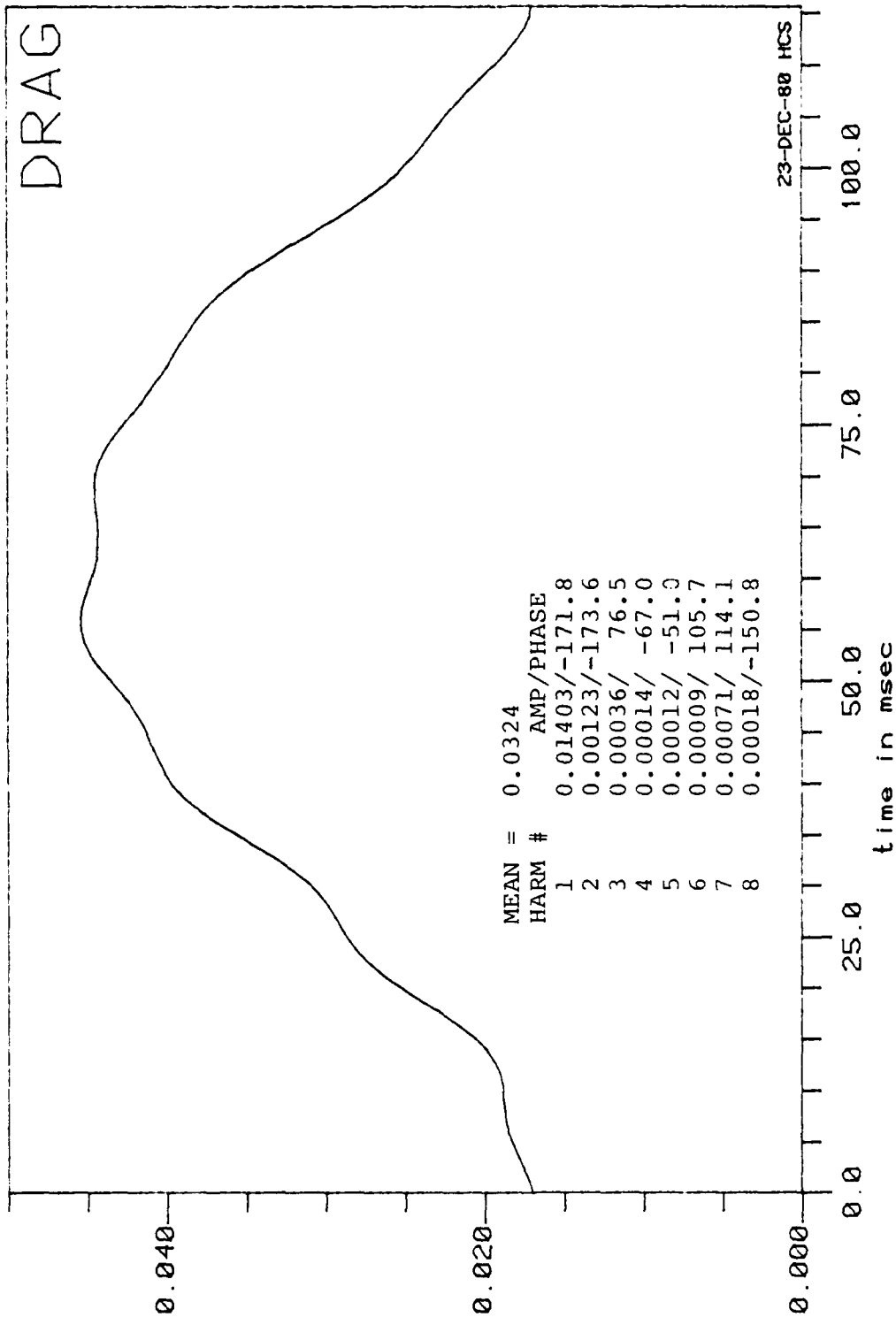

Figure 33: Drag Coefficient vs. Time, $\overline{C_{pa}}$ = .14

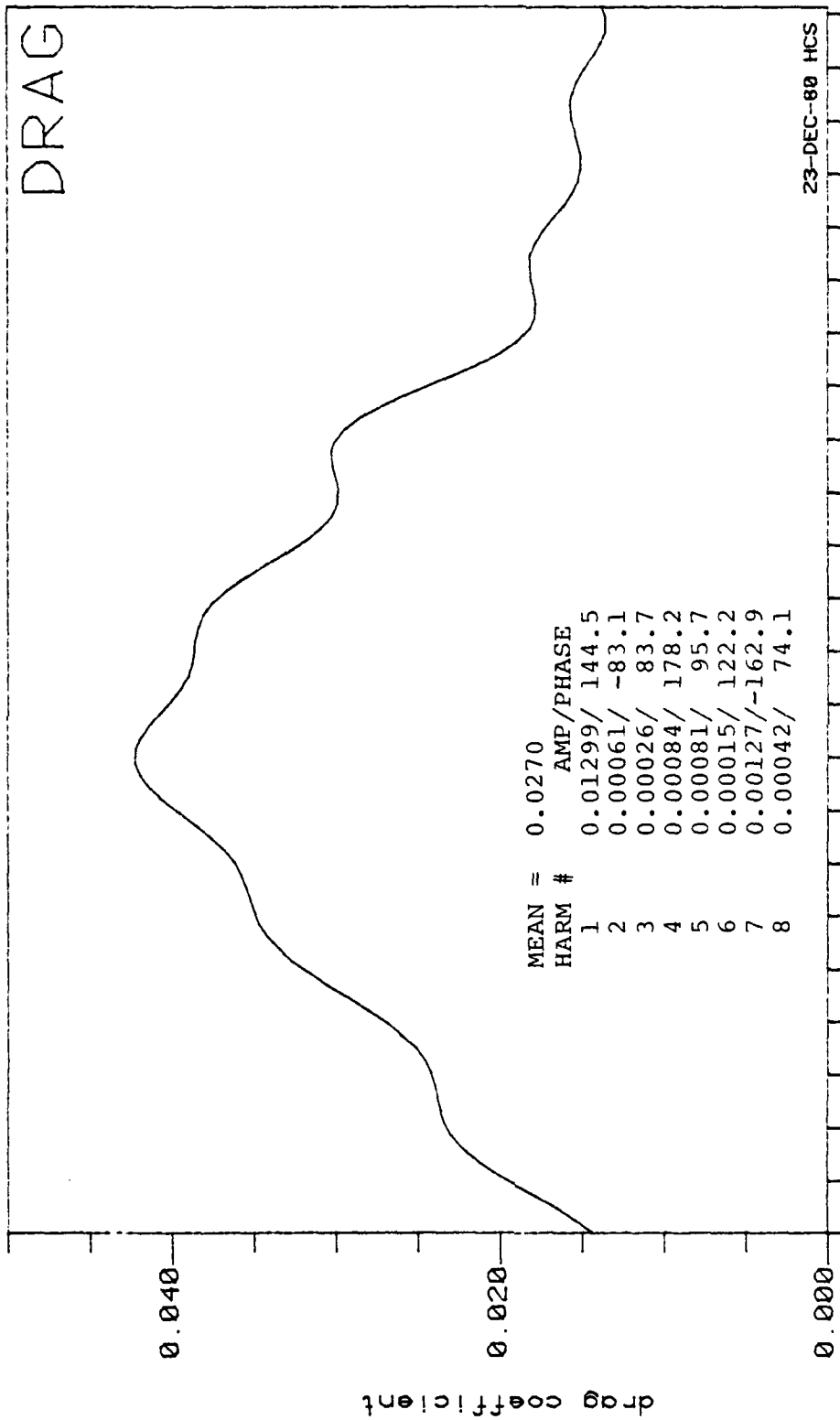

Figure 34: Drag Coefficient vs. Time, $\overline{C_{pa}} = .25$

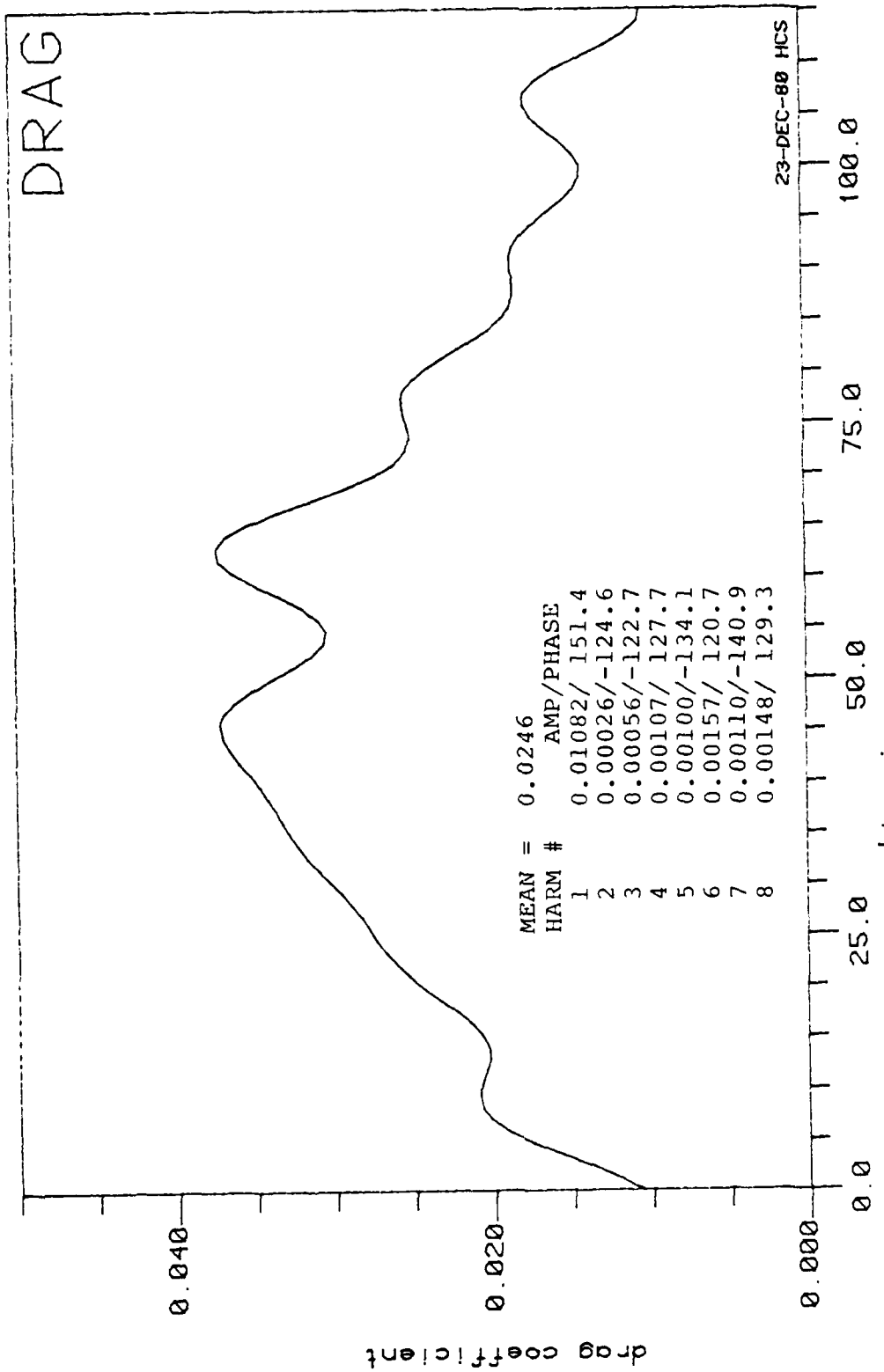

Figure 35: Drag Coefficient vs. Time, $\overline{C_{pa}} = .40$

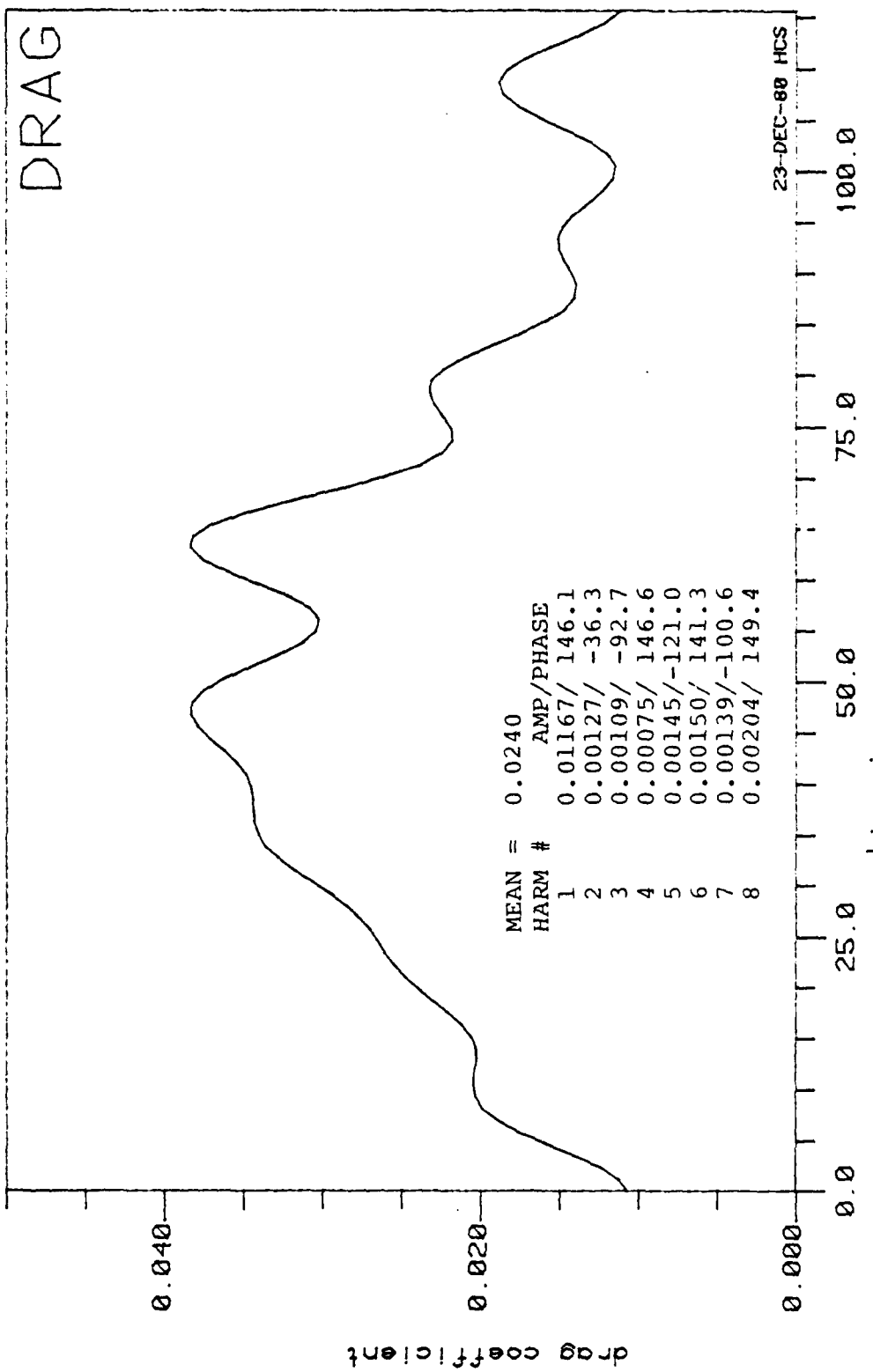

Figure 36: Drag Coefficient vs. Time, $\overline{C_{pa}}$ = .53

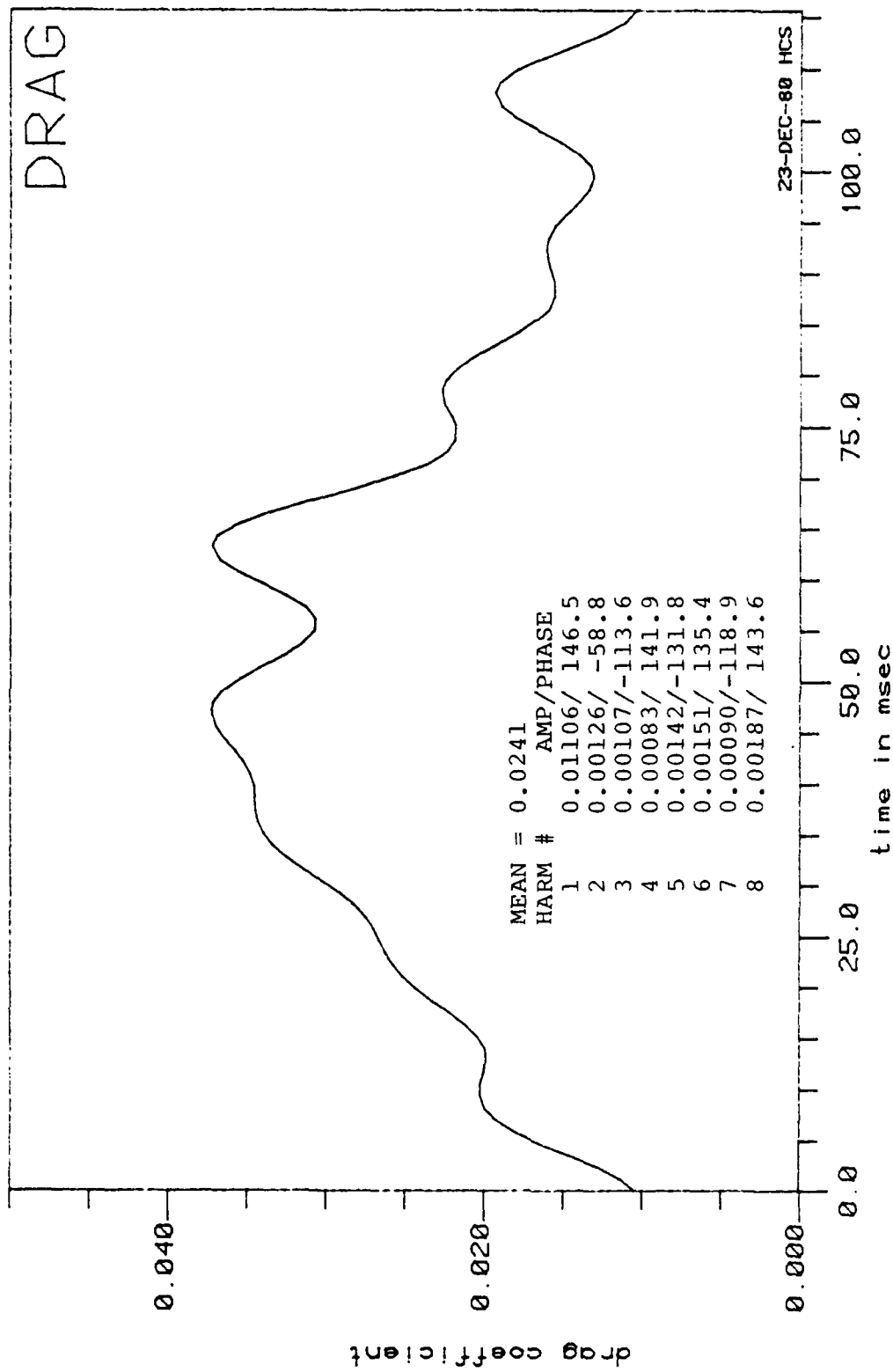

Figure 37: Drag Coefficient vs. Time, $\overline{C_{pa}} = .72$

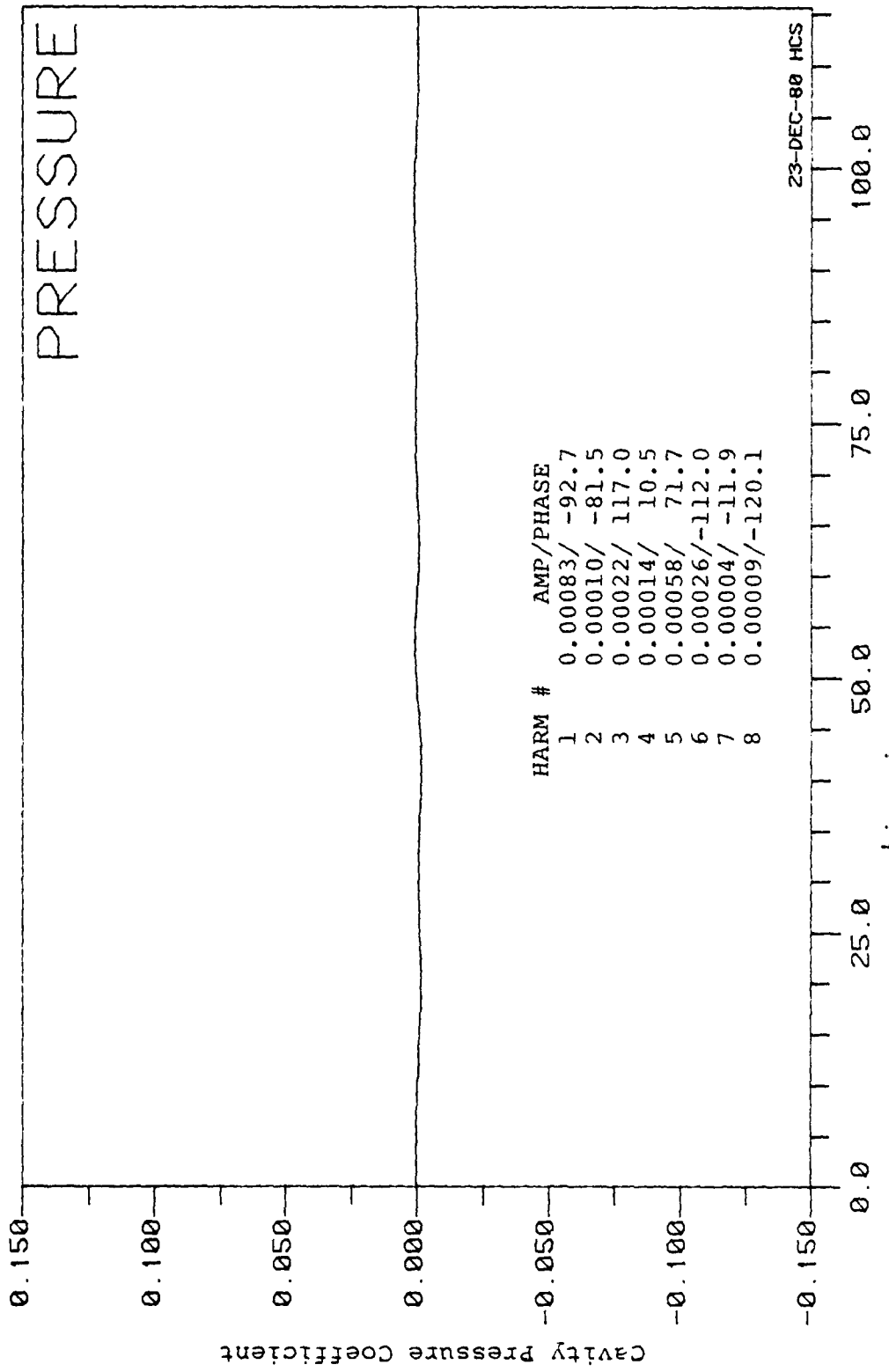

Figure 38: Cavity Pressure Coefficient vs. Time, $\overline{C_{pa}} = 0$

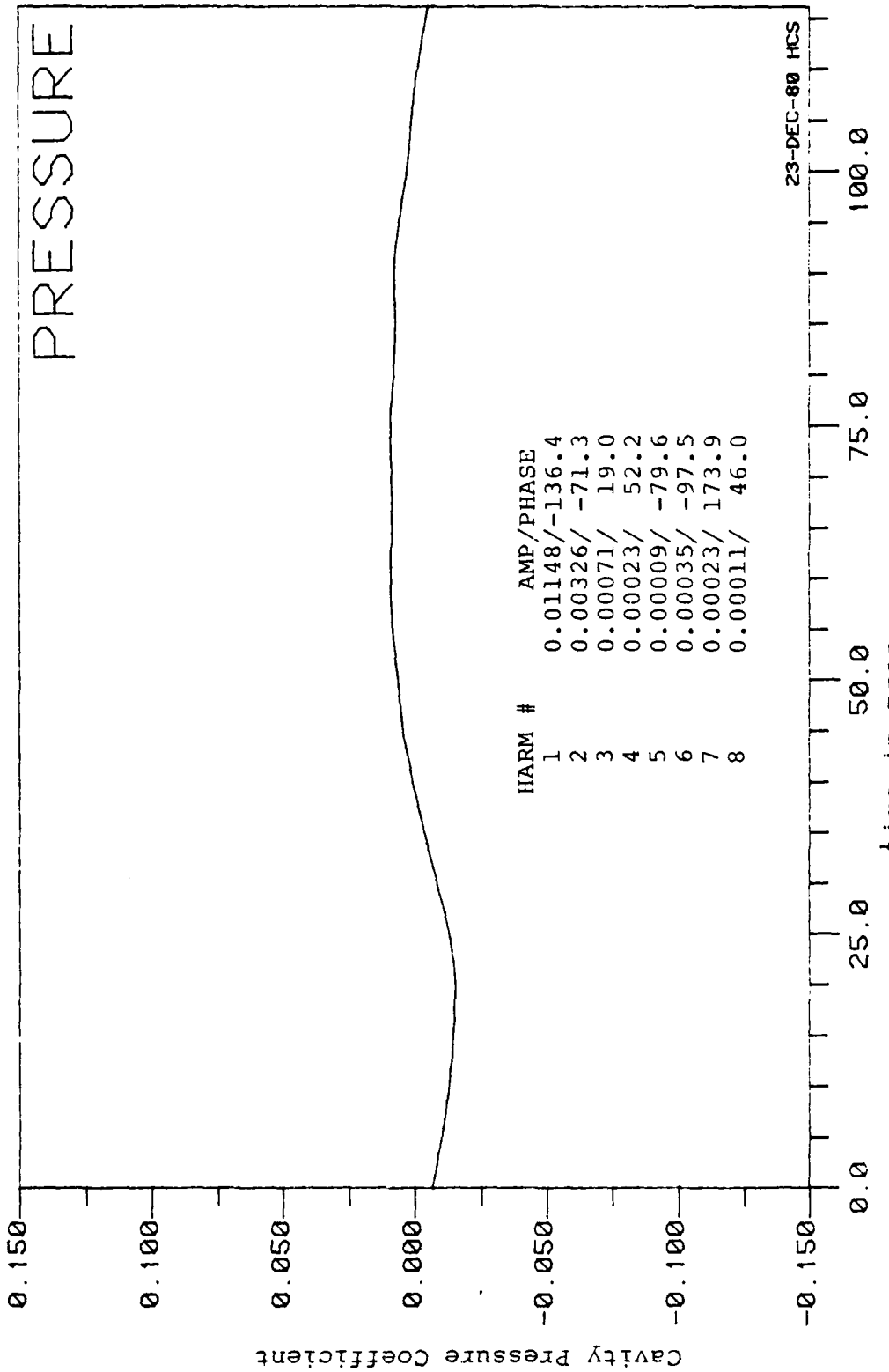

Figure 39: Cavity Pressure Coefficient vs. Time, $\overline{C_{pa}}$ = .03

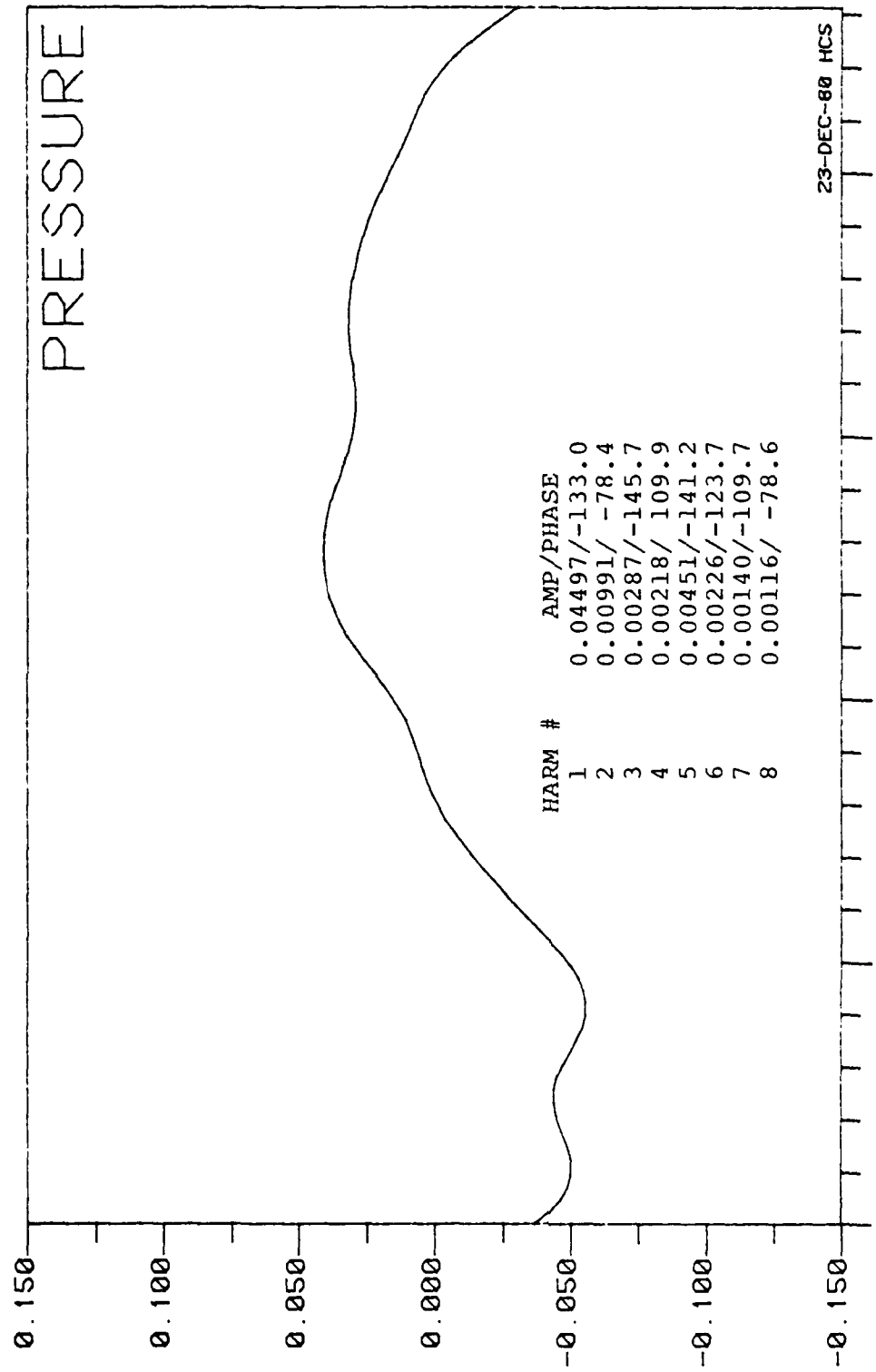

Figure 40: Cavity Pressure Coefficient vs. Time, $\overline{C_{pa}}$ = .14

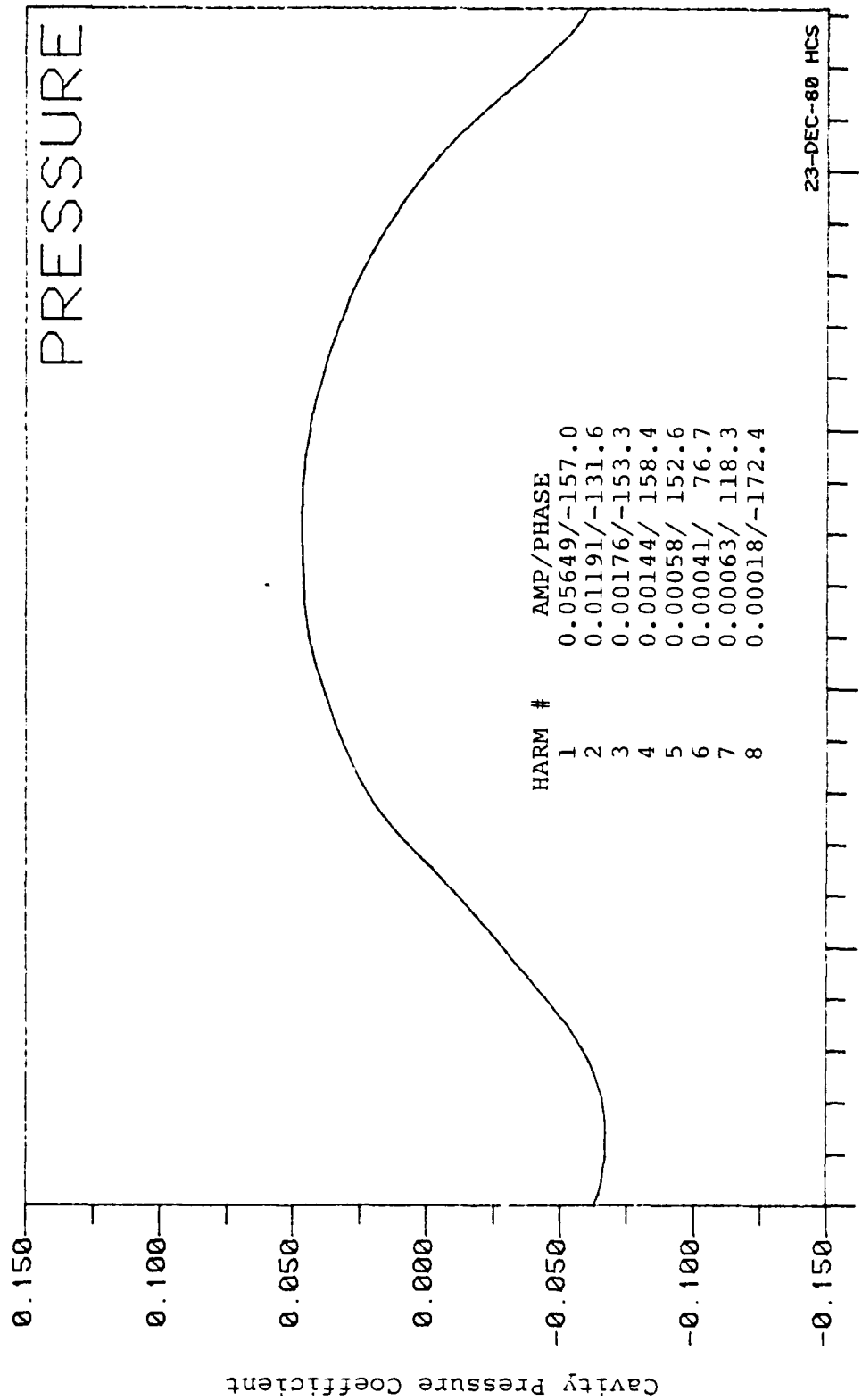

Figure 41: Cavity Pressure Coefficient vs. Time, $\overline{C_{pa}}$ = .25

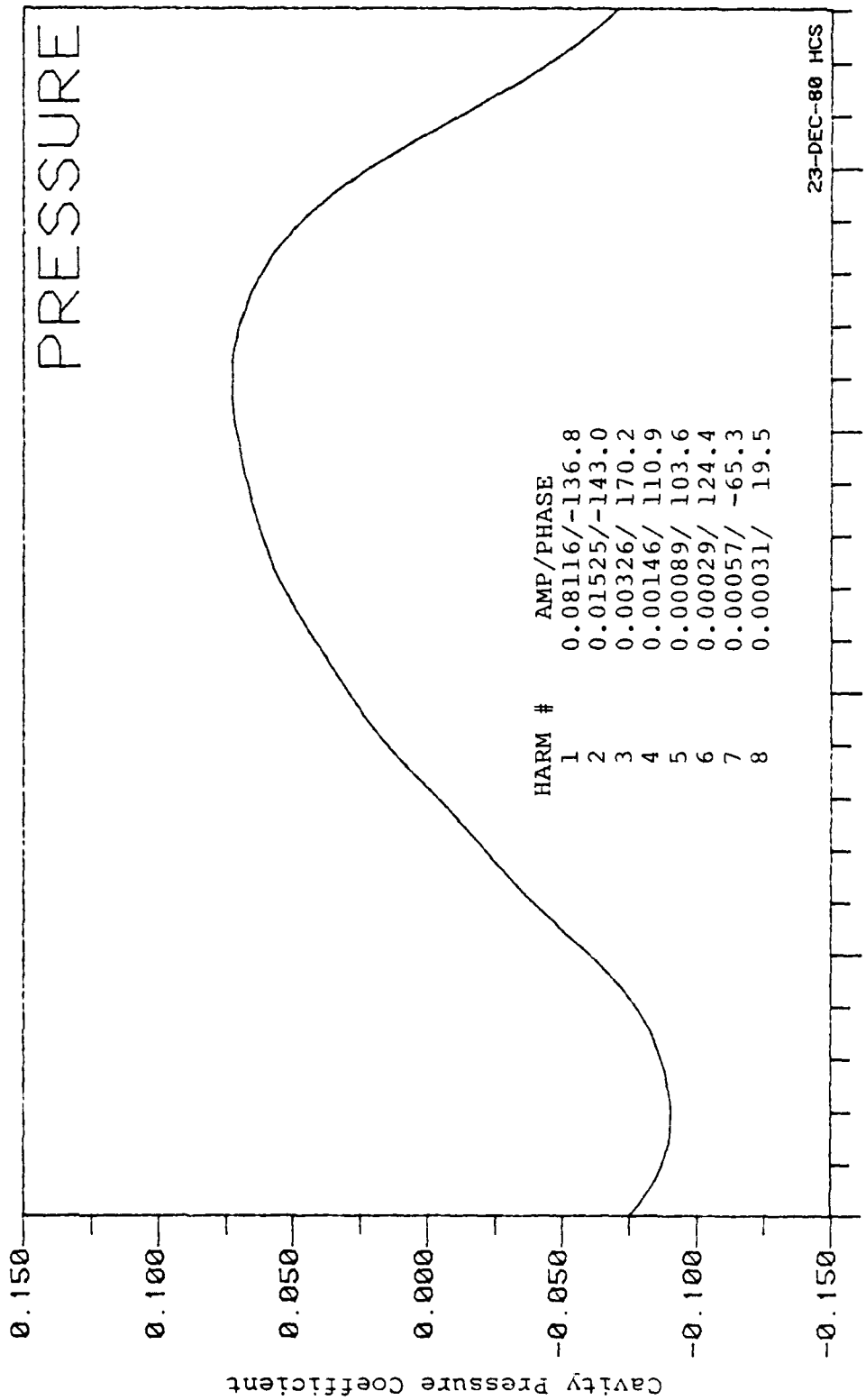

Figure 42: Cavity Pressure Coefficient vs. Time, $\overline{C_{pa}} = .40$

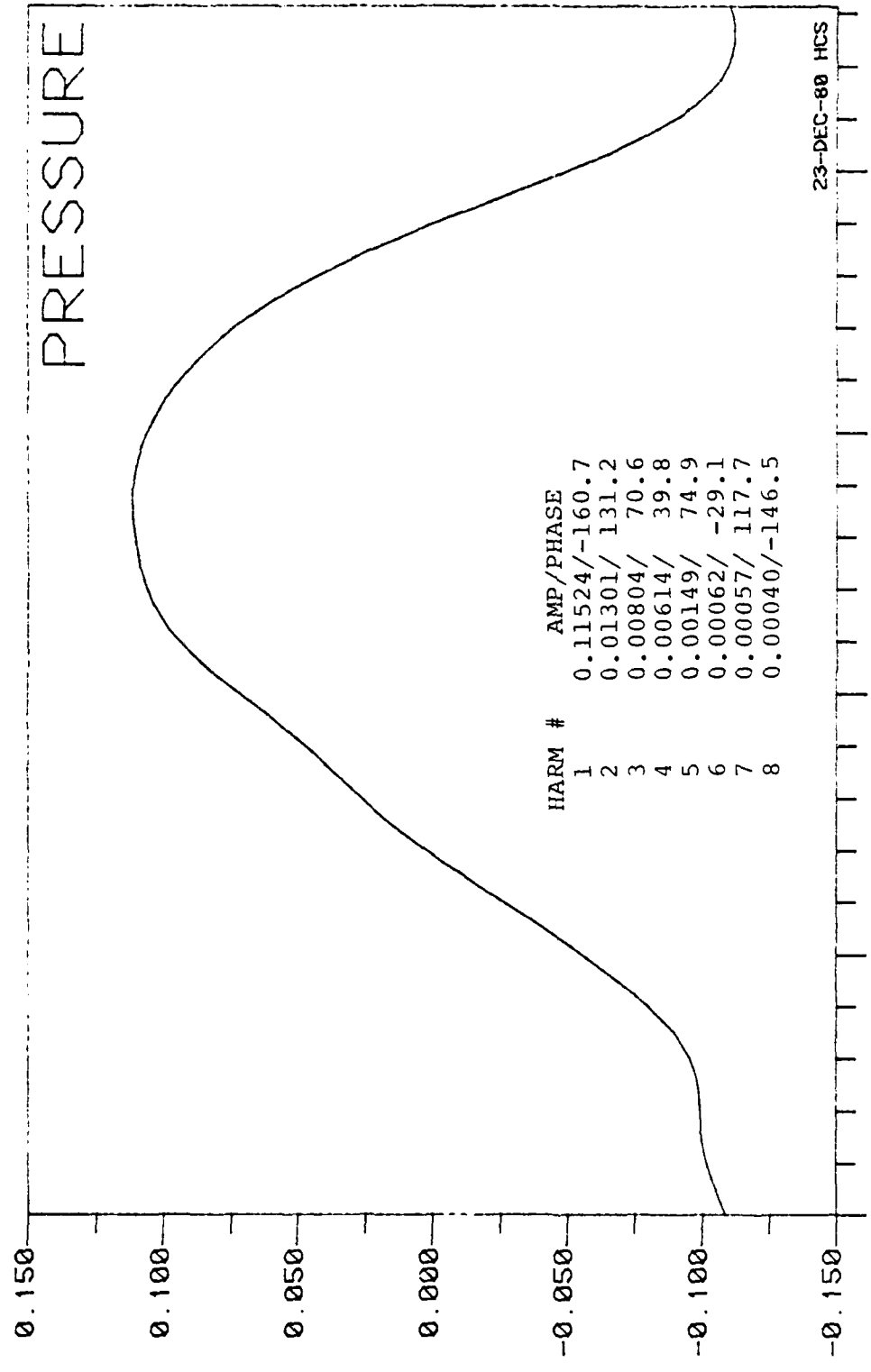

Figure 43: Cavity Pressure Coefficient vs. Time, $\overline{C_{pa}}$ = .53

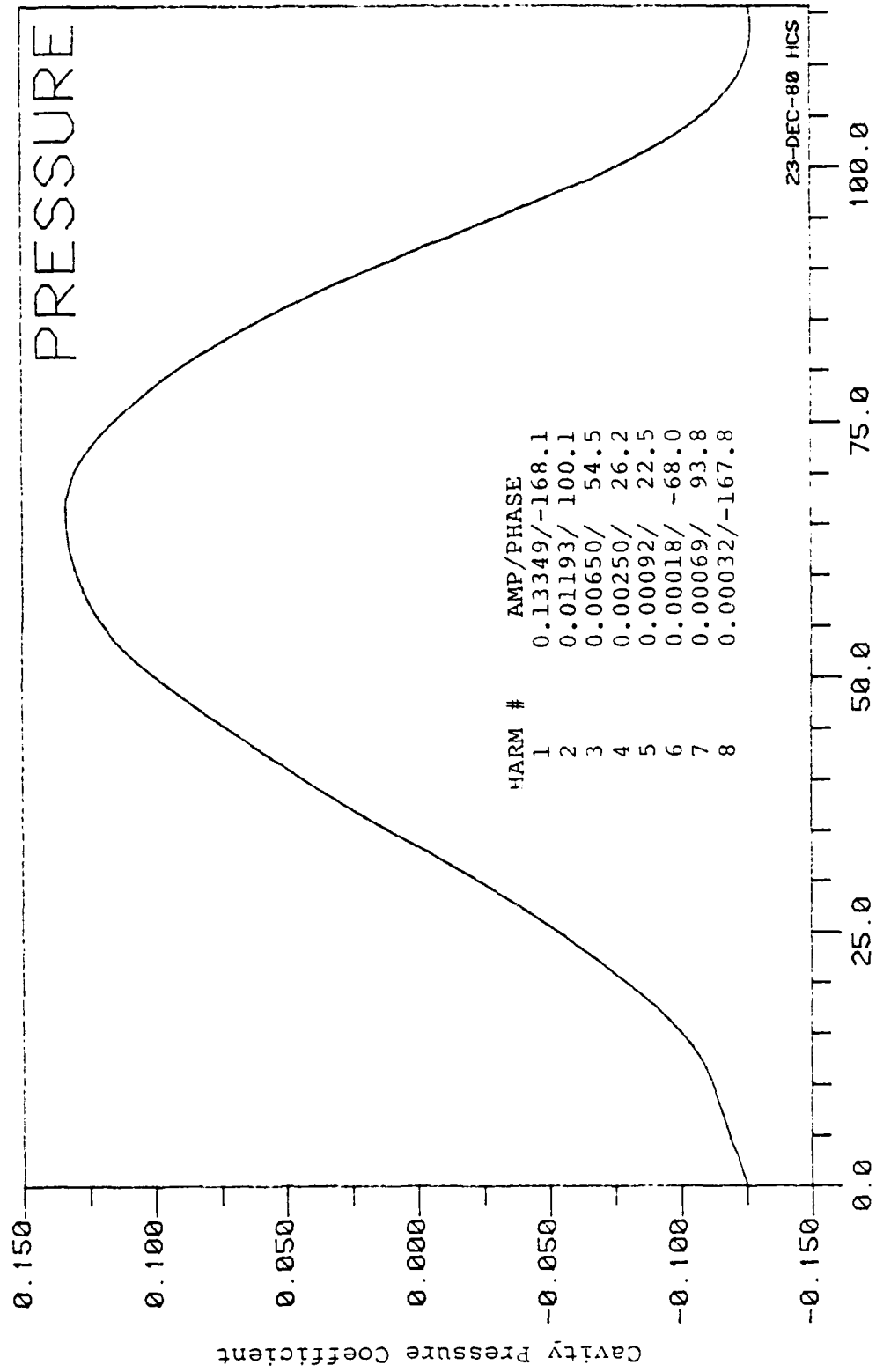

Figure 44: Cavity Pressure Coefficient vs. Time, $\overline{C_{pa}} = .72$

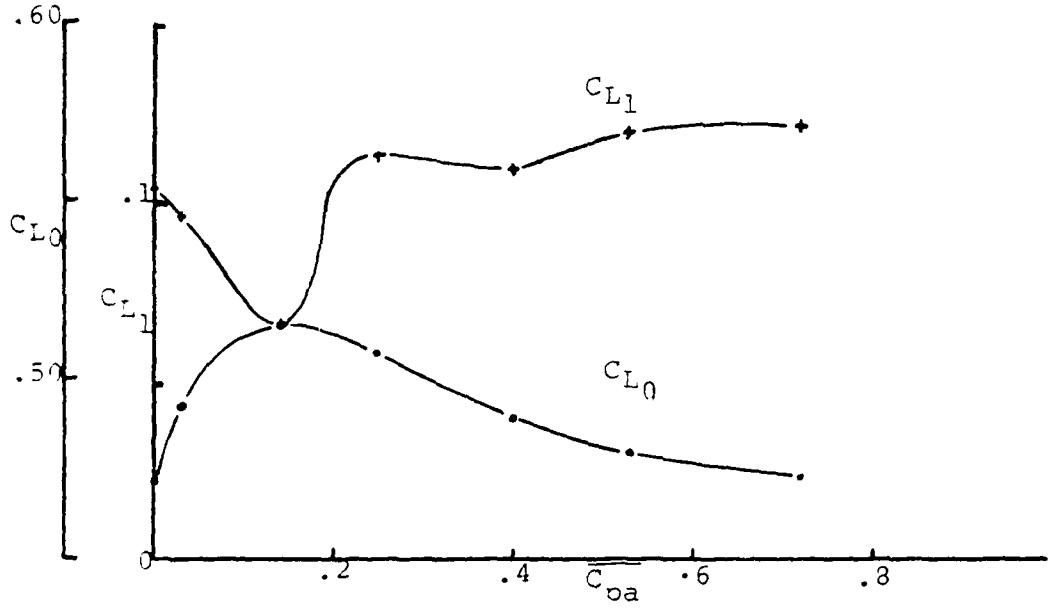

Figure 45: Mean and First Harmonic of Lift Coefficient vs. $\overline{C_{pa}}$

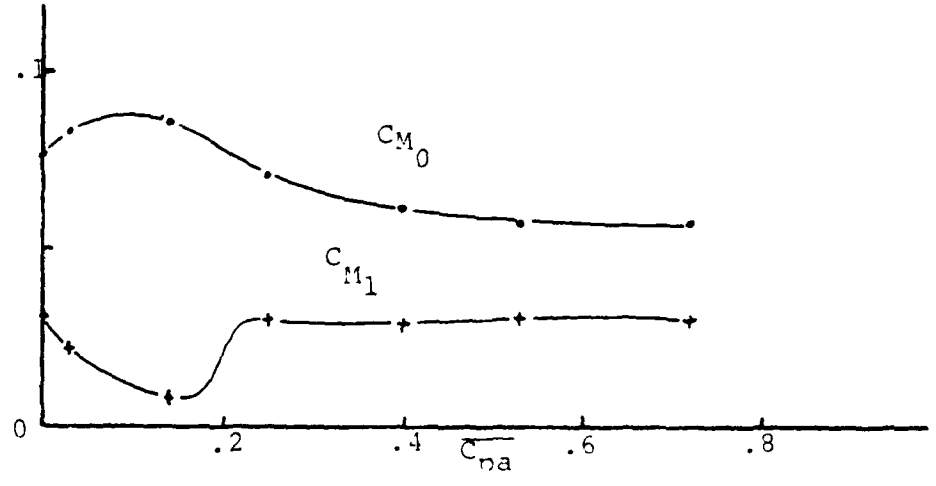

Figure 46: Mean and First Harmonic of Moment Coefficient vs. $\overline{C_{pa}}$

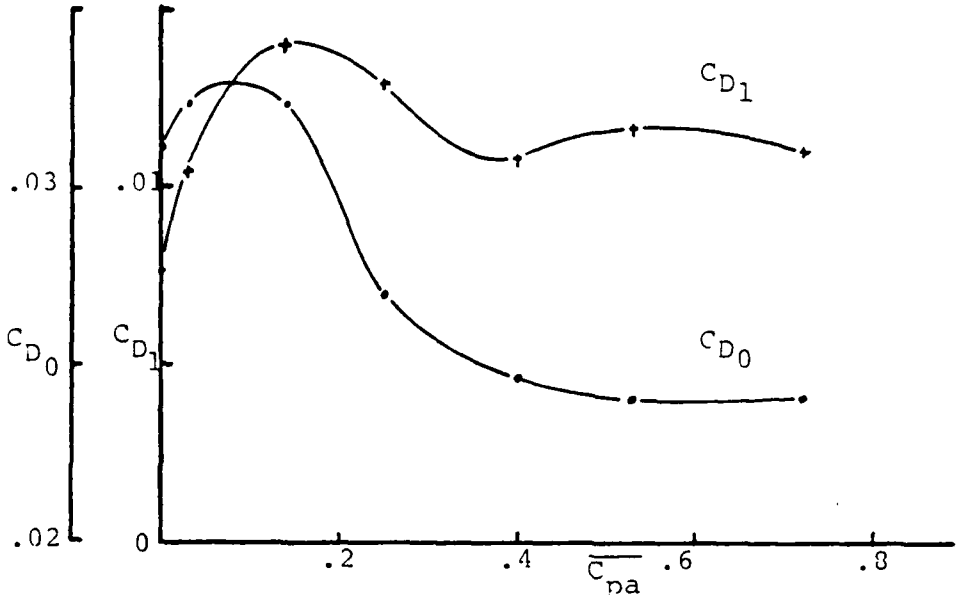

Figure 47: Mean and First Harmonic of Drag Coefficient vs. $\overline{C_{pa}}$

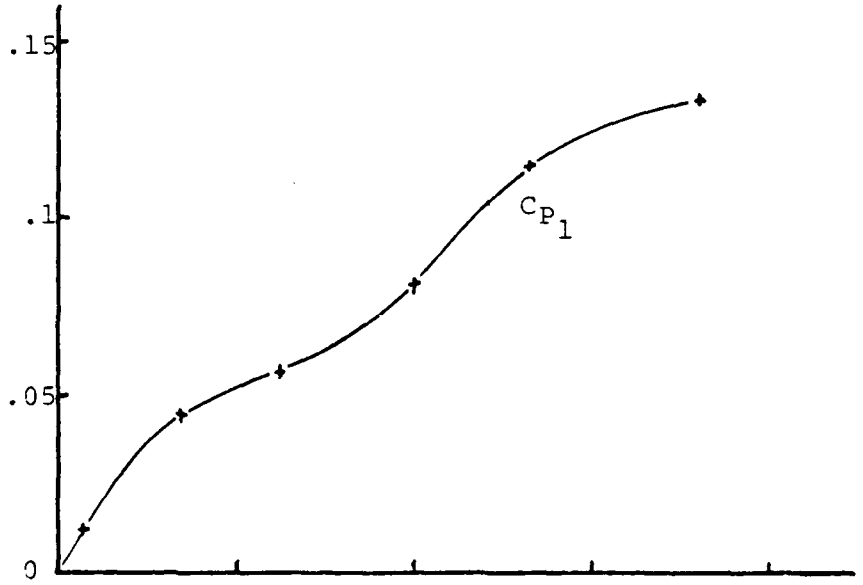

Figure 48: First Harmonic of Cavity Pressure Coefficient vs. $\overline{C_{pa}}$

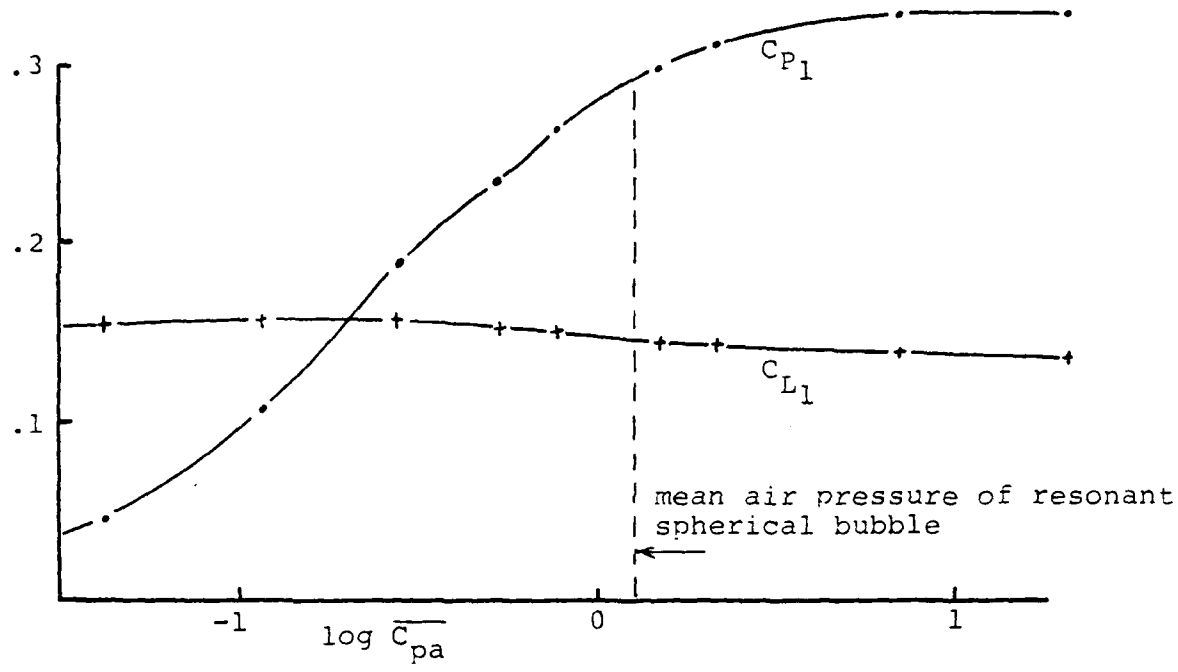

Figure 49: Calculated First Harmonics of Pressure and Lift Coefficients, σ = .7

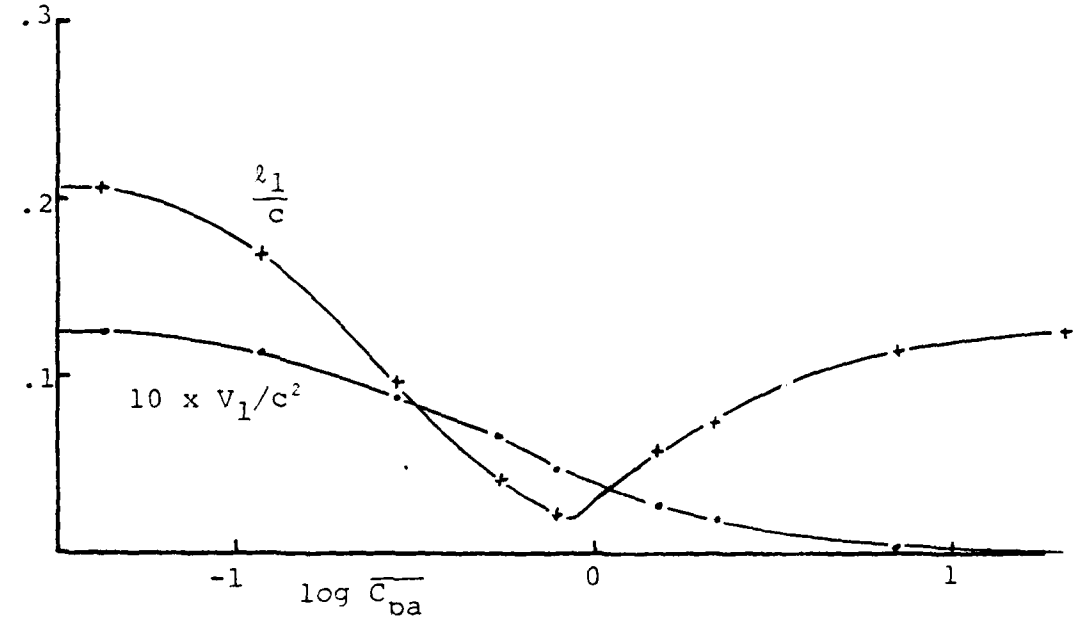

Figure 50: Calculated First Harmonics of Cavity Length and Volume, σ = .7

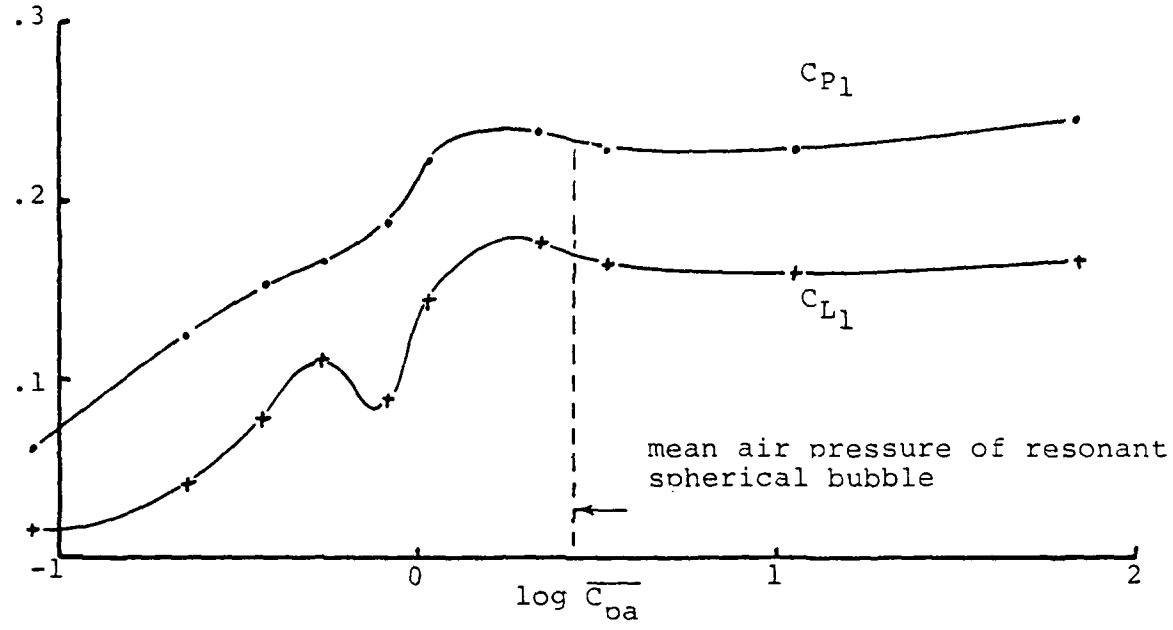

Figure 51: Calculated First Harmonics of Pressure and Lift Coefficients, σ = .5

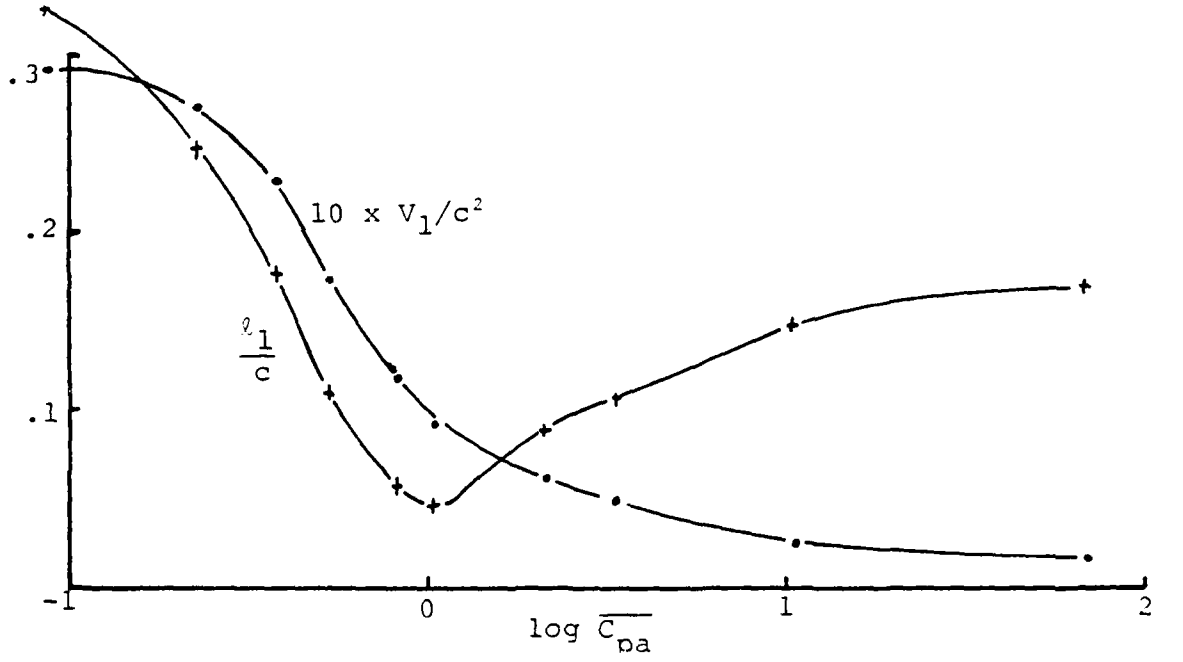

Figure 52: Calculated First Harmonics of Cavity Length and Volume, σ = .5

Appendix A

CALIBRATION OF THE DYNAMIC MEASUREMENT SYSTEM

In order to measure unsteady forces on the cavitating hydrofoil, knowledge of the dynamic amplification and phase distortion associated with the dynamometer, foil, and driving system was essential. A substantial portion of the effort in performing this experiment was the refinement of a calibration technique which would provide this system transfer function.

The dynamic system is shown in figure 1. A stub shaft on the port side of the foil is held in a socket on a two-component dynamometer, which measures lift and drag on the foil. The driving shaft of the foil passes through the bearing case of a three-component dynamometer on the starboard side of the tunnel. The bearings isolate the dynamometer from moment forces on the foil, so that the three component dynamometer sees only two components: lift and drag. A load cell on the pushrod driven by the rotating eccentric reads all moment loads.

Five-hundred pound Lebow model 3345 load cells were used in lift and drag with the three component dynamometer, as well as for the pushrod. Steel flexures necked down over 11 mm to 2.5 mm in diameter link the lift and drag load cells to the dynamometer frame and central spider, and serve to isolate the load cells from spurious loading. The two component dynamometer is a

Lebow model 6643 with a 1000 pound load cell in lift, and a 500 pound load cell in drag. Load cells are factory mounted in the Lebow 6643, and cannot be swapped out and optimized for a particular experiment.

It is instructive to view the foil and dynamometer system in terms of simple dynamic elements: mass, stiffness and damping. The bearing case, spider, foil and driving shaft are the live mass, and together have a mass of about 22 kilograms (kgm). The hydrodynamic added mass is the same order of magnitude. The least stiff part of the measuring system is the combination of the load cells and their isolating flexures. The 1000 pound load cell has a stiffness of 45,000 kilograms force per centimeter (kgf/cm), the 500 pound load cells have a stiffness of 22,000 kgf/cm. The flexures, in series with the load cells, have a stiffness of 37,000 kgf/cm. Mechanical damping is provided by the seals around the foil shaft, but plays a very small role in total damping. Hydrodynamic damping dominates, and occurs when vorticity is shed into the wake. Any vibration of the foil which occurs when the fluid is moving causes changes in the lift of the foil. These changes in lift are attended by shed vorticity, which is a pathway for the system to lose energy into the wake. This process damps the vibration.

Added mass and damping are functions of fluid velocity, and are somewhat dependent on the presence of cavitation. To properly

reproduce the characteristics of the system during testing, it is clear that any calibration technique would have to accomodate the full range of cavitation test conditions: low tunnel test pressures, high fluid velocities and any foil position.

An analytic approach to the dynamic problem was rejected as being impossibly complex. It was felt that values for stiffness and mechanical damping would be difficult to obtain, and that the idealization of the real hydrodynamic problem to one tractible for the purposes of calculating hydrodynamic damping would be of questionable value. An experimental approach was considered necessary.

An electromechanical shaker was available for continuous excitation of the foil. This technique involves applying a known vibratory force to the foil, then comparing measured loading on the foil with the applied loading to arrive at the transfer function. Objections to this approach stem from the cumbersome nature of the required connection between the shaker and the foil. Inasmuch as the connecting rod from the shaker to the foil must carry both compressive and tensile loading, it must be rather large and heavy, which would disturb the flow field and change the system mass. The nature of the operation makes it difficult to apply loading in the drag direction, which was necessary to derive the total system transfer function. These problems are not insurmountable, and would have been overcome had a better technique not been available.

Transient calibration involves applying a steady load and abruptly removing it while recording system response. The time derivative of the record represents the response of the system to a dirac delta input rather than a step input, and the Fourier Transform of a system's response to a delta input is defined to be its transfer function. The advantages of this approach are: first, an unobtrusively small diameter wire can be used to carry relatively high applied tensile loads; second, the quick set-up and run through time of the technique; third, the ability to apply very high step loads resulting in good signal to noise ratios; and fourth, the ease with which the direction and application point of the loading can be changed. Transient calibration was selected as the most practical approach to providing a correction for non-ideality of the dynamic measurement system.

The actual procedure proved simple, quick and dependably reproducible. A small diameter hole was drilled in the foil allowing the attachment of 2.2 mm high strength piano wire. The wire was led out a small hole in the plexiglass lower window of the water tunnel, where it ended in a hook. A 10 cm loop of thin nylon braided rope (mono-filament fishing line worked equally well) connected the piano wire to a chain fall, which was used to load the foil with 130 kgm in steel blocks. The computer operator supplied an appropriate verbal cue as he initiated data acquisition from the five load cells, and a second technician melted the nylon fuse with a propane torch. The torch and nylon

line insured that no additional loading was applied during the process of releasing the weight.

Data reduction involved trivial data manipulations and the use of a DEC supplied Fast Fourier Transform (FFT) routine. The records from all five load cells were reviewed by hand and a best estimate for zero time (the instant the weights were released) was made. The clearest indication was always from the load sensing element with the fastest response: moment. The data was then shifted to that zero time and differentiated. The mean value was removed from the record and then the FFT subroutine was used to compute the transfer function, which was normalized on the measured step strength. The data was smoothed, and the "DC" value added. The result was the transfer function between a load applied to the foil and the response from each of the five load cells.

The two dynamometers were designed to optimize separation between measured lift, drag and moment. For steady measurements, it is satisfactory to assume that there is no coupling between force sensing elements, i.e., an applied lift is measured entirely in the lift load cells -- none of it appears in the drag or moment cells. However, the oscillating mechanism and the dynamics of the vibrating foil itself provide a path for lift forces to be felt in the moment cell, and moment forces to be felt in the drag cell. The system is therefore dynamically coupled, and each measured force must be viewed as a linear combination of all the applied

forces. The coupling coefficients describing this combination will be functions of frequency. Inversely, the applied hydrodynamic forces of interest in the experiment must be found in some linear combination of the measured forces. This is to say that in order to interpret the measured forces from the experiment, some matrix "H" is required such that:

$$\underline{fa}(\omega) = \underline{H}(\omega) \cdot \underline{fm}(\omega)$$

Where $\underline{fm}$ is a vector of measured forces, and $\underline{fa}$ is a vector containing the desired applied forces.

This "$\underline{H}$" matrix can be found from the result of three linearly independent transient calibration experiments, linearly independent in the sense that the ratios of applied lift, moment and drag must be different in each of the three. The solution proceeds as follows. Perform three transient calibrations such that a different combination of applied forces excites the system in each. Reduce the data and construct nine response functions: lift, moment and drag from the three experiments. Record the step strengths for each of the nine cases, and store the results in an $\underline{Fa}$ matrix where:

$$\underline{Fa} = \begin{bmatrix} Lia & Lja & Lka \\ Mia & Mja & Mka \\ Dia & Dja & Dka \end{bmatrix}$$

The nine complex elements of $\underline{H}$ are computed at each frequency bin of the FFT; for 2048 points at 2500 hertz, the FFT approximates the response function every 1.22 hertz, and so a different $\underline{H}$ matrix is calculated every 1.22 hertz. The nine curves in frequency space are plotted in figures A1 to A9.

Use of this data is straightforward. The unsteady data is reduced in a numerical Fourier Series to give harmonic strength at multiples of the oscillation frequency. The values of the $\underline{H}$ matrix are picked off corresponding to the frequency of each harmonic and used to multiply the three harmonics of measured lift, moment and drag to get applied lift, moment and drag. Thus from the Fourier Analysis of the data and a knowledge of the behavior of the measuring system, the time records from the five load cells were disassembled into frequency space, combined linearly to give applied forces, and then reassembled into the time domain to yield plots of unsteady lift, moment and drag.

The system transfer function as a function of frequency was determined for the entire spectrum of operating conditions. It was of interest to know to what parameters the system was sensitive. Flow speed was by far the most important factor, both due to the change in added mass which in turn changes the location of the resonance in frequency space, and due to the increase in damping which widens the resonance peak. The calibration data that was used was taken at the same flow speed used in the cavitation studies: 6.1 mps.

Where i, j, and k indicate the three experiments, L, M and D are lift, moment and drag, respectively, and "a" indicates that the forces are applied forces. Note that since the derivative of a step is an impulse, and the Fourier Transform of an impulse is white noise (constant amplitude in frequency) whose amplitude is equal to the step strength, this Fa matrix represents the Fourier Transform of the hypothetical applied impulsive forces. The columns of the Fa matrix are the three known fa vectors from the three experiments.

Similarly, construct a square Fm(ω) matrix containing the nine measured responses to the nine step inputs.

$$\underline{Fm} = \begin{bmatrix} Lim & Ljm & Lkm \\ Mim & Mjm & Mkm \\ Dim & Djm & Dkm \end{bmatrix}$$

Here the "m" indicates measured forces. The nine elements of Fm are, in general, complex, and are the values returned from a FFT of the time record of the lift, moment and drag load cells. Each element is a discrete approximation to a complex response function in frequency space. The matrix equation.

$$\underline{Fa} = \underline{H} \cdot \underline{Fm}$$

now contains enough information to solve for the nine elements of H. If both sides of the equation are post-multiplied by the inverse of Fm, an expression for H results:

$$\underline{H} = \underline{Fa} \cdot \underline{Fm}^{-1}$$

Other variations in operating conditions caused negligible differences. Cavitation produced only minor changes in the calibration data, and the noise that it introduced made this data less useful for data reduction than the fully wetted transient calibration information. The characteristics of the drive mechanism was another concern. When the foil is oscillating during unsteady testing, the belt drive adopts a particular tension and the flywheel has a given inertia. During calibration testing, the oscillator drive is stopped and so the calibration test poorly simulates the apparent stiffness the driver offers during test conditions. It was necessary to evaluate the potential error introduced. A series of calibration tests were done with different belt tensions and at different positions of the driving eccentric, both of which determine the stiffness the driving mechanism presents. No significant variation in transfer function data was found.

Inertial Loading

Another correc . .n to measured data arises from the inertial loading the foil and drive system imposes on the load cells. The foil and drive arm have mass; acceleration of this mass creates forces on the accelerating mechanism. The sinusoidal oscillation of the test foil causes unsteady inertial force to be felt by the load cells in addition to the hydrodynamic forces of interest in the experiment.

This unsteady inertial loading is measured by oscillating the foil in still air at the test frequency and measuring the resulting forces. These forces are subtracted from the calibrated total forces to yield the actual hydrodynamic forces. The inertial loads measured at the test frequency of 8.5 hertz were:

FORCE	AMPLITUDE (lbf)	PHASE (deg)
LIFT	2.96	1.4
MOMENT	2.16	20.2
DRAG	2.18	5.0

As should be expected with a linear system and a sinusoidal input, no tare forces were noted at frequencies other than that of excitation, 8.5 hertz.

The measuring system transfer function was considered flat enough at 8.5 hertz for a system with no added mass to make calibration of the tare readings unnecessary. Consequently, the tare forces are reported as measured.

AD-A119 800 MASSACHUSETTS INST OF TECH CAMBRIDGE DEPT OF OCEAN E--ETC F/G 13/10
EXPERIMENTAL AND THEORETICAL STUDIES OF THE EFFECT OF GAS CONTE--ETC(U)
JAN 82 R J VAN HOUTEN, H C SAYRE N00014-80-C-0224
UNCLASSIFIED 82-1 NL

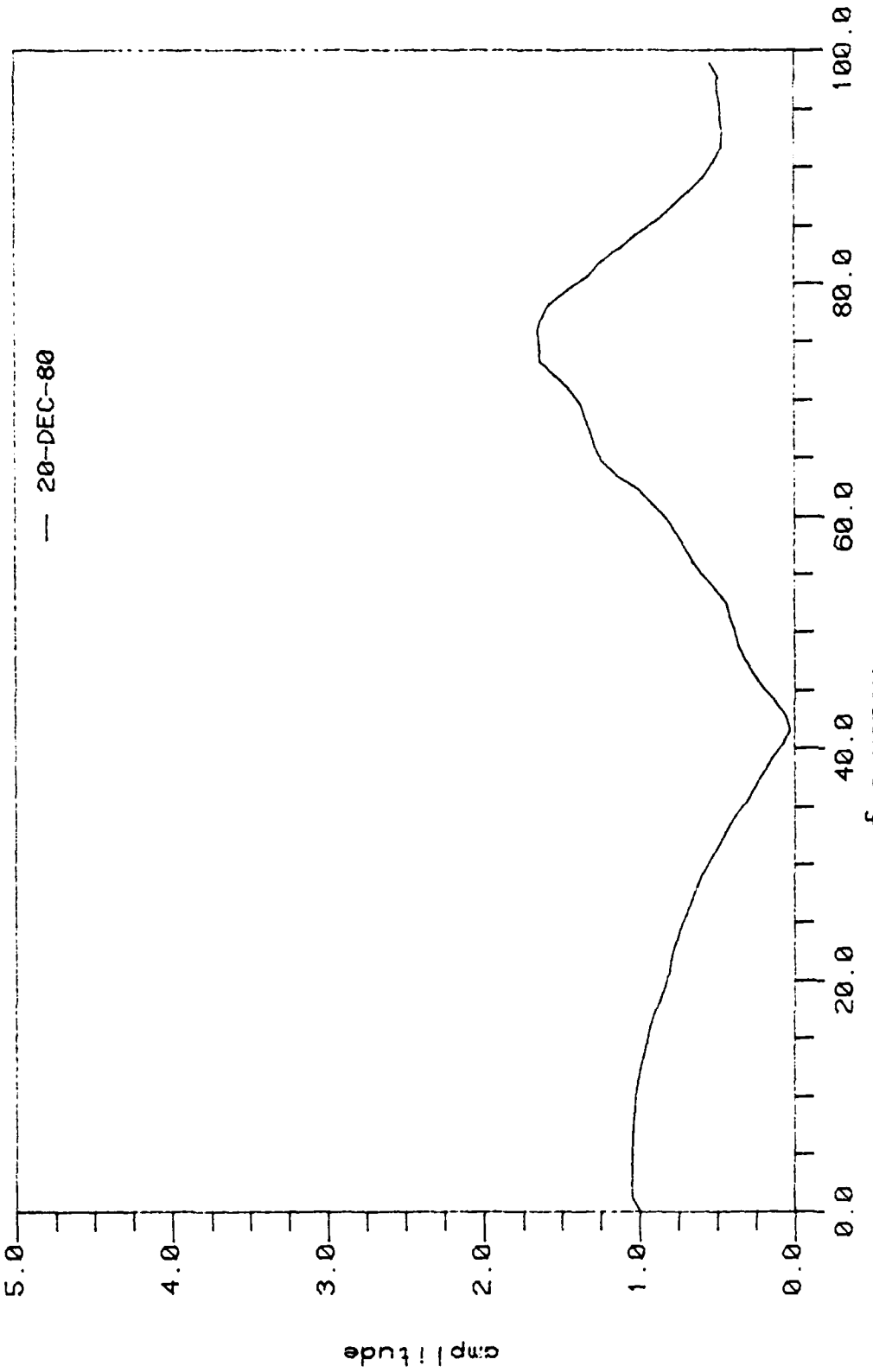

Figure A1: Calibration Matrix Element H_{11}

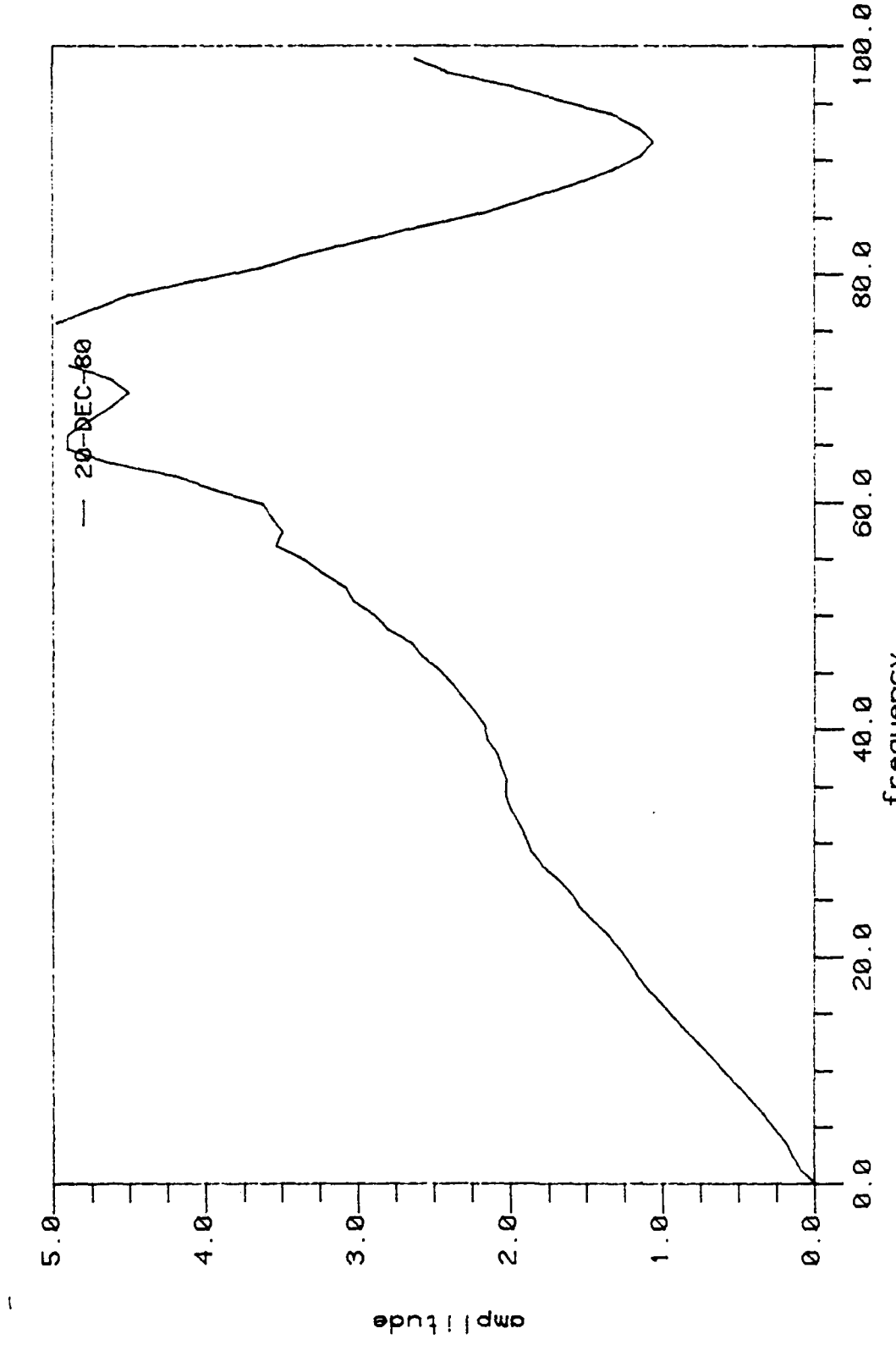

Figure A2: Calibration Matrix Element H_{12}

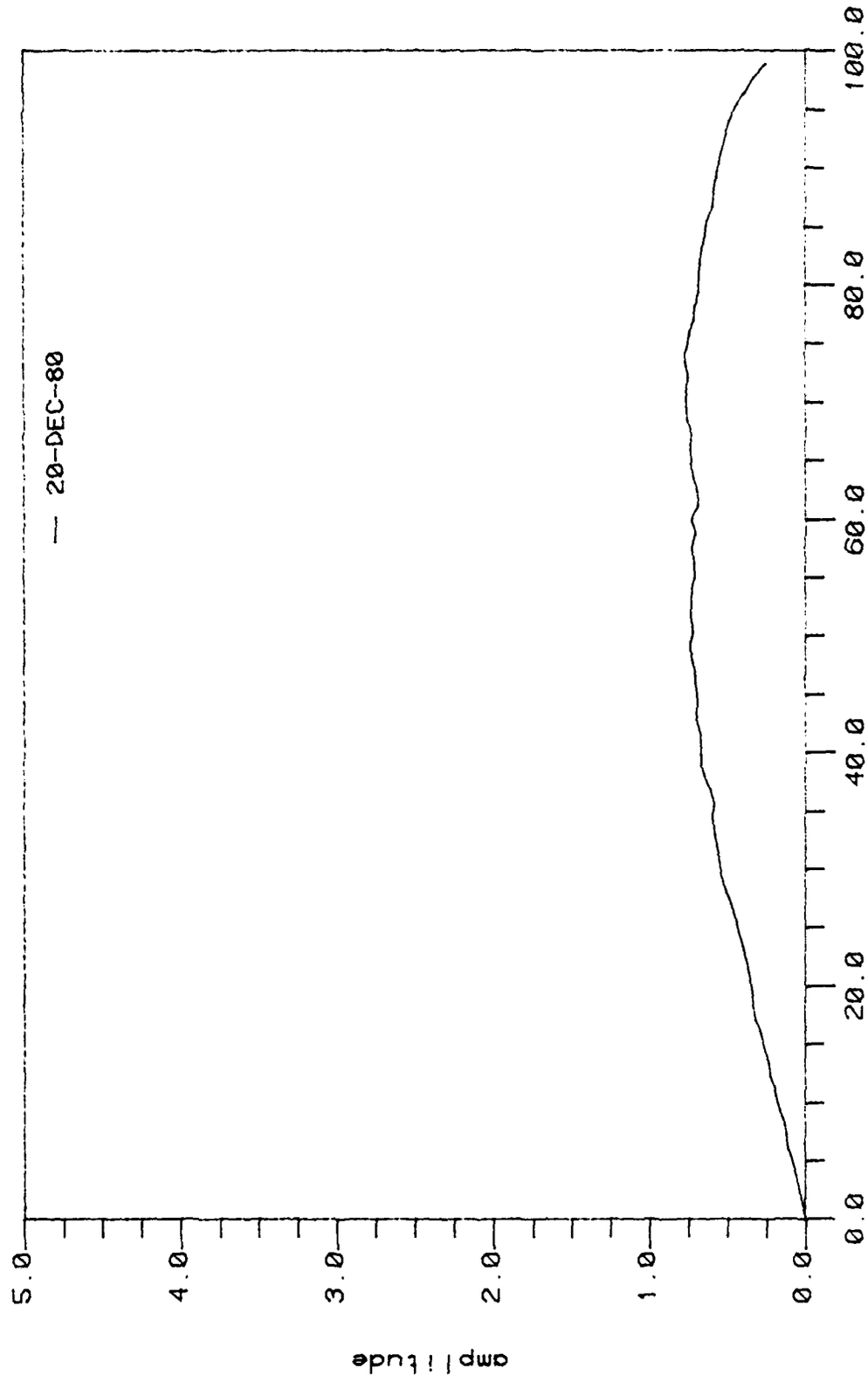

Figure A3: Calibration Matrix Element H_{13}

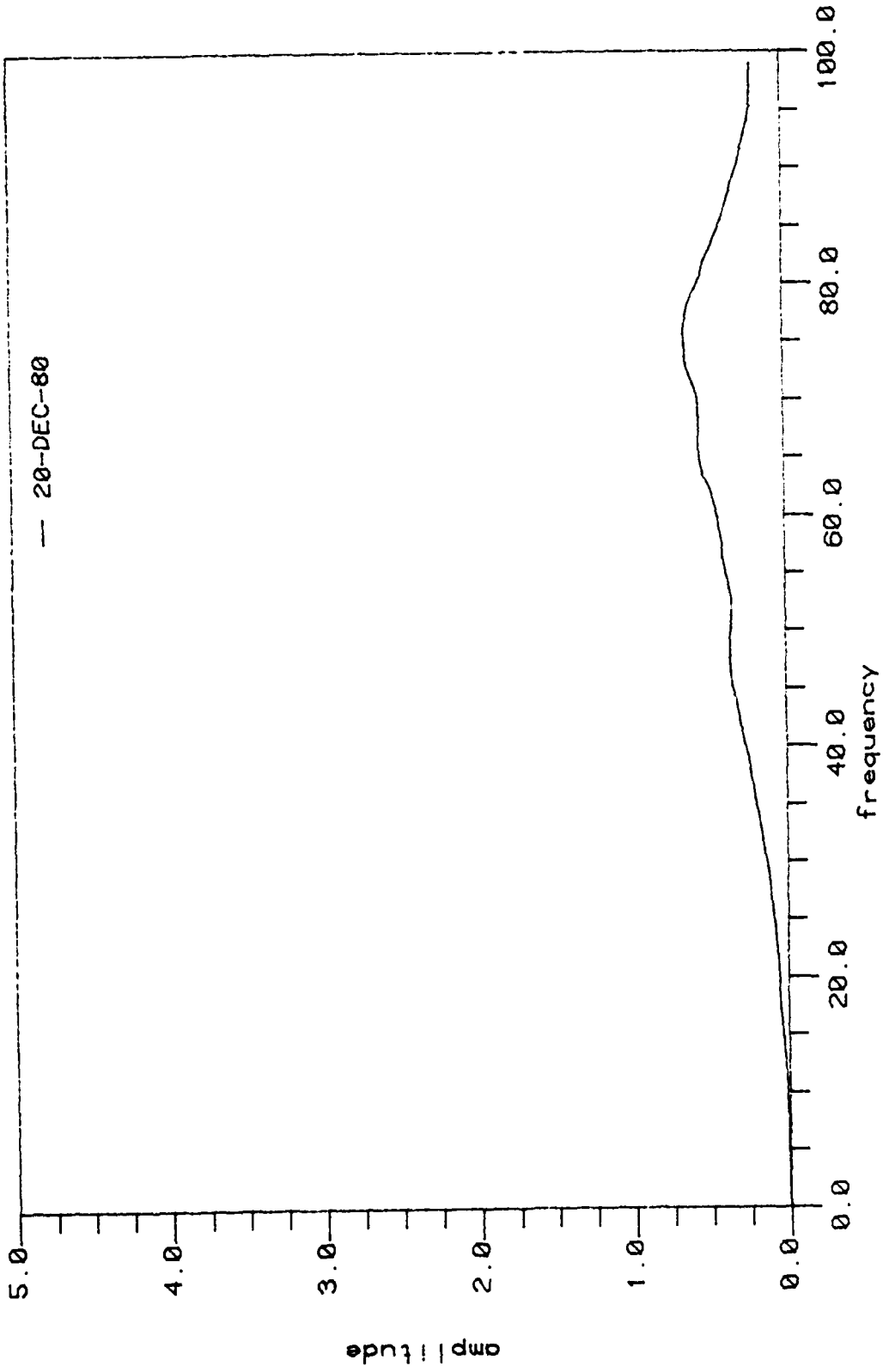

Figure A4: Calibration Matrix Element H_{21}

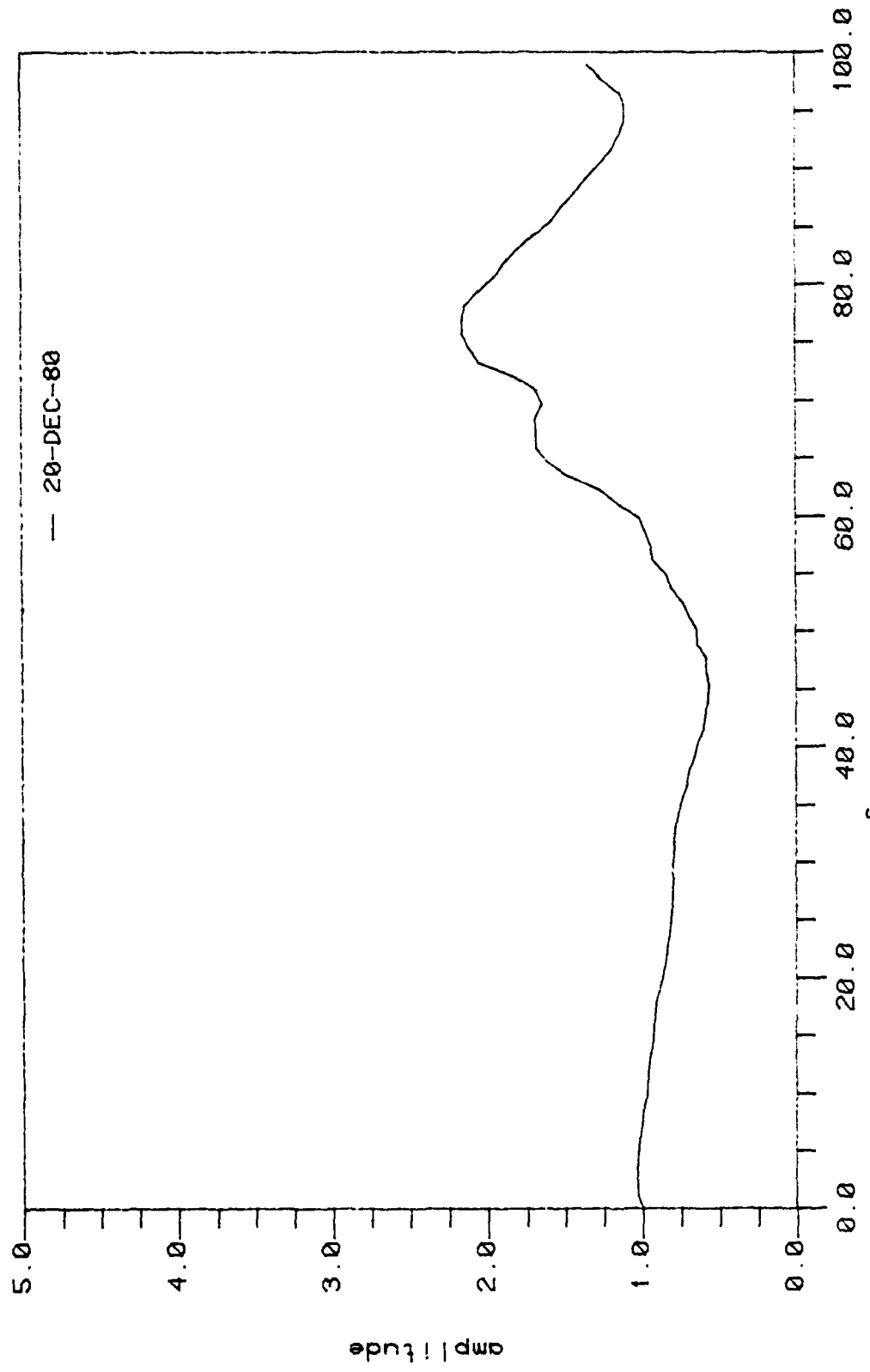

Figure A5: Calibration Matrix Element H_{22}

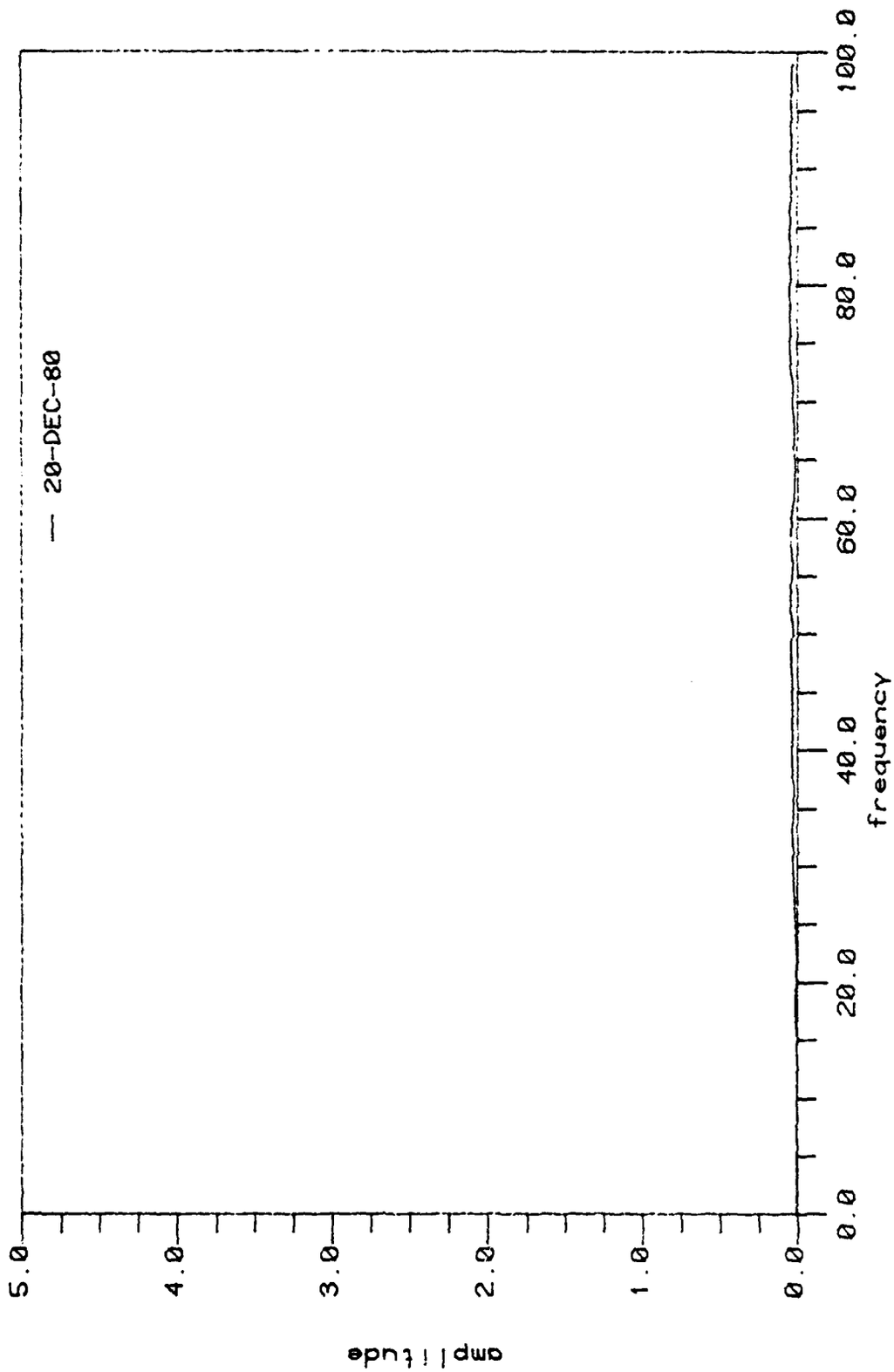

Figure A6: Calibration Matrix Element H_{23}

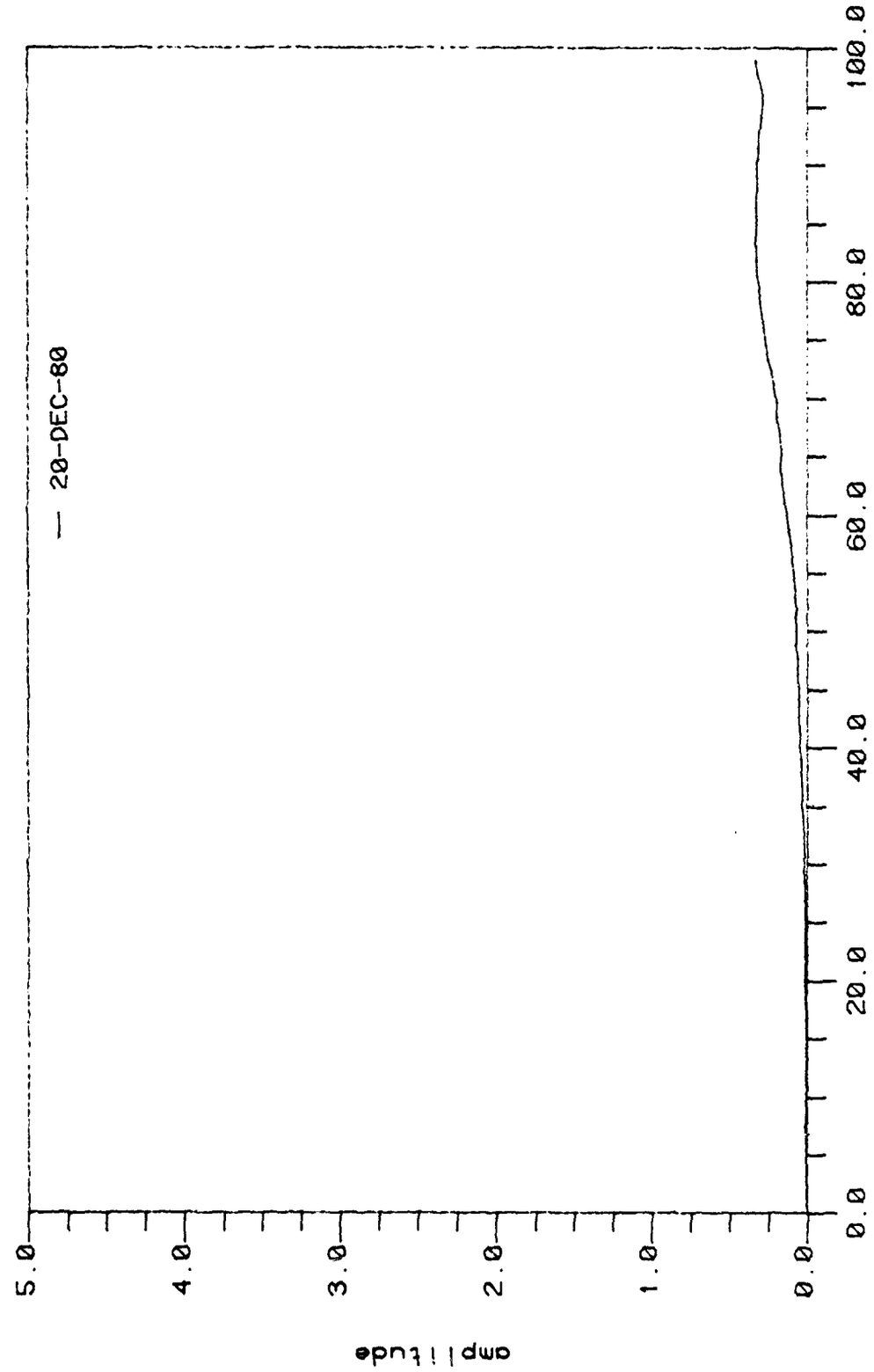

Figure A7: Calibration Matrix Element H_{31}

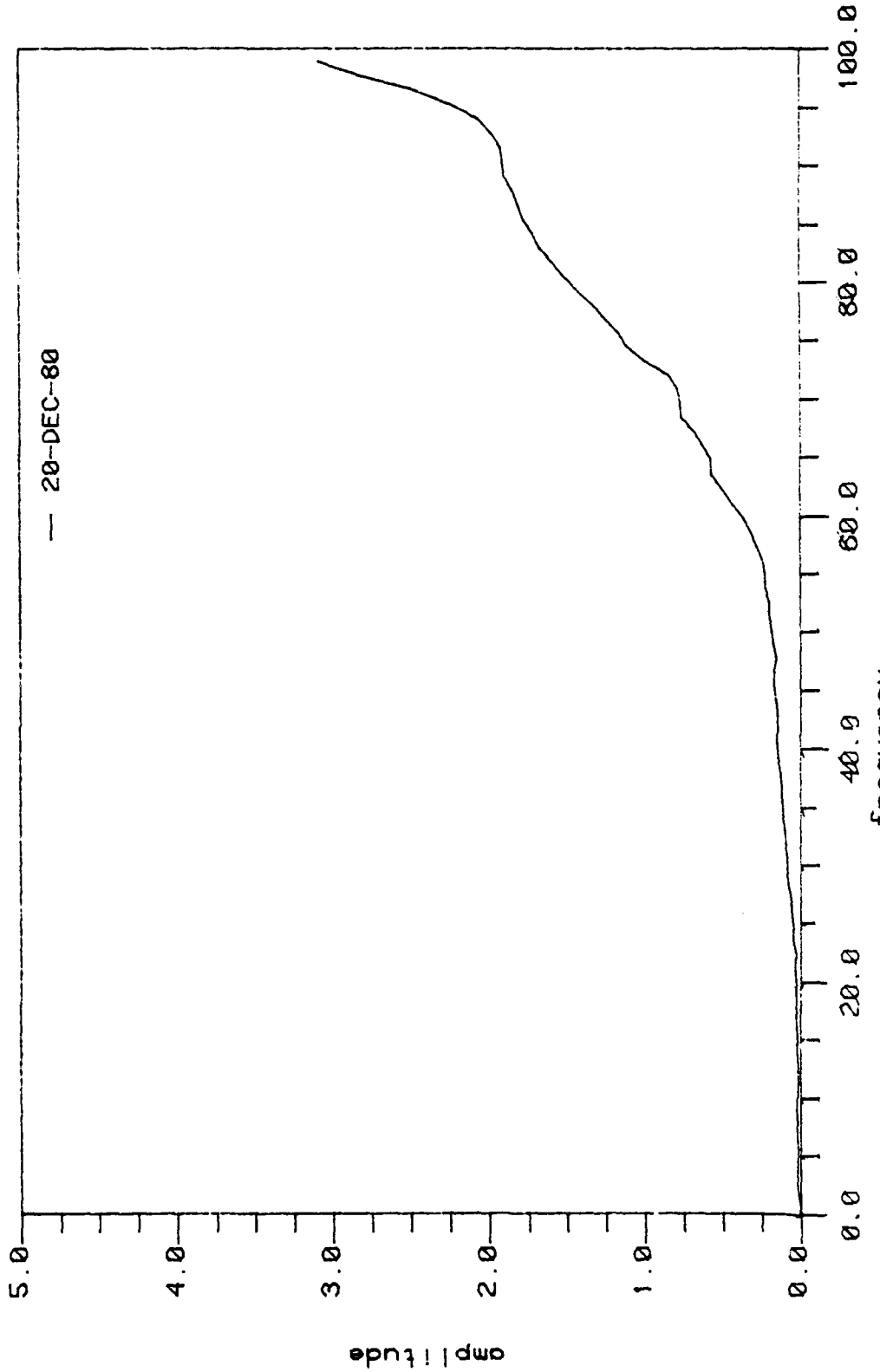

Figure A8: Calibration Matrix Element H_{32}

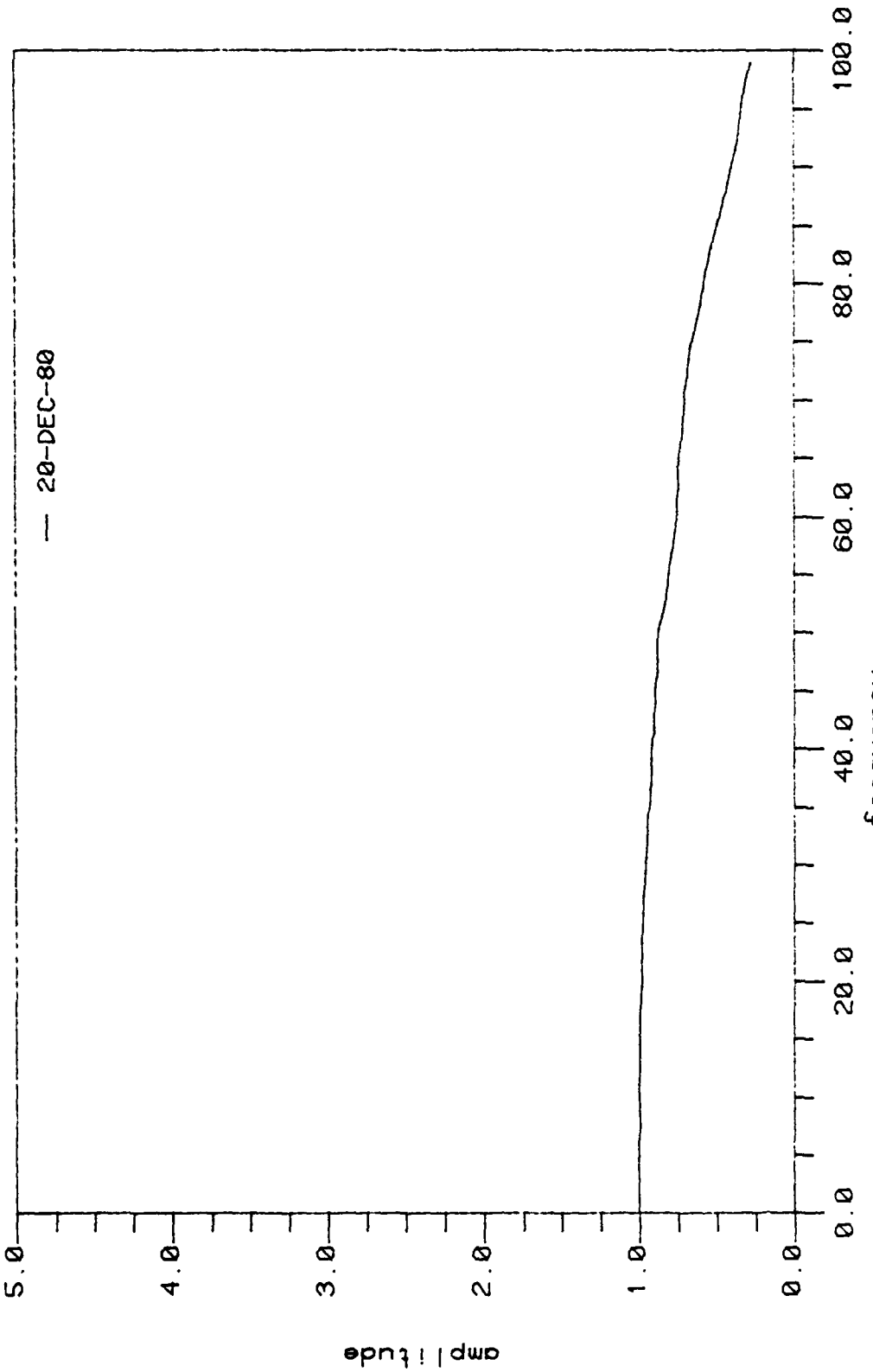

Figure A9: Calibration Matrix Element H_{33}

Appendix B

AIR ENTRAINMENT

The motivation for an investigation into natural cavity entrainment of tunnel air came in part from an observation made by Jiang and Leehey (1977). They measured cavity pressures and forces acting on unventilated supercavitating foils and noted that short supercavities had higher cavity pressures than long supercavities, suggesting perhaps that short cavities were more efficient in entraining tunnel air than long cavities. In measuring cavity pressures with two different techniques, a total head tube inserted into the cavity versus a surface pressure tap, they noted significant differences in the measured pressure, but both techniques showed the same length-pressure trend.

A possible explanation for the observed pressure dependence on length is the following: if cavitation number (which determines cavity length) is varied by changing tunnel pressure at a constant velocity, and the solubility of air in water increases with pressure, then a cavity acting in a high pressure fluid (implying a high cavitation number and a short length) is acting in a richer air environment and may be able to absorb more air across its interface with the fluid.

The ventilated cavitation experiments described in this project report required experimental equipment which was ideally

suited to verifying the Jiang and Leehey observation. It was proposed to investigate the effect of cavity length on cavity pressure by varying the cavitation number in two different ways: first by increasing the tunnel velocity at constant pressure, and second by decreasing the pressure at constant velocity. It was hoped that the results would document the functional dependence of entrainment rate on ambient pressure. From experience w ı the manometer system described earlier in measuring mean cavity pressures, the accuracy and precision were considered compa at one millimeter of mercury. Small changes in cavity pressure are readily measured.

It was not possible for the investigators to create an operating condition which led to any measurable change in cavity pressure from vapor pressure at tunnel temperature. At high pressures and high velocities or low pressures and low velocities, steady cavities were left undisturbed for up to one half hour with no measurable change in cavity pressure.

It was a concern that for short cavities manometer lines were occasionally seen to fill with tunnel water during the course of the experiment. In order to clear lines of water a small amount of air was forced through the lines into the cavity. The presence of this air in the cavity caused measured cavity pressure to rise, but as soon as the air bleed was stopped, cavity pressure returned to that of vapor pressure at tunnel water temperature. The time for the return to unventilated conditions appeared to be approximately the same as the response

time of the manometer -- about one second. Air injected into the cavity was quickly lost.

The effect of free air on cavity air entrainment is another issue. As air was bled into a cavity it escaped from the cavity and entered the recirculating tunnel water stream. After thirty seconds of continuous air injection at 150 cc/sec at standard temperature and pressure (stp), free air bubbles were numerous enough in the tunnel water to limit visibility to several centimeters. This extreme condition was created in the tunnel and pressures within unventilated cavities were recorded over time. At no point was it possible to measure a pressure higher than vapor pressure.

It appeared that it was not possible for the cavity to entrain air rapidly enough and then retain that air long enough to raise its pressure by a measurable amount. The next experiment attempted to quantify the rate of air injection that would be required by the steady cavity in order to sustain a given total cavity pressure above vapor pressure. Since an equilibrium is soon achieved between air injection and air loss, this is also a measure of rate of volume loss of the cavity.

The experiment was similar to the work of Brennan (1969) on spherical headforms. Tunnel conditions were fixed such that a steady cavity formed on the foil. The cavity pressure was recorded (vapor pressure) and then air was bled into the cavity at increasing rates. The static pressure within the tunnel was

increased so as to maintain constant ventilation number between cases; the cavity length and volume appeared nearly constant between cases as well. Total cavity pressure was recorded at each flow rate to arrive at a curve of volume loss as a function of cavity pressure. Three cavity lengths were investigated: .5 chord, 1 chord, and 2 chords.

The results of this experiment are shown in figure B1. Their interpretation is made easier if one writes the mass balance between air entering and leaving the cavity:

$$(\overline{\dot{M}_a})_{out} = (\overline{\dot{M}_a})_{in}$$

Using the ideal gas law for isothermal flow,

$$(\overline{P_a \dot{V}_c})_{out} = (\overline{\dot{V}_a})_{in} \cdot P_{atm}$$

or:

$$\tilde{P}_a \, (\overline{\dot{V}_c})_{out} = (\overline{\dot{V}_a})_{in} \cdot P_{atm}$$

where $\tilde{P}_a$ is defined as $\overline{P_a \dot{V}_c} / (\overline{\dot{V}_c})_{out}$
and will be somewhat different from $\overline{P}_a$. Dividing by $\overline{P}_a$,

$$\frac{\tilde{P}_a}{\overline{P}_a} (V_c)_{out} = \frac{(\dot{V}_a)_{in}}{\overline{P}_a} \cdot P_{atm}$$

It can be seen from figure B1 that the volume flux of air into the cavity (measured at stp) is linear against $\overline{P}_a$, which is to say that the right hand side of the above equation is constant. If the ratio $\tilde{P}_a / \overline{P}_a$ is approximately constant, so is the volume flux leaving the cavity. Since the cavity volume was held

constant over all flow rates, this indicates that the cavity loses a given fraction of its volume per unit time independent of the air to vapor mixture within the cavity. Brennan also found this linear relationship in the case of the spherical headform. He showed that this result, when coupled with a simple difussion model for air entering the cavity, yielded a linear relationship between air partial pressure and ambient dissolved air content in the case of unventilated cavities.

The difference in the slope of the mass injection versus cavity pressure curves for the partial and supercavities indicates greater volume fluxes for the larger cavities, which is expected as they themselves have larger volumes. The volumes of the cavities are very difficult to estimate, particularly for the supercavities. The 50% chord partial cavity was estimated to have a volume of 800 cc ± 30%. At the measured volume flux of 760 cc/sec, the cavity exchanges its partial air volume in just over a second. This estimate does not conflict with the estimate of transient air pressure decay time noted above.

A comparable analysis can be made of the unsteady data, which is presented in figure B2. Once again there is a linear relationship between mass flow and the air partial pressure, signifying a constant rate of loss of cavity volume. This is very surprising, considering the change in the nature of the unsteady cavity as the air partial pressure is increased. It

is also instructive to note that the volume loss rate during unsteady conditions appears to be significantly lower than under steady conditions, despite the very violent cloud collapse which occurs at low air partial pressures in the unsteady case. Klose and Acosta (1969) made a similar finding in observing that for a 2-D, wedge-shaped foil, the minimum air injection rate required for super ventilation was greater when the foil was steady than when oscillated at a reduced frequency in the range of one or two. At higher and lower frequencies, the oscillated foil required more air injection.

The very rapid loss of injected cavity air in these experiments indicates that the cavity air partial pressure rapidly comes into equilibrium with the free and dissolved air content of the tunnel water. Thus, the lack of measureable air partial pressure under unventilated conditions was not due to insufficient waiting time. The reason for the lack of consistency between these observations and those of Jiang and Leehey is not known. Under prototype conditions, the dissolved air content is expected to be quite high, resulting in a larger equilibrium air partial pressure. The magnitude of this partial pressure can perhaps be estimated by coupling experimental air loss data, such as that presented here, with a theoretical diffusion model, as was done by Brennan for a head form under laboratory conditions. The effect of free air would, of course, also have to be considered.

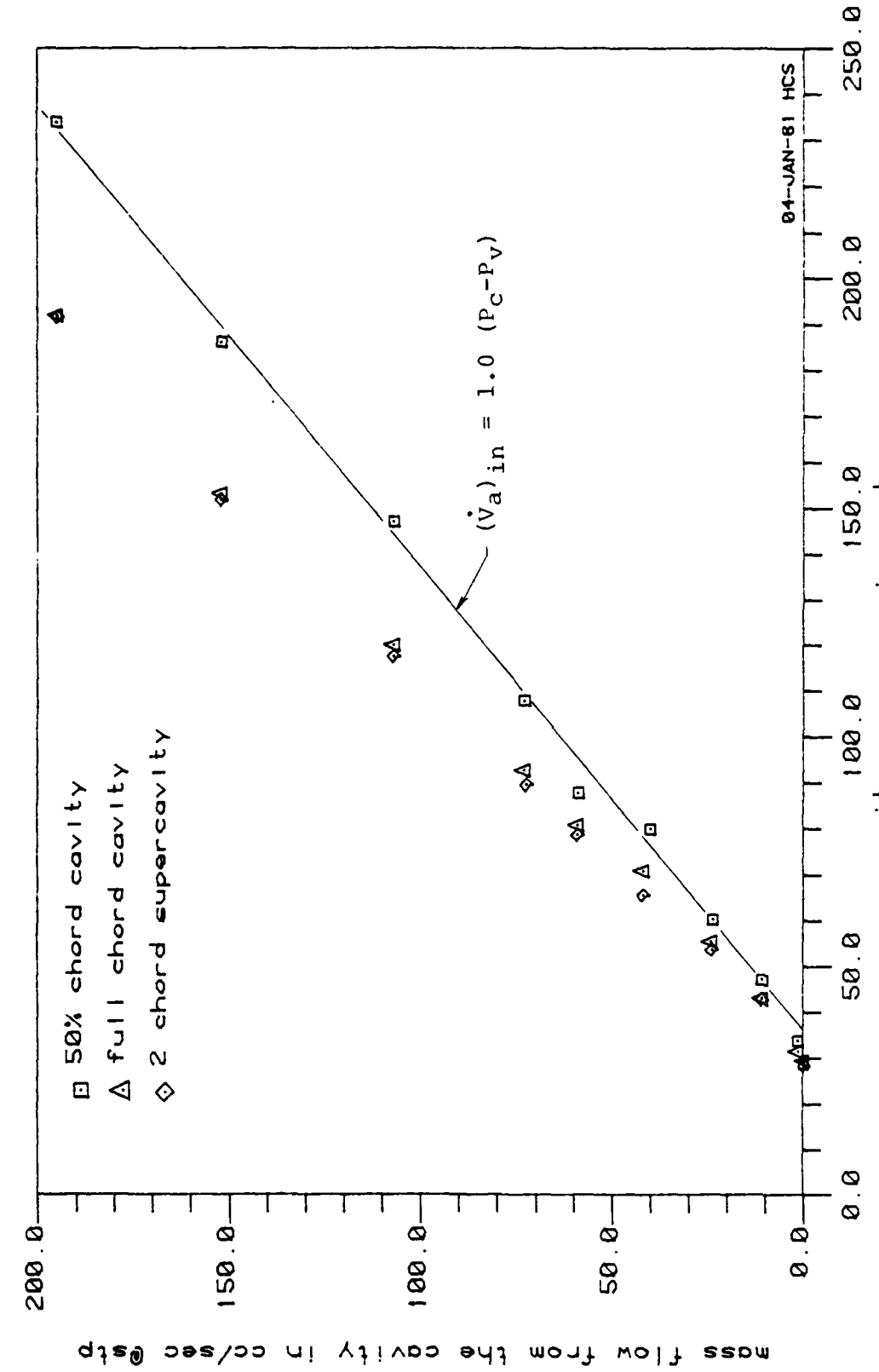

Air loss rate from a steady ventilated cavity

Figure B1

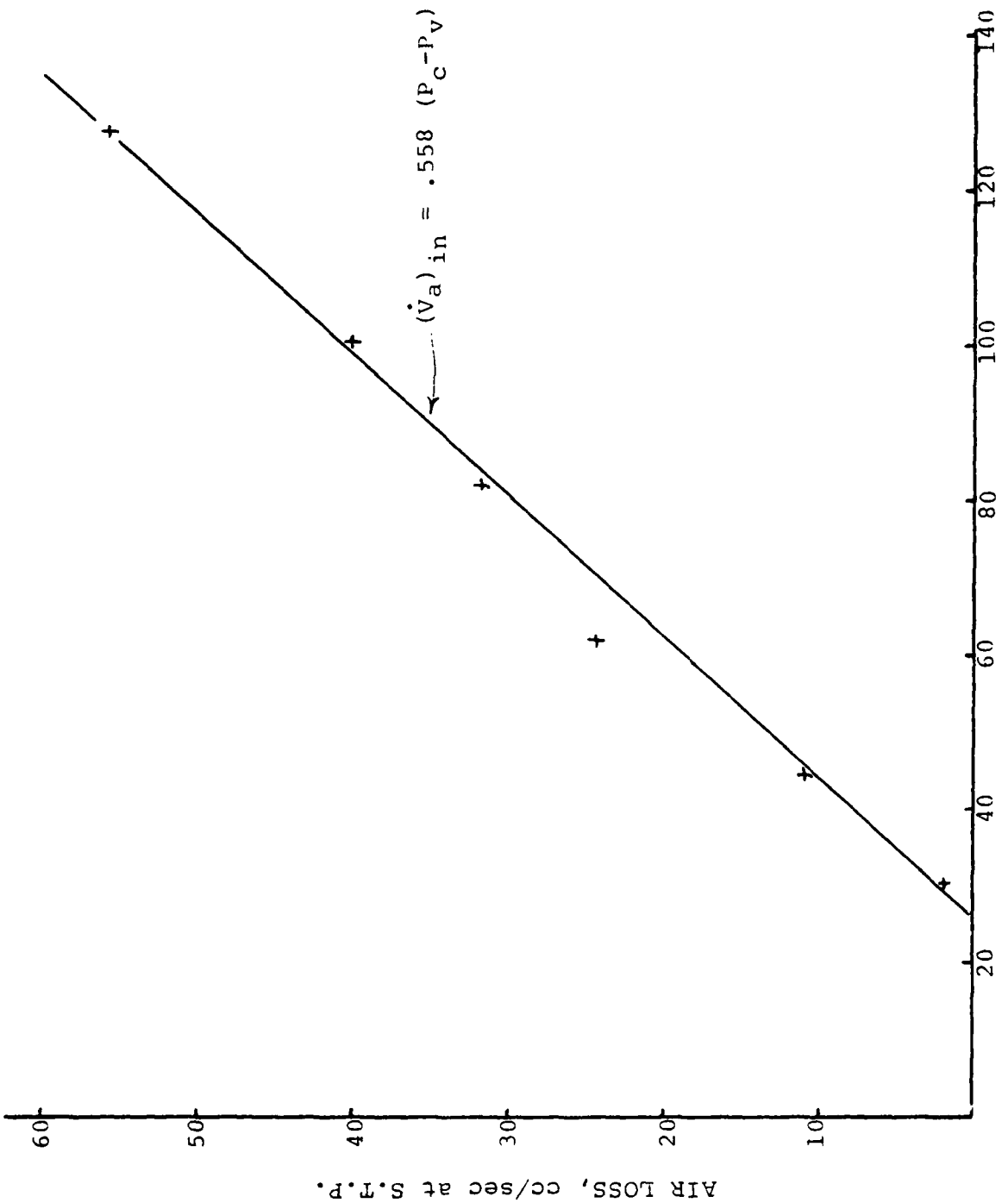

Figure B2: Air Loss Rate From an Unsteady Ventilated Cavity

END

DATE
FILMED

11-82

DTIC